Durham E-Theses

The effects of differential uplift and sediment supply on major Himalayan river systems at the mountain front

DINGLE, ELIZABETH

How to cite:

DINGLE, ELIZABETH (2012) *The effects of differential uplift and sediment supply on major Himalayan river systems at the mountain front*, Durham theses, Durham University. Available at Durham E-Theses Online: http://etheses.dur.ac.uk/3617/

THE EFFECTS OF DIFFERENTIAL UPLIFT AND SEDIMENT SUPPLY ON MAJOR HIMALAYAN RIVER SYSTEMS AT THE MOUNTAIN FRONT

Elizabeth Dingle

MSc by research

Department of Geography

Durham University

October 2011

It is well documented that in tectonically active regions, fluvial morphology responds to changes in base level. Vertical incision rates are adjusted through changes in channel morphology to balance imposed rates of rock uplift. It is common for responses in channel width, slope, grain size distribution and stream power to reflect spatial and temporal changes in rock uplift rates. Channels within tectonically active orogenic belts, such as the Himalayas, may be influenced by changes in discharge or sediment supply in addition to tectonic controls. Identifying the causes of morphological response in such areas is therefore of first order importance to enhance our understanding of landscape evolution. The Nepalese Himalayan foreland presents the ideal location to undertake this investigation, with its distinct tectonic frameworks heavily influenced by the style of foreland basin development. Thin-skinned thrust faulting over the past 1.6 Ma, has facilitated the recycling of foreland basin fill into hanging wall deposits of the frontal thrust (HFT), producing topographic entities now recognised as the Siwalik Hills. Above weak basal decollements, Dun valleys separate the frontal Siwalik Hills, and have rapidly filled with erosional detritus from the rising Himalaya. Poorly consolidated lithologies within the Siwalik Hills and Dun valleys are now being remobilised by modern incision of Himalayan River systems. It is unknown whether patterns of sediment storage and release within the foreland affect river morphology.

To understand the controls behind Himalayan river morphology, longitudinal profiles and channel slope were extracted from 90 m digital elevation models along the Gandak and Kosi Rivers about the Himalayan mountain front. Remotely sensed channel width measurements have also been made, and further supplemented with grain size data derived in the field and analysed using photo sieving techniques. Short-lived increases in channel slope are noted at the Main Boundary Thrust and Main Dun Thrust (MDT) of both rivers, in addition to a decrease in slope upstream of the HFT and Kosi Main Central Thrust (MCT). Increases in channel width upstream of the HFT and MCT (Kosi) are also consistent with morphological response to tectonic uplift. Where characteristic responses in morphology are absent at identified tectonic structures, it is likely that changes in lithology or anthropogenic modification of flow have overwhelmed tectonic influences. No increase in grain size upstream of recognized fault locations was noted on the Gandak, and it is proposed that an alternative mechanism dictates grain size patterns at the mountain front. On passing downstream of the MDT, an absence of direct hill slope inputs and a greater proportion of seasonal tributary inputs is reflected by a narrowing of grain size distributions, loss of Greater Himalayan lithologies, and decrease in D_{84} (by 50 mm).

These differences between geometry and grain size of the Gandak and Kosi Rivers are interpreted in terms of the style of foreland basin evolution. A lack of foreland accommodation above the strong basal decollement of the Kosi River facilitates continuous exportation of erosional detritus out of the mountain front. Widely spread D_{84} grain size distributions along the Kosi are dominated by regular inputs of coarse hill slope material from unstable relief produced by exceptional rates of uplift, above closely spaced frontal tectonic structures. It is interpreted that the weak basal decollement characterising the Gandak region has produced more stable hillslopes and accommodation for sediment within the Chitwan Dun. The fine grained and well sorted grain-size distributions of the Gandak noted between the MDT and HFT reflect an absence of direct hill slope inputs and a presence of seasonal tributary derived material. This study concludes that active tectonic structures strongly influence channel geometry at the mountain front. Grain size patterns are believed independent to differential uplift, and are considered a function of lateral sediment inputs, the nature of which reflects the structural evolution and tectonic history of the foreland basin.

Abstract

Declaration and Statement of Copyright

Contents

Acknowledgements

Tables

Chapter 1: Introduction

1.1 The role of tectonic deformation in shaping channel geometry

It is widely acknowledged that active tectonics play a key role in shaping fluvial geomorphology within the Himalayas (Seeber and Gornitz, 1983, Lave and Avouac, 2000; Lave and Avouac, 2001; Kirby *et al*., 2003; Jain and Sinha, 2005). Changes in channel morphology may be expected where rivers flow across active tectonic boundaries or features (Schumm *et al.,* 2000; Ouchi, 1985). Channels may respond to changes in valley slope, initiated by tectonic activity, through variations in aggradation, incision patterns and channel sinuosity (Schumm *et al.*, 2000). The specific response will depend on the magnitude and duration of the perturbation, in addition to the properties of the material of which the river is incising into. This relationship between fluvial morphology and tectonic uplift is of firm enough grounding, that first order insights of relative patterns of rock uplift can be extracted from channel profile analysis alone (Kirby *et al*., 2007).

Channel morphology is defined by a number of parameters including channel width, bed roughness, bedrock exposure and grain size distribution (Johnson and Whipple, 2007), but the response and interactions between these variables when one is adjusted remains unclear. It is known that river channels adjust their morphology in order to convey the flow and sediment supplied to them, as the morphology of the channel determines the distribution of velocity, shear and ultimately incision rates on the channel (Leopold and Maddock, 1953; Johnson and Whipple, 2007). Independent controls such as channel slope, where changes are initiated by tectonic perturbations, will also instigate a response in channel morphology. Slope and channel width are key variables in setting stream power, which determine the rate at which energy is transferred to the channel bed or walls, and therefore spatial patterns of erosion and sediment transport:

$$\Omega = \rho g \frac{Q_w}{W} S \qquad [1]$$

where Ω is unit stream power (W/m), ρ is water density (1000 kg/m^3), g is acceleration due to gravity (9.8 m/s^2), S is channel slope, W is channel width (m) and Q_w is water discharge (m^3/s).

To balance stream power, and therefore erosion, with an imposed change in rock uplift, parameters that may be modified with both relative ease and speed from equation [1] are channel width and slope. Through adjusting these parameters, the spatial pattern of erosion within the channel is reorganised to promote faster or slower vertical incision as required. These parameters may continue to be adjusted until a state of equilibrium between rock uplift and vertical incision is established.

Changing spatial patterns of erosion are not only consequences of altered channel morphology, initiated as a response to a change in base level, but may also be products of negative feedback systems initiated by alternative forcing factors. Negative feedback systems may promote changes in channel morphology in order to re-establish equilibrium between channel morphology and the water and sediment they must convey, in response to external perturbations inflicted on natural river systems. The nature of perturbations acting upon river channels in orogenic settings extends beyond direct tectonic forcing, and morphological responses will manifest themselves in a number of ways, and persist for variable time scales. Perturbations which may force a river into a state of disequilibrium, and therefore initiate a morphological response, may also originate from a change in discharge, sediment supply or sediment calibre (Leopold and Maddock, 1953; Knighton, 1998; Holbrook and Schumm, 1999; Finnegan *et al*., 2005; Finnegan *et al.,* 2007; Whittaker *et al*., 2010; Yanites and Tucker, 2010). It is therefore important to identify the cause of morphological responses in tectonically active regions.

Traditionally the response of alluvial channels to tectonic perturbations has received greater attention than the response of bedrock channels within existing literature (Ouchi, 1985, Schumm *et al*., 2000, Holbrook and Schumm, 1999). Responses within alluvial channels are closely observed in controlled flume experiments, allowing for a greater understanding of the processes initiated in both space and time. More recent work by authors such as Finnegan *et al.* (2005) and Yanites and Tucker (2010), has focused on the morphological response of bedrock channels to tectonic perturbations using both flume experiments and field observations, and produced a very distinct set of conclusions. For this reason, the morphological responses within alluvial and bedrock channels to tectonic uplift shall now be considered separately.

1.2 The response of alluvial channels to tectonic perturbations

It is anticipated that in alluvial uplifted regions with reduced channel slope (either over growing folds or upstream of active faults), a loss of stream power will occur which should promote sediment deposition and storage (Holbrook and Schumm, 1999). This in turn should produce wider, shallower channels, with an increase in braid index and number of braid bars within alluvial channel reaches (Figure 1.2). Grain size is also a common proxy for identifying areas experiencing tectonic uplift (Holbrook and Schumm, 1999). In theory, there should also be an increase in bed grain size immediately upstream of either the fault (assuming dip-slip faulting) or axis of maximum rock uplift rate (Figure 1.1) reflecting a decrease in stream power (Holbrook and Schumm, 1999) and in the ability of the river to mobilise larger particles from the channel bed. As the river passes over the region of maximum rock uplift rate, relative channel slope increases allowing for a greater stream power and vertical erosion of aggraded sediment, resulting in a narrower channel with a lower width-depth ratio.
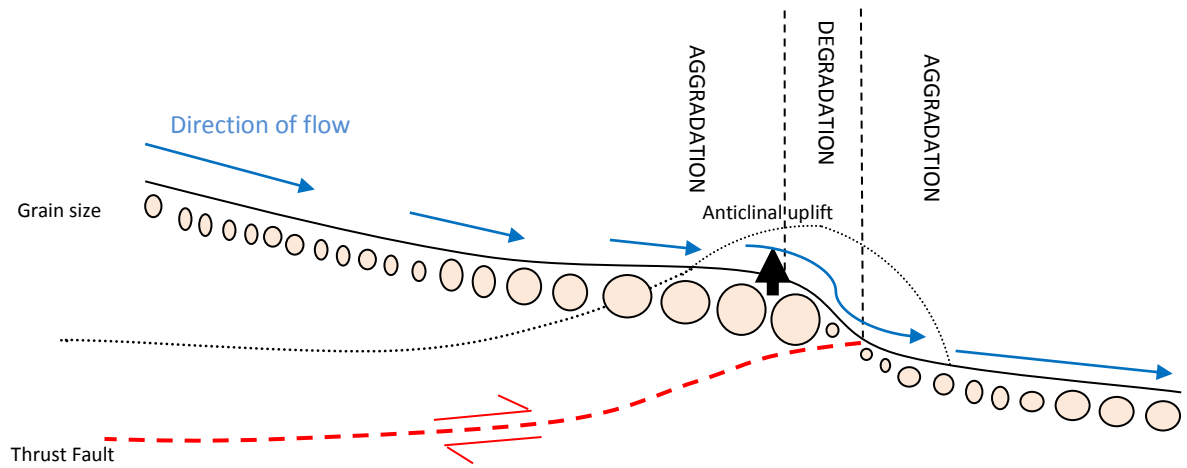
Figure 1.1 *Cross sectional view of a river passing over a region of rock uplift. Changes in grain size are also shown to correspond to variations in channel slope. Around the region of maximum uplift, the river incises into the bed.*
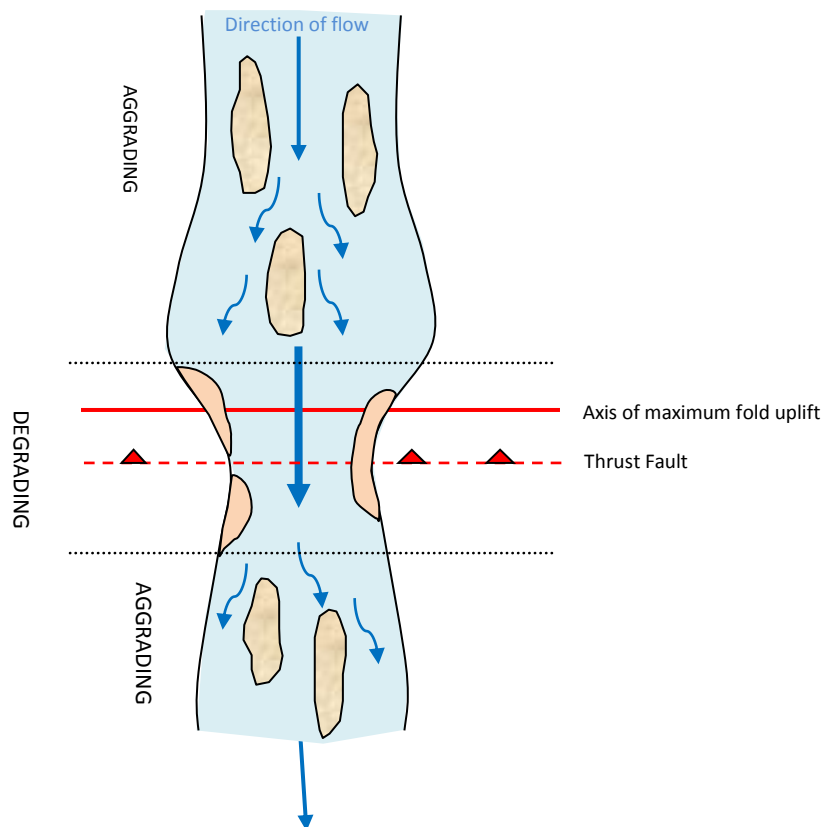
Figure 1.2 *Plan view of an alluvial-mantled channel flowing over a region of rock uplift. The thickness of the flow arrows also indicate the depth of flow. As the river flows over the region of maximum rock uplift the channel narrows, forming alternate bars, and incises where slope is locally increased. Upstream and downstream of this zone, the channel widens and flow becomes shallower with an increase in bar formation.*

Meandering alluvial channel experiments have demonstrated increased thalweg sinuosity on the downstream side of uplifted regions, where slope becomes locally steepened (Ouchi, 1985). On the upstream side of the same series of experiments by Ouchi (1985) where slope was locally reduced, flow velocity has slowed and the thalweg pathway diminished. In comparison, uplifting braided channels were also modelled and key responses observed included aggradation and the development of multiple thalweg channels upstream of the uplifted area, and a steeper degrading channel with a singular thalweg and alternate bars on the downstream side. Therefore the response of alluvial channels to tectonic perturbations will vary depending on existing channel patterns. However, channel patterns are also a function of flood peaks, mean discharges and types of sediment load (Holbrook and Schumm, 1999), so to determine if channels are responding to tectonic perturbations, the influence of changes in these other variables must be considered. For example, a change in discharge may promote a response in channel width, depth or velocity, as shown with simple power functions (Leopold and Maddock, 1953):

$$W = aQ^b \qquad [2]$$

$$D = cQ^f \qquad [3]$$

$$V = kQ^m \qquad [4]$$

where D is depth (m), Velocity is V (m/s) and a, b, c, f, k, and m are empirical constants. It has been widely shown that b is ~0.5 for alluvial rivers, as seen in a number of studies summarised in Knighton (1998).

Where changes in sediment load may occur during more regular peak flows or floods, there may be insufficient time for slope to adjust (Leopold and Maddock, 1953) to produce the greater flow velocity needed to transport increased sediment loads, and so the channel must rely on other variables (e.g. roughness, width) to accommodate it. This can be shown in Manning's Equation whereby multiple factors are related to flow velocity:

$$V = R^{2/3} S^{1/2} (1/n) \qquad [5]$$

[where R= hydraulic radius (m) and n= roughness coefficient]

1.3 The response of bedrock and mixed bedrock-alluvial channels to tectonic perturbations

Finnegan *et al*. (2005) redefined traditional hydraulic scaling laws for the steady state width of bedrock channels. Previous bedrock incision models commonly assume channel width (W) as a power law function of discharge (Q) as seen in equation 2. In regions of spatially non-uniform rock uplift rates, Finnegan *et al*. (2005) concluded that discharge-derived width scaling laws (e.g., eq. 2) do not hold true within bedrock channels and proposed an expression incorporating channel slope (S), roughness (n) and width-depth ratio (α):

$$W = \alpha \, [(\alpha + 2)^{2/3}]^{3/8} \, Q^{3/8} \, S^{-3/16} \, n^{3/8} \qquad [6]$$

Scaling channel width as a sole function of discharge fails to incorporate steepened channel reaches with elevated stream power, which favour vertical incision thus producing a narrower channel. Equation [6] as derived by Finnegan *et al.* (2005) accommodates for narrowing of channels in reaches with elevated slope, such as regions experiencing high rates of rock uplift, or more resistant lithologies. This relationship is demonstrated to only hold true where width-depth ratios and roughness factors are constant down the channel. With the introduction of sediment into the bedrock channel, the validity of this scaling relationship requires reassessing. Theoretically, natural channels should be able to adjust their width to accommodate changes in sediment supply (Yanites and Tucker, 2010). Where alluvial cover is locally increased in mixed bedrock-alluvial channels, vertical incision is reduced. In order to maintain the same rate of vertical incision, erosion is focused on channel walls to increase channel width and therefore the surface area of the channel bed available to incise. In cases where alluvial cover is thicker or more extensive, the channel is forced to steepen to increase stream power, and therefore its erosive potential (Figure 1.3) to maintain vertical incision rates equal to the imposed rock uplift.

With increasing sediment loads, the relationship between channel width and slope is shown to steepen (Yanites and Tucker, 2010). At moderate to high erosion rates, a greater change in channel width than slope would be expected in response to increased sediment supply. At the same time however, with increased discharge levels, the effect of sediment load on channel width is reduced (Yanites and Tucker, 2010). Similar findings were also achieved by Hartshorn *et al.* (2002) on the LiWu River (Taiwan) whereby valley lowering was thought to be driven by frequent and modern intensity flow, with peak flow events having a greater control on channel width. Abrasion by sand and finer suspended materials contributed to maximum levels of erosion during moderate flow events in the LiWu River, in addition to less frequent impacts by saltating boulders along the bed. Therefore, both discharge and sediment yield are found to be key in setting bedrock channel geometry in this particular setting.
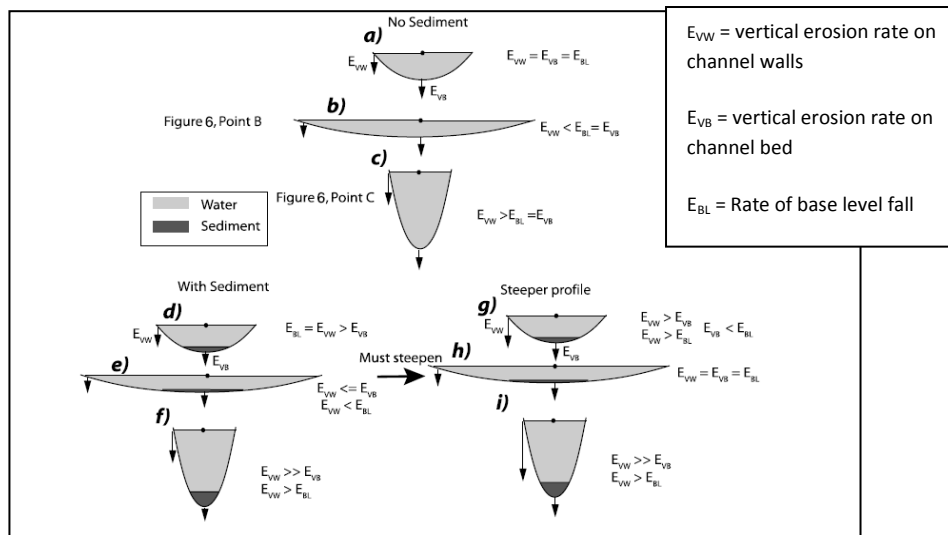
Figure 1.3. *Source: Yanites and Tucker (2010). The presence of sediment can drastically alter the geomorphological response of bedrock channels to an imposed erosion rate.*

Lave and Avouac (2000) demonstrated significant differences in channel slope between the Bagmati and Bakeya Rivers in the Himalayas of central Nepal, despite both passing over the same frontal fold axis. These differences were originally attributed to differing drainage areas and stream power. Essentially it was argued that the larger Bagmati River maintained a more consistent gradient as it passed over the fold unlike the Bakeya, which displayed a steepening profile on the downstream side of the fold. Interestingly, Yanites and Tucker (2010) concluded that the Bagmati River showed minimal change in slope as was able to adjust its shear stress almost entirely through changes in channel width, to maintain rapid erosion rates. The Bagmati also has a significantly larger sediment load than the Bakeya, which in keeping with the model in Yanites and Tucker (2010), should produce a steeper relationship between channel width and slope (Figure 1.4). Amos and Burbank (2007) noted abrupt channel narrowing about the active Ostler fault system in New Zealand. Above a particular uplift threshold, channels were then required to steepen in addition to narrowing to maintain the same levels of vertical incision. Rom these examples, it is apparent that the rate of imposed uplift, stream power and sediment load are crucial in determining morphological responses to rock uplift.
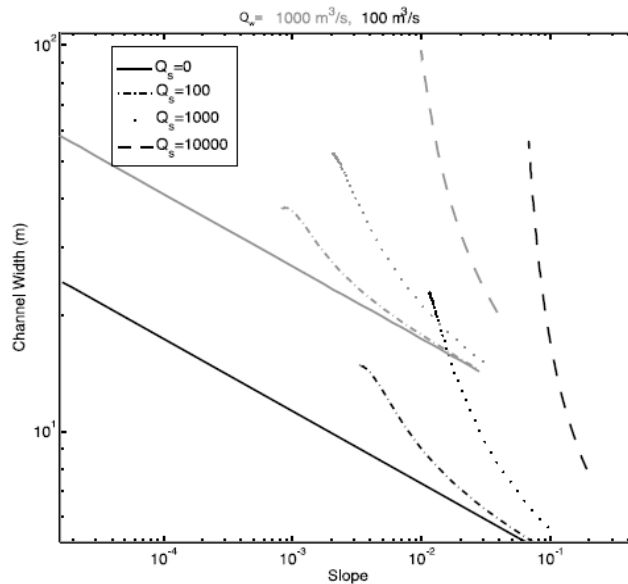
Figure 1.4. *Relationship between channel width, slope and sediment supply (Q_s) shown for two different discharge values (source: Yanites and Tucker, 2010). As sediment supply increases, the relationship between slope and channel width steepens away from a linear scaling relationship as seen in sediment free channels and discussed by Finnegan et al. (2005).*

Other issues were raised by Whittaker *et al.* (2007) and Whittaker *et al.* (2010), where it was noted that bedrock river channel morphologies in the Central Apennines are responding transiently to periods of increased fault movement. In this instance, traditional hydraulic scaling laws relating channel width to drainage area or discharge are also lost. Particular characteristics of regions undergoing transient responses to elevated fault slip rates include over steepened reaches (long profile convexities), narrower valley widths and increased coarse fraction grain sizes. Fluvial systems that have undergone base level drops are reported to contain knick points which migrate across systems whilst within a transient state (Wobus *et al.*, 2006a). Geometric analysis by Kirby *et al.* (2007) suggested that fluvial systems that respond to changes in boundary conditions as a kinematic wave will produce straight forward transient responses with constant vertical knick point velocities. Where thresholds concerning sediment flux and transport stages exist and are exceeded, the transient response is likely to be complex with diffuse changes in channel gradient or over-steepening of reaches downstream of knick points. Observed channel geomorphology may therefore depend on numerous factors. The speed at which channels respond to perturbations may also dictate channel geometry or longitudinal profiles, as channels may have not yet re-achieved a state of equilibrium or 'steady-state'. Overall catchment response times to tectonic perturbations have been shown to be in excess of 10^6 years (Whittaker *et al.*, 2007). Measurements taken across channels undergoing transient responses to alterations in the rate of tectonic uplift may vary from those taken from the same channel after it has re-established to steady state. If width were to adjust faster than slope to a tectonic perturbation, initial measurements may indicate that channel width alone has altered to

7

accommodate variations in erosion, neglecting possible slower alterations in slope. The time scales at which responses manifest themselves in landscapes must also be appreciated when examining morphological variables.

1.4 Sediment storage and recycling in the Himalayas

Recent work by Granet et al. (2010) on trans-Himalayan Rivers suggested a difference between coarse and fine-grained sediment end member transfer times, and transfer histories, based on Uranium series isotope disequilibria in suspended and bed load sediments of the Gandak River. Despite both end members originating from the Himalaya Range, the longer transit times (>100 ka) displayed by the coarse-grained end member, sampled on the alluvial plain and close to the Ganga confluence, were attributed to a larger sediment residence time implying that the sediment had undergone temporary storage, possibly within the Gandak floodplain. Time estimates for fine-grained end members to transfer from the High Himalayas to the Gandak-Ganga confluence are given as ~23-27 ka. As further noted by van der Beek *et al.* (2006) unusually old AFT ages within the present Karnali River sediments downstream of the Siwalik Hills (~300 km west of the Gandak) indicate recycling of sediments across the Sub-Himalayas. This infers that the intermittent storage and release of sediments within the Sub Himalayas may play an role in Himalayan River sediment dynamics.

Intermonate or 'Dun' valleys are ideal sites within the Sub-Himalaya for storage of large quantities of sediment. The Siwalik Hills represent the southernmost topographic front of the Himalayan orogen, and are products of intense deformation along the Himalayan Frontal Thrust (HFT) (Lave and Avouac, 2001; Kimura, 1999). The HFT is a east-west trending thrust fault which separates the Siwalik Hills from the Indo-Gangetic Plain to the south. At present, the Siwalik Hills are undergoing uplift at an exceptionally high rate of ~10-15 mm/yr (Lave and Avouac, 2001) due to accommodation of a large proportion of Himalayan shortening on the HFT. It is believed that thin-skinned thrust faulting and fault-propagation folding of foreland basin sediments in the hanging wall of the HFT during the last 1.6 Ma (Valdiya, 1998) formed the Siwalik Hills and the intermonate valleys or 'Duns' separating the hills (Lave and Avouac, 2000, Lave et al., 2005). It is speculated that Duns form as a consequence of the style of tectonic deformation and sequencing of faulting initiated during early basin development (Simpson, 2010).

Prior to thrusting of the Siwalik Hills (Mid-Miocene), the Siwalik Basin (Himalayan foreland) contained large quantities of eroded Higher and Lesser Himalayan crystalline rocks (primarily schist and gneiss), exported by tran-Himalayan river networks. This coarse and more resistant fraction then became incorporated as weak, poorly-lithified sedimentary deposits within the now-uplifted Siwalik Hills. The lithologies that underlie the Siwalik Hills are generally described as claystones, siltstones and weakly-consolidated conglomerates which have

undergone locally intense deformation (Lave and Avouac, 2000; Singh *et al.*, 2001; Thakur and Pandy, 2004).

The development of foreland basins such as the Siwalik Basin is strongly modulated by the strength of the basal decollement as shown by Simpson (2010). Differences in the viscosity of the detachment may strongly affect patterns of deformation and fault activity across foreland basins. As can be seen in the results of Simpson (2010) in Figure 1.5, foreland basins may segment into series of smaller 'piggy-back' basins where they evolve above thin, low viscosity detachments creating large areas of accommodation within the foreland basin (model r8). Activity on tectonic structures within the basin is also sporadic. In contrast, where cover sequences are compressed over strong detachment planes it is noted that deformation remains focused on the outermost structure and at a more continuous rate (model r1).
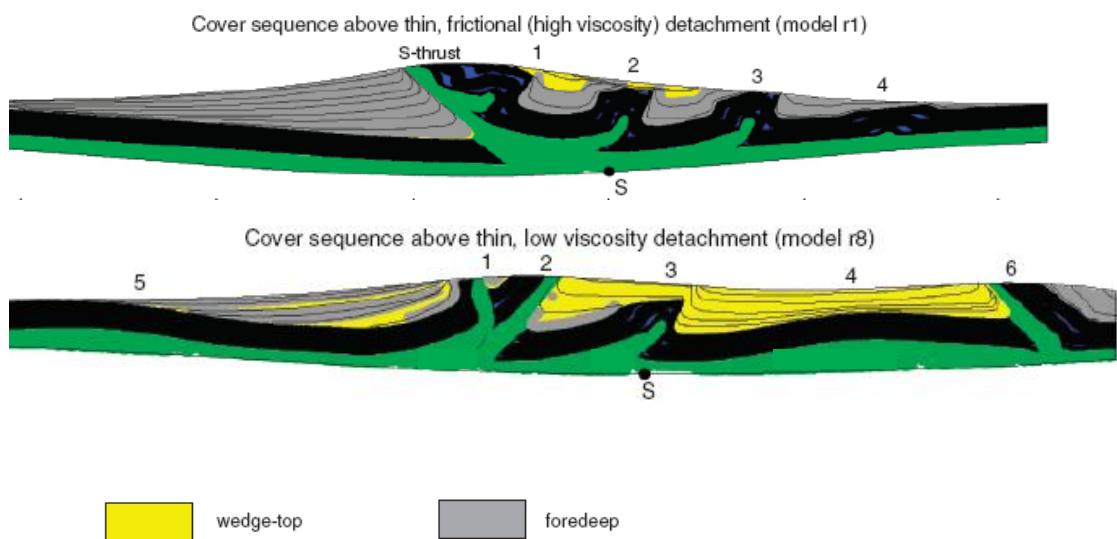
Figure 1.5 *Model run results from Simpson (2010) after 30 % shortening on experiments using different mechanical behaviour (strength of decollement). The decollement is represented by the green layer, whilst the cover sequence is represented in black. The upper image represents a scenario with a strong basal detachment producing focused deformation about the outermost thrusts. The lower image represents shortening over a weaker basal decollement producing a more complex series of piggy-back basins above the fold-thrust belt, with deformation distributed over a larger area of the foreland.*

Piggy-back basins, in the instance of model r8 in Figure 1.5, are likened to Duns by a number of sources (Kimura 1995, Kimura 1999, Singh *et al.*, 2001) which characterise extensive areas of the Himalayan foreland. Using the findings of Simpson (2010), it can be presumed that foreland basins that have developed in this manner should display different characteristics to those formed over strong basal detachments. Foreland basins containing Dun valleys should therefore

provide accommodation for large volumes of erosional detritus from the adjacent rising orogen. It would be expected for the foreland to be characterised by lower relief as a result of distributed deformation and sporadic activity on tectonic structures. In such circumstances deformation is divided across multiple structures over a larger distance, and sporadic fault movement also produces more intermittent sediment production than that of basins without Dun valleys. Where Dun valleys are absent, deformation should be focused on the outermost structure producing high relief (as a result of higher rates of rock uplift above individual faults) and a more continuous sediment output as a result of more regular sediment production and a lack of foreland accommodation. Based on the findings of Simpson (2010), it would be expected for catchments containing Dun valleys to have a lower sediment load than those without.

The low relief of the Siwalik Hills is presumed to limit sediment input into fluvial networks which can be generated by physical erosion, and Singh *et al.* (2008) assume that sediment input from these deformed Neogene molasse deposits (Lave and Avouac, 2001) has been minimal. However, with the high rock uplift rates estimated for this area, and the rapid down cutting of rivers crossing the region in response (Lave and Avouac, 2001), a large volume of sediment must have been eroded to maintain this low relief. Modern estimates place existing relief to represent ~15 % of the total rock eroded across the Siwalik Hills since faulting initiated (Barnes *et al.*, 2011). The erosion of Siwalik sediment has resulted in the rapid accumulation of conglomerate within Duns in low relief areas of the Siwalik Hills.

For simplicity, if it is assumed that the Siwalik Hills are composed of Neogene sediments, then overlying sediments with the Duns must be of at least the same age or younger. Therefore, the upper Dun fill should comprise upper Neogene or Quaternary sediments. However, these upper Neogene or Quaternary sediments within the Duns are likely to contain large quantities of ancient re-eroded (or 'recycled') Lesser and Greater Himalayan crystalline sediments (Szulc *et al.*, 2006). Initially, these recycled sediments would have been exported from the rising Himalayas and deposited in the foreland prior to the Neogene. They then would have been incorporated and uplifted into the Siwalik formations and eventually re-stripped from the uplifted Siwalik Hills by Quaternary fluvial erosion, and finally redeposited in the Duns during the late Neogene and Quaternary periods. This then presents the possibility that these recycled deposits are now being remobilised again by present-day fluvial incision of tributaries traversing the Dun surface, and redeposited into the modern River. Petrology studies by Tamrakar *et al.* (2008) revealed a significant proportion of recycled sediments within Rapti River sands within the Hetauda-Chitwan Dun basin in central Nepal (Figure 1.6), which supports this theory.
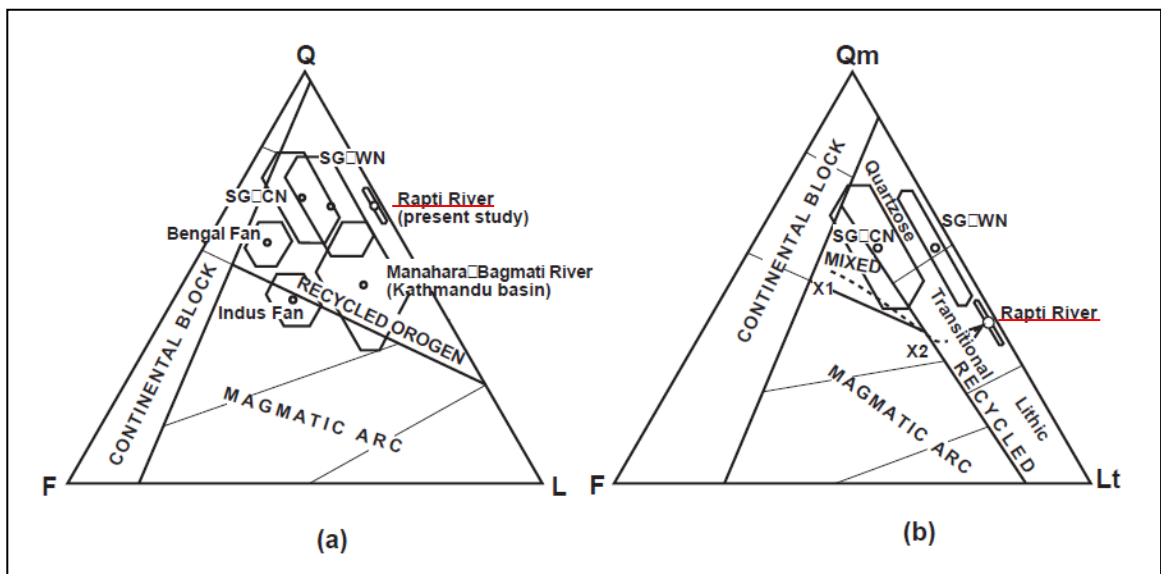
Figure 1.6. *Recycled orogeny provenance field plots displayed in an (a): Quartz (Q), Feldspar (F) and Lithic fragment (L) triangle diagram and (b): Monocrystalline quartz (Qm), Feldspar and Lithic fragment + polycrystalline quartz (Lt) triangle diagram (source: Tamrakar et al., 2008). As can be seen in both triangle diagrams, the Rapti River sands are classified as from a recycled orogen provenance field with a high quarto-lithic composition. One explanation given to explain this high quartz content (and increase in quartz roundness further downstream) is the incorporation of recycled quartz derived from Siwalik and Dun deposits.*

This further raises the question as to if, and how, an input of recycled Himalayan sediment from the Siwalik Hills could influence modern river morphology. As noted by Attal and Lave (2006), sediment source characteristics can exert strong controls on the evolution of river sediments. This can be in the form of differing abrasion coefficients of natural lithologies, or the particle size and size distribution of hill slope sediment supply. It is possible that a significant recycled sediment contribution could affect channel roughness and grain size distribution.

1.5 The Kosi and Gandak Rivers
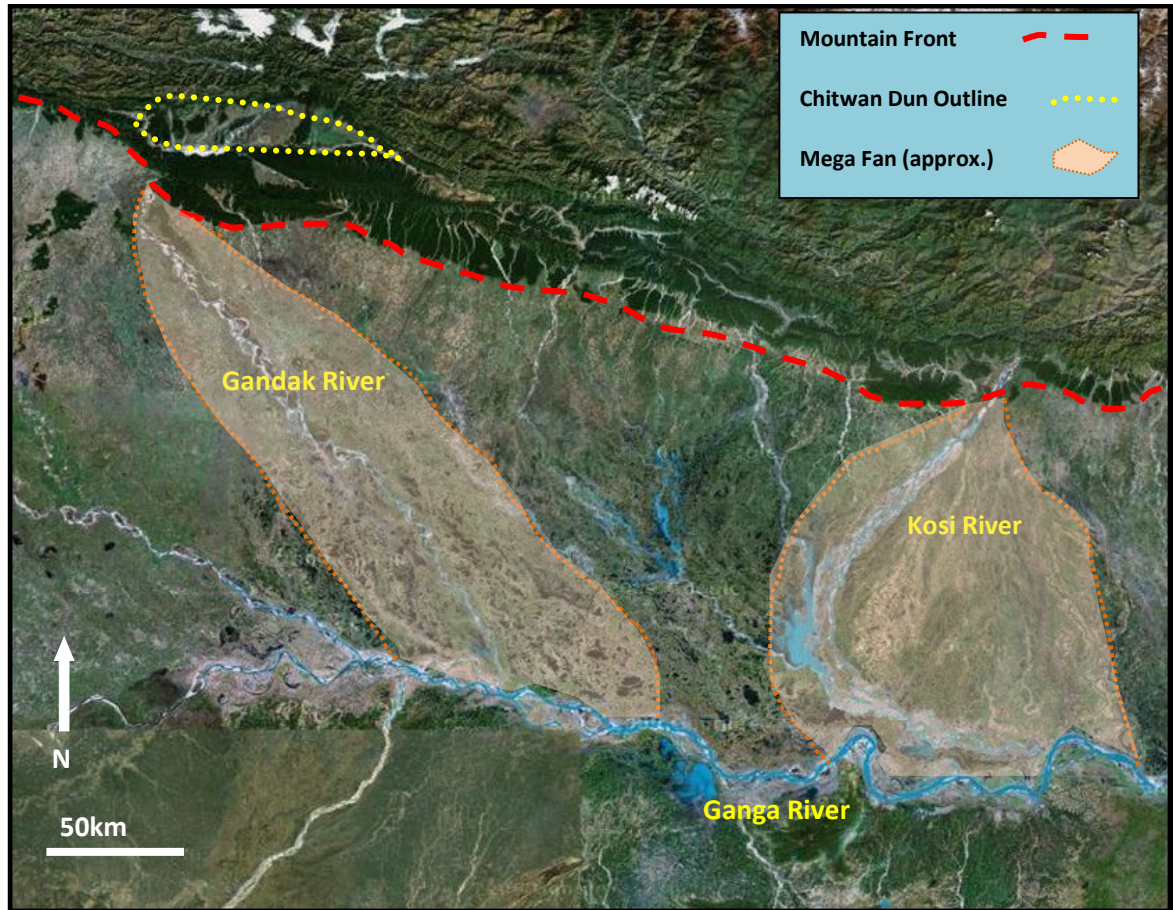
Figure 1.7 *Google Earth image of the Gandak and Kosi Rivers exiting the Himalayan mountain front (Siwalik Hills) and crossing the surface of their respective sediment mega fans prior to joining the larger Ganga River system.*

The Kosi and Gandak trans-Himalayan rivers are both classified as mountain fed rivers (Sinha and Friend, 1994; Jain and Sinha, 2003; Tandon *et al.,* 2006) originating from regions deep in the Himalayas and characterised by high relief and precipitation. Both the Kosi and Gandak Rivers are comparable in their large annual discharges (1792 and 1555 cumecs respectively) and high modern sediment loads in excess of 80 Mt/yr (Jain and Sinha, 2003). In both cases, vast sediment fans have also developed on entering the East Gangetic Plains, where topographic gradients are considerably reduced prior to joining the larger Ganges River system (Figure 1.7). Trans-Himalayan Rivers evolve from largely bedrock to alluvial channels on exiting the mountain front where huge quantities of deposited erosional detritus have formed these vast sediment fans (Figure 1.7). Transitions from bedrock to alluvial channels occur where total sediment supply is equal to or greater than the transport capacity of the channel. Abrupt transitions are most common where steep mountain rivers emerge onto plains with significantly reduced slopes (Ferguson, 2003) which initiate a reduction in shear stress and stream power. This causes the river to deposit its load, in this case the vast quantities of detritus stripped from

the rising Himalayas, as the sediment supply exceeds the transport capacity of the channel. The preferential entrainment of finer grained material causes a rapid downstream fining in bed load, until the river bed composition is entirely sand. The East Gangetic Plains (EGP) are characterised by aggrading river systems, such as the Kosi and Gandak, with high sediment yield and low unit stream power in rapidly subsiding areas proximal to active thrust faults. For comparison with the West Gangetic Plains, unit stream power in the EGP is given as 6-20 W/m^2 in comparison to 40-43 W/m^2 in the West (Jain and Sinha, 2003).

On exiting the Lesser Himalayas and passing through the Sub Himalaya onto the Gangetic Plains, the fluvial morphological signatures of these rivers diverge. The Gandak is characterised by more consistently braided channel patterns whilst the Kosi is observed to change systematically between a braided, straight and finally meandering pattern by ~160 km downstream of the mountain front (Jain and Sinha, 2003). Recent studies using Sr and Nd isotope tracing have highlighted a massive contrast in contemporary sediment flux and catchment erosion rates between the Kosi and Gandak rivers and catchments (Singh *et al.,* 2008). Whilst the Kosi sediment flux and erosion rates are given as 60-130 Mt/yr and 1 mm/yr respectively, the Gandak produces significantly higher values at 450-510 Mt/yr and 6 mm/yr.

Increased sediment supply within channels has demonstrated to strongly influence channel pattern through bar development and braiding (Frostick and Jones, 2002) so it is possible that this contrast in sediment supply between the Kosi and Gandak is responsible for the difference in channel patterns. Based on annual Sr and Nd isotopic measurements of bed material, the annual contribution of the Gandak River during 2003-06 to the Ganges mainstream sediment load is estimated at over 50 % despite the Gandak catchment covering only a minor (5 %) area of the Ganges catchment. The larger Kosi catchment (8 % of the Ganga catchment) has a minor contribution, estimated at ~6 %, to the total Ganga sediment fraction. This raises two important questions: (1) where is this additional sediment sourced from, and (2) does this sediment initiate a morphological response in the Gandak River?

The Gandak River presents an ideal situation to investigate whether sediment storage and release from the Sub-Himalayas influences channel morphology. Prior to exiting the Himalayan mountain front, the Gandak flows into the Chitwan Dun as identified on Figure 1.7. The positioning of the Gandak River and the Chitwan Dun thus presents an ideal situation to undertake research building on findings by both Singh *et al*. (2008) and Simpson (2010) to establish to why observed morphology differs from modelled outputs. Based on conceptual tectonic assumptions (Simpson, 2010), it would be expected for the Gandak to have a lower sediment load than the Kosi. However, results from Singh *et al*. (2008) suggest the exact opposite based on contemporary sediment yields within the Gandak catchment, which contribute over 8 times the amount of sediment than the Kosi to the Ganga sediment load for at

least the 2-year study period (2004-06). Sediment stored within the Dun may contribute a fraction of itself into the Gandak River sediment load due to incision by tributaries crossing the Dun surface. As noted by Attal and Lave (2006), sediment source characteristics can hold a strong influence on the evolution of river sediments so it is important to consider how this freshly eroded 'recycled' fraction from the Dun could potential influence the characteristics of the Gandak River sediment load and deposits. Intermittent climatically driven erosion as noted by Tandon *et al.* (2006) and Suresh *et al.* (2002) initiated after the Last Glacial Maximum, may explain the exceptionally high sediment loads of the modern Gandak River. The Kosi River shall provide suitable control due to an absence of Duns within its catchment, yet is characterised by similar discharge values, catchment size and climatic conditions allowing for a direct comparison to the Gandak River.

1.6 Research Hypothesis

Whilst previous studies have focused separately on the dynamic interaction of Himalayan rivers and their sediment fans in the Gangetic Plains (Mohindra *et al.*, 1992; Singh *et al.*, 1993; Chakraborty *et al.*, 2010), and the effect of active tectonics on Himalayan river profiles (Seeber and Gornitz, 1983; Hodges *et al.*, 2004; Montgomery and Stolar, 2006; Robl *et al.*, 2008), few have considered the controls on trans-Himalayan river morphology, especially as the rivers exit the mountain front. Little is known as to how Himalayan rivers adjust their morphology in response both to downstream and along-strike variations in rock uplift rates, and to patterns of sediment input from the Siwalik Hills.

The following hypotheses are therefore raised:

H1: Channel geometry of trans-Himalayan rivers is a function of active tectonic structures

H2: Grain size distributions coarsen as trans-Himalayan rivers exit the Himalayan mountain front as a result of active tectonic structures

Morphological comparisons shall be achieved by combining channel width and channel gradient data from remotely sensed data sources down a defined reach of each river. The Gandak reach will span from ~5 km upstream of the Main Boundary Thrust (MBT) to 5-10 km downstream of the Himalayan Frontal Thrust (HFT), and the Kosi reach from ~5 km upstream of the Main Central Thrust (MCT) to ~5-10 km downstream of the HFT. These limits have been chosen as cover the main foreland tectonic structures, which will allow examination of channel morphology (primarily width and slope) with respect to the structures within each reach. The geographical position of the tectonic structures will be taken from existing literature and compared with field observations where possible. Measurement of the channel bed grain-size distribution will also be undertaken along these study reaches in order to understand the pattern of any variation and its links to the tectonic deformation field or sediment supply of the rivers.

H3: Inputs of recycled Siwalik lithologies from local mass-wasting lead to a coarsening of grain size distribution within trans- Himalayan rivers at the mountain front

H4: Patterns of sediment storage and release within Dun valleys modulate channel morphology to a greater degree than rock uplift at the Himalayan mountain front

Rivers passing through Dun valleys prior to exiting the mountain front demonstrate multiple bedrock-alluvial channel substrate changes. In theory, there should be two gravel-sand transitions where Duns are present in the Sub-Himalaya, in comparison to just one where they are absent. Similarly to entering the alluvial plain, whilst passing into the alluvial Dun it would also be expected for the bar deposits to be dominated by fine grained materials so any coarser local Siwalik inputs should be easily detectable if present.

On entering the Siwalik Hills, an increase in the proportion of local Siwalik lithologies, as opposed to modern Greater Himalayan lithologies is expected within channel and bank deposits. These are likely to be derived from local hillslope failure, or tributary inputs that deliver sediment from the Siwalik Hills into the Dun valley floor. Likewise to findings by Attal and Lave (2006) further upstream on the Marsyandi River, it would be expected for the grain size distributions of these hillslope inputs to be coarser than those of main river deposits that have undergone fluvial sorting and abrasion. Local inputs of eroded Siwalik Hill sediment from a number of tributaries may influence sediment grain size within the Dun, prior to passing into the bedrock gorge through the frontal HFT anticline. Grain size distributions will be collected in the field to ascertain whether a contribution of recycled Himalayan material, transported by local tributaries, is also present in the modern rivers. If a contribution of re-eroded Himalayan material from the Dun exists, it must be considered how this will be distinguished from present day inputs. Due to time constraints with this project, it will not be possible to conduct geochemical analysis of these sediments, such as those conducted by Singh *et al.* (2008) or Galy *et al*. (1999). However if the input of recycled Himalayan material is present, the coarser resistant crystalline fraction sourced from the Greater Himalayas during its earlier relief building and consequent erosion, should be evident in modern fluvial deposits. If the contribution is great enough, it would be anticipated for there to be an increase in grain size downstream of the confluences of which tributaries crossing the Dun surface meet the main river body.

By using grain size distributions, it may be possible to establish whether Dun valleys (and therefore the loci of sediment production) modulate channel morphology of trans-Himalayan Rivers. If only a minor sediment contribution exists from the Dun, it is likely that the massive sediment load of the river would buffer the Dun signal and therefore it is unlikely that sediment input from the Dun is important. If significant local Siwalik inputs are detectable through grain

size signals however, it would suggest that the input of stored sediment within the Dun is significant in terms of the modern river's sediment load.

1.7 Thesis Structure

After introducing the motivation behind this thesis in this introductory chapter, the following chapter will focus primarily on tectonic frameworks, geology and fluvial morphology on regional and local scales. It will also explain the development and characteristics of major tectonic structures within both the Himalayas as a whole and the study regions. Finally, it will discuss the complexity of Himalayan Dun valley formation and introduce the Chitwan Dun.

The third chapter will be dedicated to the methods that shall be used to test my hypotheses. This will begin by considering remotely sensed data and how it can be manipulated, and follow with techniques to be implemented in the field. The chapter shall then conclude with how the field data will be analysed, and finally consider the errors and limitations associated with each method.

The fourth chapter will present the results acquired from the methods in the preceding chapter. The fifth chapter will allow for discussion of any trends or relationships which may be extracted from the data in the results chapter, and allow for the interpretation of processes which may have produced such results. The sixth and final chapter shall contain conclusions drawn from the discussion, which shall then be related back to the original hypotheses in an attempt to falsify or prove each. This final chapter will also present the opportunity to propose ways to further this research.

Chapter 2: Study Area

2.1 Regional tectonic background

The high relief, seismic activity and rapid surface processes that characterise the Himalayan orogen are a direct product of the continent-continent collision between India and Eurasia, initiated during the period 65-50 Ma (Powell and Conaghan, 1973; Valdiya, 1998; Szulc *et al.*, 2006). The subsequent northward migration and subduction of the Indian continental plate beneath the Eurasian plate has resulted in the accretion of Indian plate material at this boundary, and the initiation of a southward progressing deformational front (DeCelles *et al.*, 1998). The intense exhumation (Szulc *et al.*, 2006) experienced as this deformational front has progressed has resulted in the initiation of numerous thrust faults (Lave and Avouac, 2000) running parallel to the mountain front. Patchworks of chaotically deformed, compressed and displaced geologic masses separated by a series of periodically active thrust fault systems now typify much of the Himalayan orogen. The majority of convergence between India and Eurasia is presently accommodated along the outermost and youngest structure, the Himalayan Frontal Thrust (HFT) (Wobus *et al.*, 2005). Holocene shortening rates of the HFT are estimated at 21±1.5 mm/yr, which has led to focused deformation across the Himalayan foothills at the modern deformational front (Lave and Avouac, 2000).
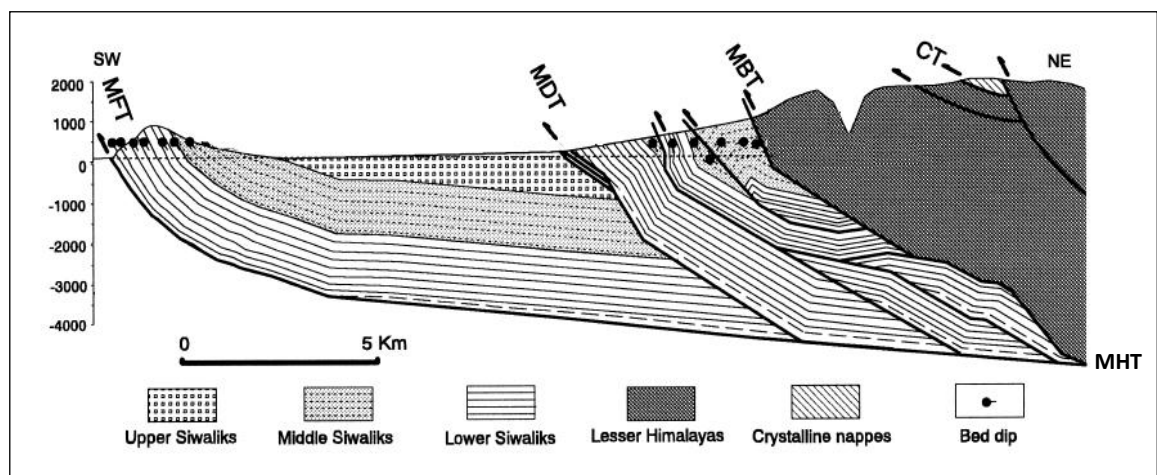
Figure 2.1 *Cross section through the Himalayan foreland with major structures identified. Image modified from Mugnier et al. (1998); based on balanced cross section through the Karnali area, western Nepal. Due to intense deformation about the mountain front, the Main Dun Thrust (MDT) has also developed, and can be seen with the HFT (also known as the MFT) and Main Boundary Thrust (MBT) which are all connected at depth to a basal detachment, the Main Himalayan Thrust (MHT).*

Understanding how differential uplift is accommodated across the Himalayas has proven exceptionally difficult (Wobus *et al.*, 2005; Hodges *et al.*, 2004) with a combination of active

and passive uptake models proposed (Pandey *et al.*, 1995; Bilham *et al.*, 1997; Hodges *et al.*, 2004). Traditional passive uptake models (Bilham *et al.*, 1997; Pandey *et al.*, 1995), relate uplift to movement of rock in the hanging wall over a ramp in the Main Himalayan Thrust (MHT) whereby no active surface breaking north of the HFT is recognized. Hodges *et al.* (2004) presented an active uptake model whereby out-of-sequence thrusting was incorporated to also account for a zone of rapid uplift observed in the Higher Himalaya region. The active model suggested that the zone of rapid uplift resulted from relative movement on the hanging wall blocks of individual faults, attached to the MHT at depth, which extend near to the surface of the Higher Himalaya. In accordance with the active uptake model proposed by Hodges *et al.* (2004), the HFT, the Main Boundary Thrust (MBT) and Main Central Thrust (MCT) are considered to connect to the MHT which is a single detachment, or decollement, at depth (Figure 2.1). There is also the possibility that both models have been valid at different points throughout the Quaternary. Stress accumulation and transfer across the MHT and its attached thrusts is a less well-understood process. It is generally believed from geodetic observations that stress accumulates elastically beneath the MCT/Higher Himalaya and is periodically released via a slip pulse along the MHT, ultimately being registered as permanent displacement on the HFT (Wesnousky *et al.*, 1999; Lave *et al.*, 2005).

2.1.1 Activity of tectonic structures within the Himalayan foreland

The HFT, the youngest of the major thrusts attached to the MHT, has been seismically active throughout the Quaternary period. Further north, the MBT is presumed to have been activated at ~10 Ma (Meigs *et al.*, 1995) based on dated stratigraphic units and apatite fission-track ages, but was then succeeded by the HFT system during the Quaternary. Episodic seismic events reveal that much of the slip along the HFT occurs intermittently through large magnitude earthquakes (Pandey *et al.*, 1995; Kayal, 2001; Jouanne *et al.*, 2004; Lave *et al.,* 2005), such as the Medieval event (M_w ~ 8.8) presented by Lave *et al.* (2005). Earthquakes associated with blind faulting are thought to contribute to permanent deformation of frontal fold structures, despite a lack of surface rupture (Lave *et al.*, 2005).

The HFT is laterally discontinuous along the Himalayan foreland due to the production of imbricate fans and splay branches formed off each main thrust (Mugnier *et al.*, 2005). Additionally, an oblique component to the India and Eurasia collision (McCaffrey and Nabelek, 1998; Jouanne *et al.*, 1999) results in inconsistent uplift rates across the length of the HFT. It may therefore be expected for the magnitude of uplift accommodated by the HFT to vary across the Himalayan foreland. Networks of laterally less extensive faults have also formed off the MBT, which branch off and run parallel to it. One example is the Main Dun Thrust (MDT), which developed as a result of ongoing compression and crustal deformation initiated during the Himalayan orogeny (Figure 2.1).

Mugnier *et al.* (2005) presented evidence for displacement in the order of 3.5-8 m and 2-3 m in excavated trenches above the surface rupture of the HFT and MDT respectively, as a result of episodic slip across the shallower part of the MHT decollement surface during large magnitude Quaternary earthquakes. This also highlights a difference in shortening rates between the faults as a result of differential uplift. Holocene shortening rates are given as 14 mm/yr and 4 mm/yr for the HFT and MDT respectively (Mugnier *et al*., 2003). The larger shortening rate across the HFT reflects the focusing of seismic events at this location, and the presence of fault scarps in the Dehra Dun region (Wesnousky *et al*., 1999) suggests that earthquakes of magnitudes greater than M ~8, which have been of sufficient size to rupture the ground surface above the HFT, have also occurred. Mugnier et al. (2005) also considered evidence for recent activity along the MBT, which is thought to occur in the order of ~1 mm/yr suggesting that the magnitude of activity along the MBT is at present much lower than that of either the MDT or HFT. Lateral variability in uplift rates along these major frontal structures is also reflected in a lack of reliable records of major seismic events since the 1200's in western Nepal, resulting in it being considered to lie within a seismic gap (Mugnier *et al.*, 2005). This lack of documentation should not eliminate the possibility of unrecorded events however.

2.2 Geological background of the Himalayas

The Nepalese Himalaya is classified into four major geographic regions or bands based on geological features and characteristics. A geological map is provided in Figure 2.2.

2.2.1 The Sub-Himalayas and the Siwalik Hills

The Sub Himalayas lies between the Lesser Himalayas and the Indo-Gangetic Plains. The Siwalik Hills represent the youngest and southernmost region of notable topography (<1000 m) on the southern margin of the Sub Himalayas. Dun valleys, formed by thin-skinned tectonics (Lave and Avouac, 2001) associated with Quaternary movement along the HFT, separate the topographic highs of the Siwalik Hills from each other. Sediments composed primarily of the ~ 5000 m thick Siwalik Group underlies the Siwalik Hills. The Siwalik Group dominates much of the Sub-Himalayan stratigraphy (Kimura, 1999). The fluvial deposits of the Siwalik Group are further sub-divided into the Lower, Middle and Upper Siwalik lithostratigraphic units (Bernet *et al*., 2006). Upper Siwalik deposits are constrained to a minimum age of ~0.5 Ma using magnetostratigraphic dating (Thakur and Pandy, 2004), whilst the Middle and Lower Siwaliks are believed to have deposited during two periods each at ~8-10 and 3.5 Ma, and ~15 and 8-10 Ma respectively (Bernet *et al*., 2006). The Upper Siwalik group is then extensively overlain by Late Pleistocene or younger Dun gravels (Singh *et al.,* 2001). The Siwalik Group displays a clear coarsening sequence (Figure 2.3), which was associated by Seeber and Gornitz (1983) to the intensification of the Himalayan orogeny during the Plio-Pleistocene period. Alternatively,

Schelling (1992) attributed the same pattern to the southward migration of the Himalayan topographic front initiated during the middle Miocene.
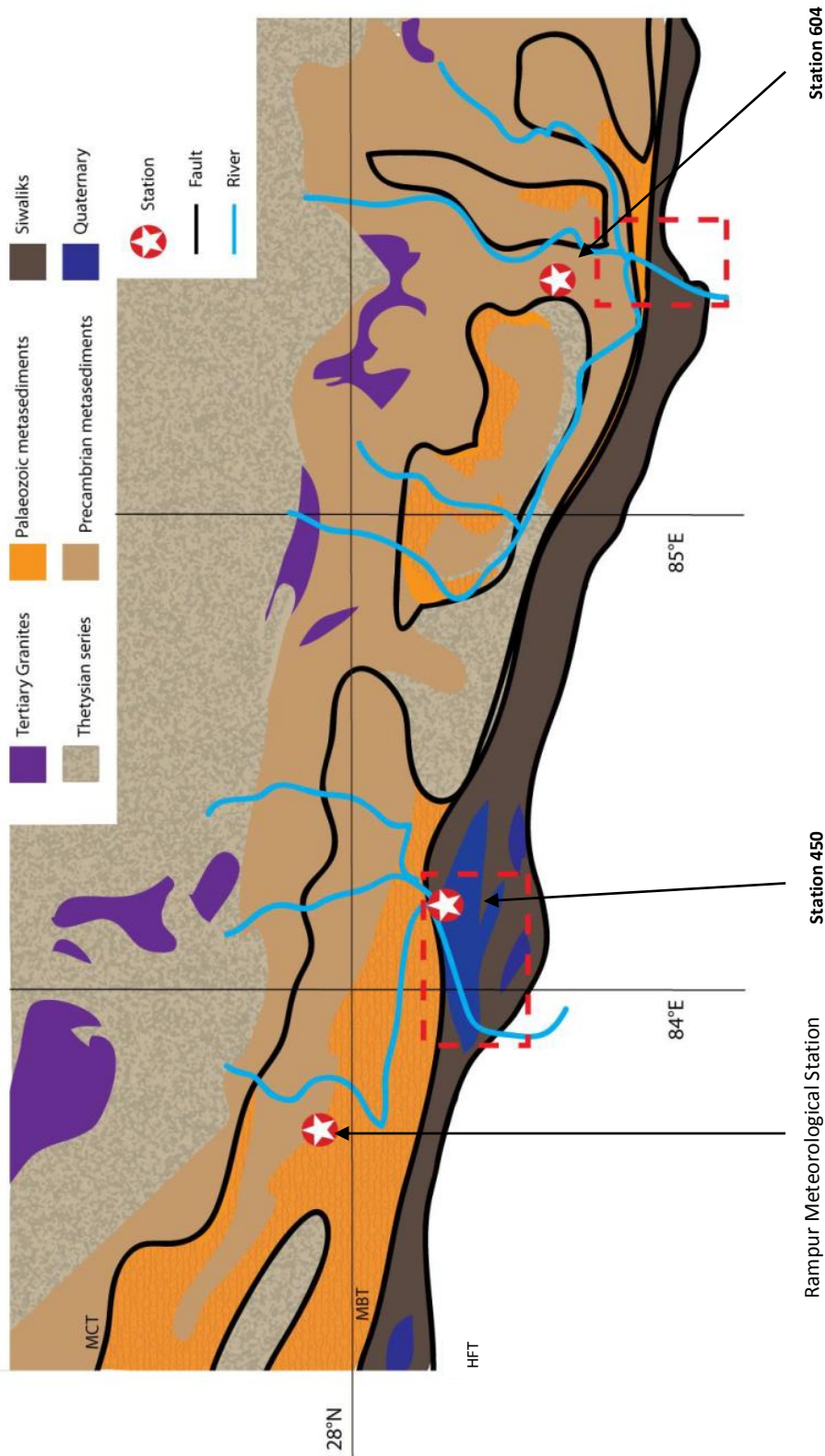
Figure 2.2 *Geological map of the Himalayas, modified from Lave and Avouac (2001). The Gandak (known as the Narayani locally) in the west of this image, and Kosi to the east, are both identified by red boxes. The major tectonic structures and geologic units which they both cross are also identified. Within the study reaches, both rivers cross Precambrian and Palaeozoic metasediments, Siwalik and Quaternary units. Streamflow data has been acquired from stations 450 and 604 for the Gandak and Arun Kosi Rivers respectively, at the locations identified by red and white stars.*

2.2.2 The Lesser Himalayas

To the north of the Sub-Himalaya, the MBT that initiated ~10 Ma (Meigs *et al.,* 1995), marks the transition to the Lesser Himalayas. As presented by Kayal (2001) the seismic activity of the MBT varies across the Himalayas, to the extent that in particular regions, the MBT is not even classified as a seismogenic fault. Substantial earthquakes have been noted below the estimated plane of detachment at 50-80 km depth in north-eastern and eastern Himalayan regions, suggesting that deep-seated hidden faults lie transverse to the MBT that allow for strike-slip movement to occur (Kayal, 2001). North of the MBT, the Lesser Himalayas represent a further increase in topography (2000-3000 m) and the geology is somewhat distinct from that of the Sub-Himalayas. Low-grade metasediments dominate local geology, and may be grouped predominantly as phyllites, gneisses, quartzites with limited granite fractions (Schelling, 1992; Lave and Avouac, 2001). These sediments have also been heavily deformed and compressed in the footwall of the MCT to the north of the region. The extent of compression has been sufficient to overturn and horizontally force folds over each other, producing features known as 'nappes'. These displaced and uprooted folds dominate large areas of the surface of the Lesser Himalaya (Valdiya, 1998). Rock uplift rates within the Lesser Himalaya are found comparable to long-term fluvial incision rates which are estimated at only a few millimetres per year (Lave and Avouac, 2001), in comparison to the much larger long-term rates of the Sub-Himalaya (10-15 mm/yr) and Higher Himalaya to the north (4-8 mm/yr).
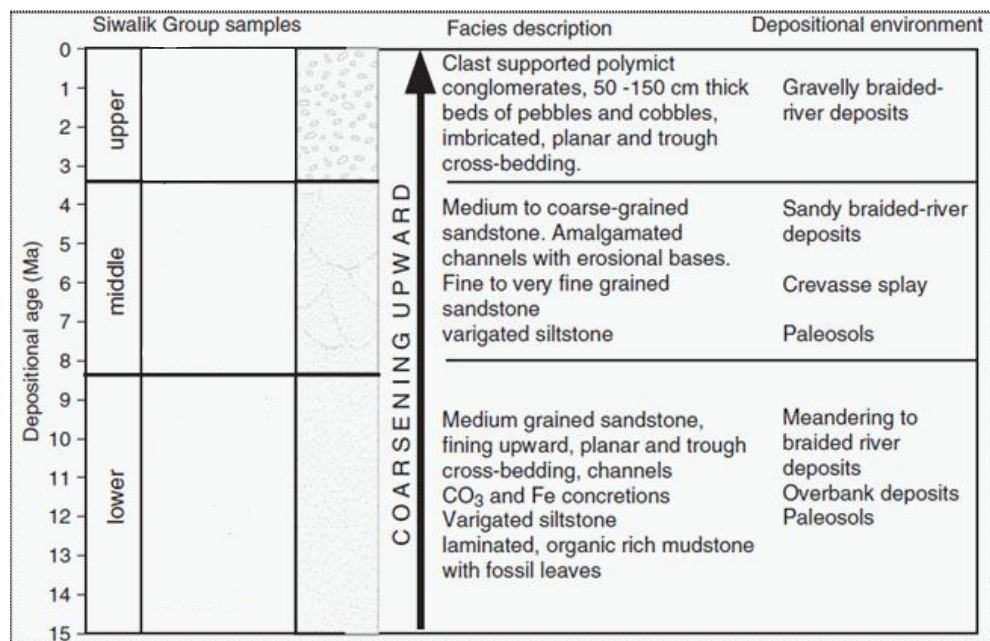
Figure 2.3 *Generalised stratigraphic section of the Siwalik Group in western Nepal modified from Bernet et al. (2006), highlighting the upwards coarsening sequence and contrasts in sediment composition within the Siwalik Group.*

2.2.3 The Higher Himalayas

The transition between the Lesser Himalaya and more northerly Higher Himalaya is marked by the MCT, which is at present presumed to be dormant (Kayal, 2001). Since the initiation of the MCT between 25-15 Ma (Schelling, 1992), north-south horizontal shortening across the eastern Nepalese Himalayan has been estimated between 210-280 km, which was thought to have occurred whilst the MCT was active. During earlier stages of the Himalayan orogeny when the MCT was activated, Higher Himalayan crystalline rocks were believed to have been thrust along the MCT and southwards over the Lesser Himalayas (Schelling, 1992). The lithology of the area is predominantly crystalline and is characterised by high grade metamorphic gneisses, leucogranitic plutons of Miocene origin (Lave and Avouac, 2001) and kyanite-bearing metamorphic rocks (Schelling, 1992). An abrupt physiological change is also notable (Wobus *et al.*, 2005) in the south of the Higher Himalayan region, with uplift rates accelerating to 4-8 mm/yr (Lave and Avouac, 2001), independent to the now inactive MCT. Here, topography in excess of 6000 m is evident but is restricted within a 50 km wide belt running parallel to the mountain front (Lave and Avouac, 2001). It is possible that tectonic thrusting extends close to the surface at the High Himalaya- Lower Himalaya transition to produce these observed physiological changes. This would require accommodation along an unmapped fault attached to the MHT (Hodges *et al.*, 2004). Wobus *et al.* (2005) suggest a gradual ramp in the MHT within the middle crust to explain the distinct change in physiography between the Lesser Himalayas and Higher Himalayas, but struggled to explain why broader changes (such as a more gradual change in landscape morphology) expected with such a ramp have not manifested in the landscape. Wobus *et al.* (2005) eventually reached a similar conclusion to Hodges *et al.* (2004), whereby an unmapped thrust fault (as the MCT is assumed dormant) is thought to accommodate shortening about the isolated belt of rapid uplift.

2.2.4 The Tethyan Himalayas

The Tibetan Plateau extends north of the High Himalayas with elevations in the region of 5000m. It is separated from the Higher Himalayas by a north-dipping, top to the north shear zone (Schelling, 1992) referred to as the Southern Tibetan Detachment System (Van der Beek *et al.*, 2006). The geology of the region is predominantly composed of carbonate and clastic Tethyan sediments (Singh *et al.*, 2008) from the Cambrian-Eocene epoch (Powell and Conaghan, 1973).

2.3 Regional structural evolution: the Siwalik Basin and Dun valley formation

Between 20 and 18 Ma, the MBT broke the Himalayan crust and the region lying directly south of the thrust began to subside (Valdiya, 1998). This resulted in the production of an elongated foreland basin across the southern front of the Himalayas, known as the Siwalik Basin (Valdiya,

1998). The Siwalik Basin would have filled rapidly with erosional products from the rising Himalayan orogen to the north, exported by extensive trans-Himalayan river networks into the foreland. Along the northern margin of the Siwalik Basin, continual movement on the newly emerged fault systems (MBT/MDT) resulted in the production and transfer of eroded sediment into the newly formed Siwalik accommodation. Consequently, sediment within the basin also underwent intensive compression, deformation and folding. Neotectonic activity during the past 1.6 Ma within the Siwalik region has incorporated these weak molasse deposits into the hanging walls of thrust faults, producing positive topographic entities in the form of rows of elongated ridges, now known as the Siwalik Hills. Focused deformation at the orogen front further resulted in the production of an active fault-bend fold on the hanging wall of the HFT, which is also characterised by variable rock uplift rates along strike (Kirby and Whipple, 2001).

The exact evolutionary style of Himalayan Dun valleys, or piggy-back basins, is contentious, with an initial hypothesis based on diachronous evolution as a result of oblique convergence, (e.g. Kimura, 1999), being challenged by the more recent work of Singh *et al.* (2001) and Simpson (2010). Singh *et al.* (2001) suggested that Dun formation was a result of synchronous thrusting on the MBT and HFT in response to Himalayan frontal deformation. Simpson (2010) considered the role of mechanical behaviour of fold-thrust belts and the consequential deformation and sequence of fault activation (Figure 1.5), based on the strength of basal decollement. Where weak basal decollements were included in the model, foreland basins developed into wedge-top basins. These wedge-top basins initiated contemporaneously, but further development occurred discontinuously as deformation failed to remain constant at any one location for substantial periods of time.

By ~0.22 Ma the Siwalik basin had accumulated ~7000 m of sediment (Valdiya, 1998). Singh *et al.* (2008) utilised Sr and Nd isotopes to ascertain sediment provenance of river sediments in the Ganga Basin, concluding that sediment within the Siwalik basin is primarily reworked material from the Higher and Lesser Himalaya crystalline rocks.

2.4 Regional climate, morphology and surface processes of the Kosi and Gandak Rivers

The Himalayan mountain front has a sub-tropical climate with average monthly temperatures ranging annually between 8-35 °C in January and June respectively (taken from Rampur meteorological station between 1995-2006), and more than 80 % of the total annual rainfall falling between June-September during the monsoon season (Neupane and Shrestha, 2009). At Rampur meteorological station, situated ~60 km north-west of Narayangarh (identified on Figure 2.2), annual rainfall for the period 1990-95 is given as 2214 mm (Neupane and Shrestha, 2009).

Monthly streamflow for the Narayani and Arun Rivers for 1976-77

[source: Department of Irrigation, Hydrology and Meteorology for Nepal]
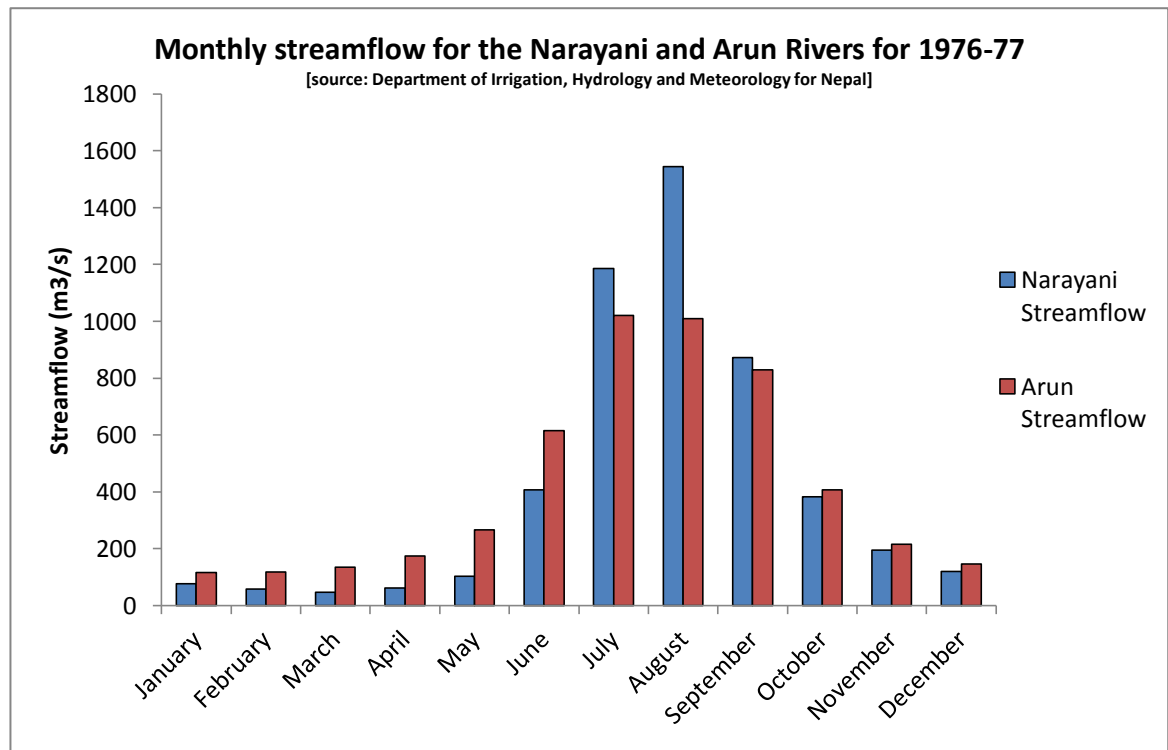
Figure 2.4. *Monthly streamflow data from Department of Irrigation, Hydrology and Meteorology for Nepal (DIHM) averaged for the years 1976-77. Peak streamflow recorded both the Narayani and Arun stations, as identified in Figure 2.2, occurs between June-October, with mean peak flows in those years of 1544 and 1020 m^3/s respectively.*

For the River Kosi, mean annual non-monsoon and monsoon discharges are estimated at 1175 m^3/s and 5156 m^3/s respectively (Sinha *et al.,* 2008), however comparative data from this study for the Gandak are unavailable. The streamflow readings in Figure 2.4 are smaller than these more contemporary values, which may be explained by an inconsistency between methods and sampling locations. Discharge has been recorded and averaged for the period 1985-2002 by Sinha *et al.* (2008), and is taken from the Baltara station near to the Ganga confluence so has a much larger catchment area. Streamflow records collected by the Department of Irrigation, Hydrology and Meteorology (DIHM) for Nepal (Figure 2.4) reflect a monsoon dominated hydrograph across the Narayani (Gandak) and Arun (Kosi) Rivers for only a two-year period.

The Kosi River consists of seven tributaries (the Arun, Sun Kosi, Tamakoshi/Tamba Kosi, Tamur, Dudh Kosi, Indravati and Likhu) and is itself, like the Gandak, a tributary to the larger Ganga River. The Kosi's largest tributary, the Arun, originates inside the Tibetan Plateau. South of the Arun, Sun Kosi and Tamur confluences the Kosi is referred to as the Sapt Kosi. The Gandak River originates from the Nhumbine Himal Glacier at the Tibet border, and is fed by seven Himalayan tributaries (Daraudi, Seti, Madi, Kali, Marsyandi, Budhi and Trisuli). The Gandak then flows south eventually to its confluence with the Ganga River at Triveni.

The headwaters of the Kosi and Gandak Rivers lie in the Tethyan Sedimentary Series of the Tibetan Plateau, which lies within the rain shadow of the Higher Himalaya (Singh *et al.*, 2008). This translates that sediment generated from this region is limited, and therefore erosional products within the modern Siwalik Basin should be dominated by re-eroded Siwalik deposits (from the Siwalik Hills) and modern Greater Himalayan lithologies.

Significant variations in channel patterns and migration styles are notable between the Kosi and Gandak rivers on exiting the Himalayan mountain front. The Kosi River is renowned for its highly avulsive and unstable nature as it crosses its mega fan surface (Wells and Dorr, 1987; Singh *et al.*, 1993; Sinha and Friend, 1994; Sinha *et al.*, 2005, 2008, Sinha, 2008; Chakraborty *et al.*, 2009;). Multiple studies have been conducted on the migration of the Kosi River over its mega fan surface for the past two centuries, and whilst it is observed that the river has undergone a significant migration to the west, the individual stages of this avulsive migration have historically been less well understood. A westward migration of >113 km was noted by Chakraborty *et al.* (2009) during the last two centuries. Early work by Wells and Dorr (1987) characterised the shifts as uni-directional, autocyclic and stochastic because no correlation between avulsions and seismic activity could be noted for the last 200 years. A more recent assessment by Chakraborty *et al.* (2009) hypothesized that the behaviour of the Kosi represents that of an oscillating rather than that of a migrating river, based on the thickness of sediment deposits, and the sedimentation rates that must have existed to produce them over the time period. Chakraborty *et al.* (2009) suggested that the Kosi moves via random nodal avulsions.

Migration of the Gandak River over its mega fan surface is significantly less avulsive. Mohindra *et al.* (1992) used aerial photography and soil chronoassociation to determine a net 80 km eastward migration of the Gandak River over its mega fan surface in the last 5000 years, a significantly slower rate than that of the Kosi. In comparison to the Kosi mega fan, the area of the Gandak mega-fan is considerably larger but its shape is more elongated as shown in Mohindra *et al.* (1992) and Figure 1.7.

The Gandak Dam, situated only a kilometre downstream of the HFT, is also likely to have some influence or even disguise the channel's morphological response to the rapid uplift associated with the HFT. As noted by Surian and Rinaldi (2003), Italian rivers that undergone modification by river engineering or management show clear changes in channel width, channel pattern and incision rates over the past 100 years. With such similar morphological responses expected from both tectonic and anthropogenic structures, it may be challenging to ascertain the dominant control in changes to channel morphology about the HFT and Gandak Dam.

2.5 The Chitwan Dun
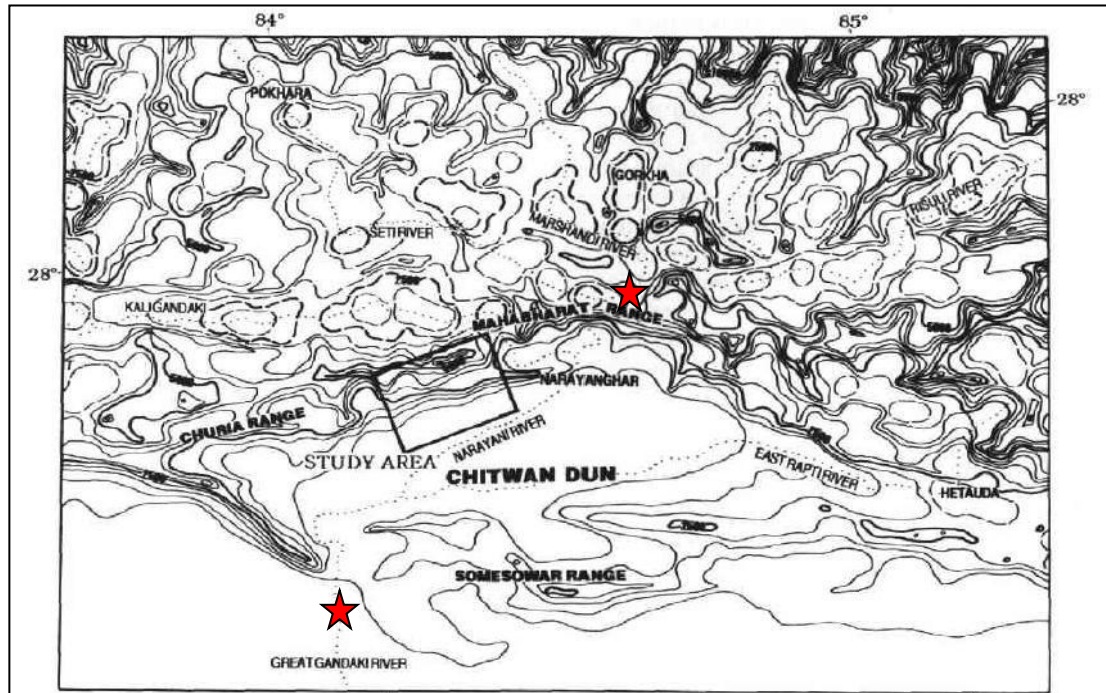
Figure 2.5 *Map of the Chitwan Dun and Gandak River study reach for this research (upper and lower limits defined by red stars).The trace of the Gandak (Narayani) and its major tributaries (East Rapti, Kali Gandaki, Seti, Marsyandi) are shown by dotted lines. (source: Kimura (1999)).*

On exiting the Lesser Himalayas, the Gandak River proceeds into the Sub-Himalayas and traverses the Chitwan Dun (Figure 2.5). The Chitwan Dun has dimensions of approximately 130 x 40 km, making it an ideal candidate for the storage of vast quantities of exported material from the rising Himalaya. A series of north-south flowing tributaries flow across the Chitwan Dun into the Gandak River, and transport sediment from the northern slopes of the Churia Range (Figure 2.6) into the Dun.

The surface of the Dun displays a low gradient as a result of the amount of erosional detritus stripped from the Himalayan range, exported by antecedent rivers into the foothills and eventually deposited within the Chitwan Dun. Information concerning the thickness of fill within the Chitwan Dun however, is unavailable. The tributaries to the north of the main Gandak River (Figure 2.6) display steeper slopes than the main Gandak as it flows through the Dun, as they originate from the hill slopes to the north of the Dun.
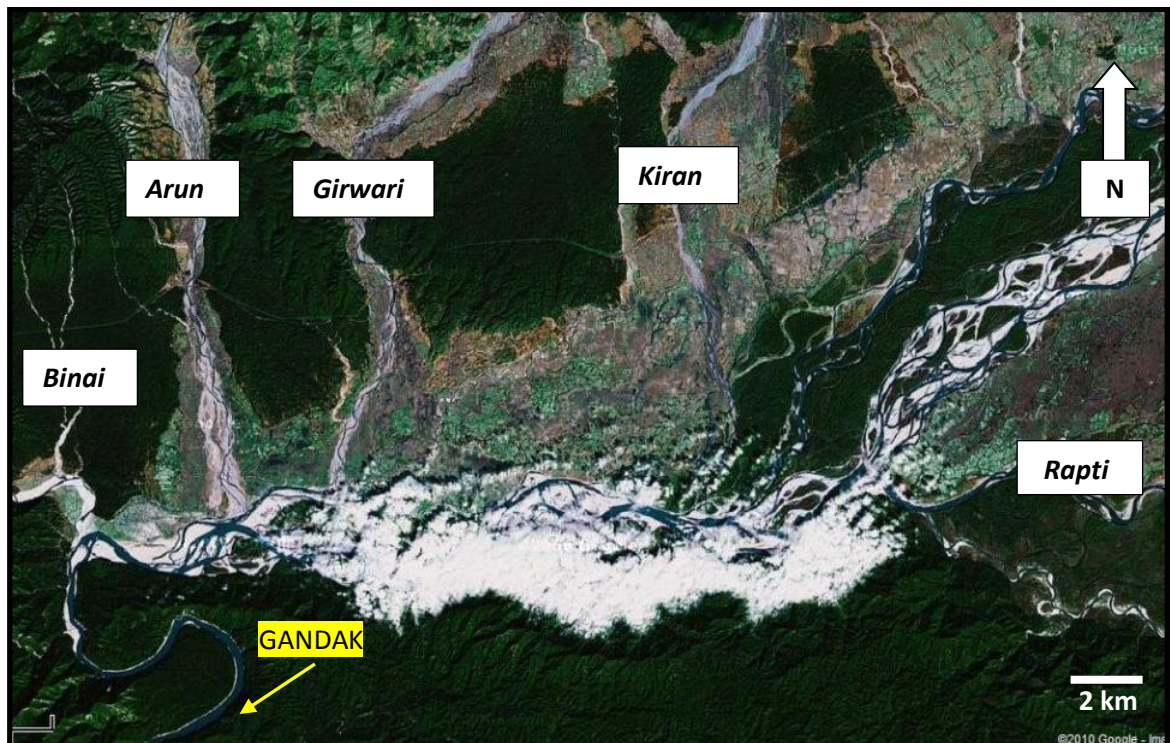
Figure 2.6 *Google Maps view of the Binai, Arung, Girwari and Kiran Kholas (tributaries) crossing the Chitwan Dun and meeting the Gandak River. The East Rapti River also joins the main Gandak body within the Chitwan Dun into the left hand (or south) bank.*

Sediment release (and fluvial transport capacity) from the Dun is largely mediated by climate (Tandon *et al.*, 2006), where higher discharges will result in incision of the stored sediment as the critical shear stress required for transport of the river bed material is exceeded. Shear stress and stream power are both functions of discharge (Yanites *et al.*, 2010) therefore; accelerated incision would be expected to coincide with periods of increased discharge. During periods of monsoon intensification after the Last Glacial Maximum and on entering the Holocene (Tandon *et al.*, 2006; Suresh *et al.*, 2002), elevated discharge levels may increase sediment export from the Dun.

2.6 Chapter Summary

The Himalayas are characterised by networks of complex tectonic structures. The recycling of ancient erosional detritus has resulted in the formation of weakly consolidated molasses which form the Siwalik Hills. How sediment is stored and removed within the Sub-Himalayas is therefore an important issue. There is a difference in morphological characteristics between the Kosi and Gandak Rivers on exiting the mountain front, and it is unknown what causes this and whether the Chitwan Dun plays any role.

Evidence of seismic events can persist within a landscape for up to 1 Ma, and with the majority of seismic movement on the HFT constrained within the Quaternary period, it would be expected for morphological responses to be maintained in rivers presently flowing over the

fault. How these morphological responses display themselves as quantifiable measures within river channels remains uncertain. There is little understanding of how the magnitude or nature of these responses changes over time either.

Sediment removal from the Chitwan Dun is likely to be a function of climate. Therefore, the most recent episode of sediment evacuation would have started during the early Holocene following the demise of the Last Glacial Maximum. It is important to ascertain whether there is still significant sediment removal from the Dun, and if so, how this may affect river morphology.

Chapter 3: Methodology

3.1 Remote Sensing

In order to observe the geomorphological changes along the Kosi and Gandak rivers, remotely sensed data from a number of sources have been utilised. Due to the inaccessible nature of both regions and associated problems with access, remote sensing is the only feasible source of data on topography, drainage networks, vegetation patterns and land use. The quality of information extracted from these datasets will depend on a number of factors, including spatial resolution and inconsistencies between data sets captured at different times because of anthropogenic modification and natural landscape evolution.

Digital Elevation Models (DEMs) have been taken from the Shuttle Radar Topography Mission (SRTM) and ASTER Global Digital Elevation Model (ASTER GDEM), and projected to UTM zones 44N and 45N (WGS 1984 datum). In addition to these resources, data obtained by the Linear Imaging Self-Scanning Sensor-3 (LISS-3) from the Indian Remote Sensing satellite (IRS-1C/1D) have been used to identify changes in vegetation and land use. The types of data used are summarised in Table 3.1.

Table 3.1. Data sources and resolutions		
Data Source	**Spatial Resolution**	**Year captured**
ASTER GDEM	30 m	2009
SRTM	90 m	2000
IRS LISS-3	23.5 m	1995-1997
Topographic Maps	1:50,000 (metric) - 1:253,440 (imperial)	1933-1983

ArcMap v.9.3 was used to display the SRTM and ASTER DEMs, to which the LISS-3 data (Figures 3.1 and 3.2) and more detailed topographic maps were georeferenced. This allowed for the extraction of data regarding channel width and slope, and for the production of longitudinal profiles of each study reach.

In order to determine if a morphological response to tectonic uplift exists, the upper limits of the study reach were placed ~5 km kilometres north of the MBT and the lower limits between 5~10 km south of the HFT.
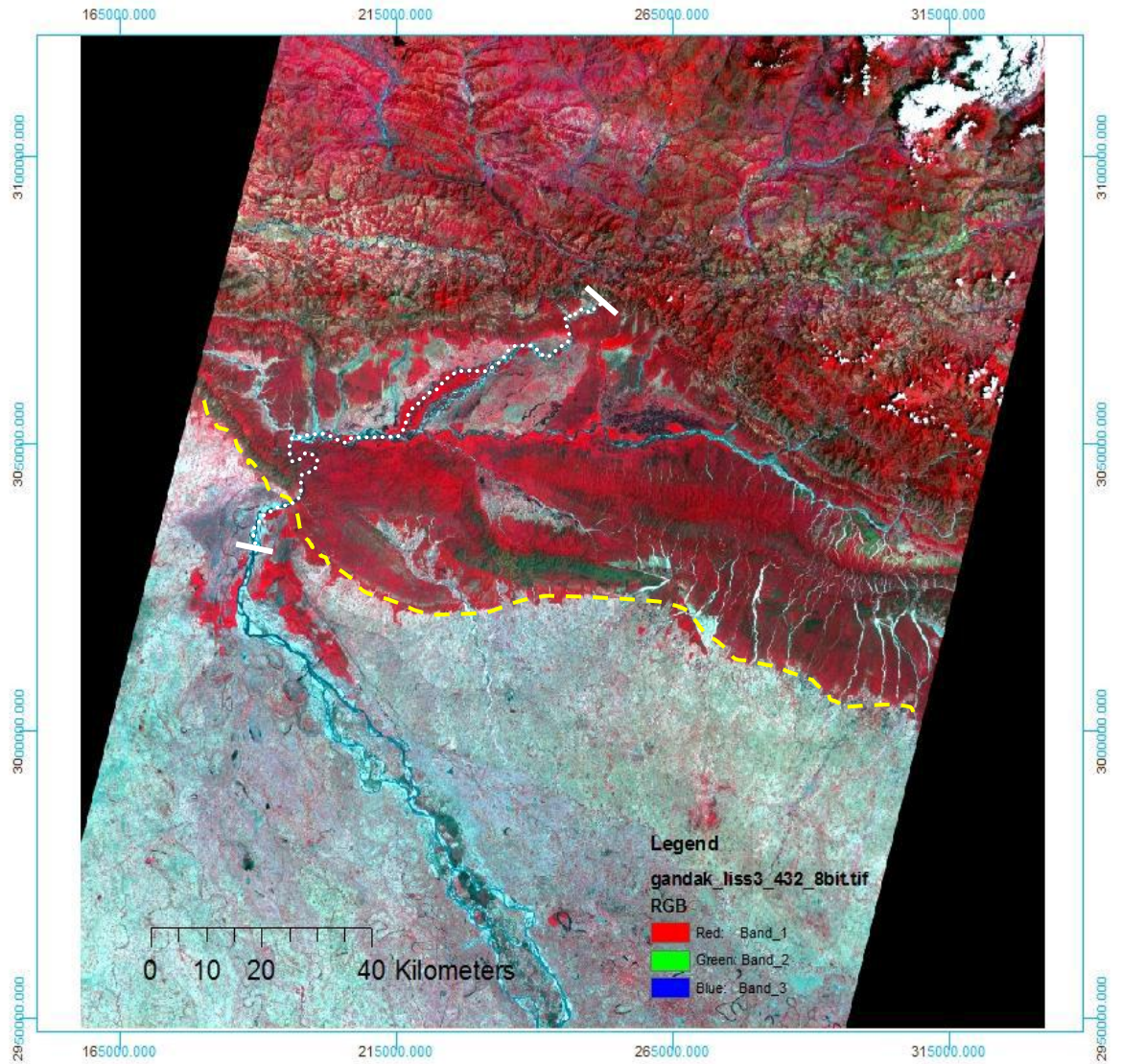
Figure 3.1. *LISS-3 projection of the Gandak study area. The dashed yellow line represents the approximate position of the Himalayan mountain front and the white lines define the study reach.*
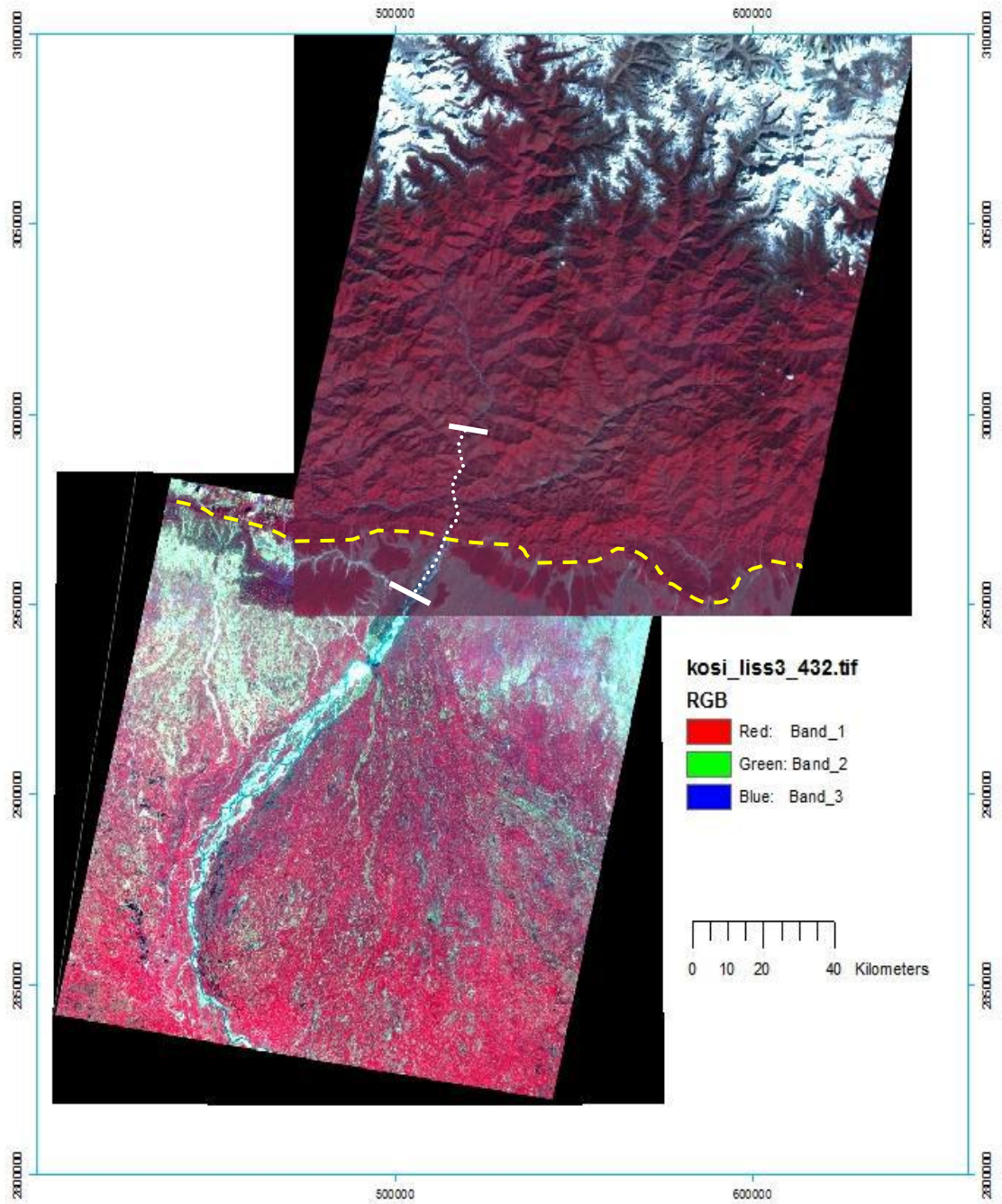
Figure 3.2. *LISS-3 and LISS-4 coverage of the Kosi study area. The dashed yellow line represents the approximate position of the Himalayan mountain front, and the white lines define the study reach.*

The study reaches as shown in Figures 3.1 and 3.2 are defined as:

	X coordinate (UTM Zones 44/45N)	Y coordinate (UTM Zone 45N)
Gandak: Upper limit	249192 (Zone 45N)	3080175
Lower limit	782447 (Zone 44N)	3029115
Kosi: Upper limit	518225 (Zone 44N)	2993354
Lower limit	511010 (Zone 44N)	2959593

Table 3.2. Study reach limits

Along each study reach, information concerning morphological variables was extracted using the following methods:

3.1.1 Remotely sensed channel width

LISS-3 operates across four spectral bands; green (0.52-0.59μm) red (0.62-0.68μm), near IR (0.77-0.86μm) and mid IR (1.55-1.70μm).   Using images produced by LISS-3, changes in vegetation and land-use are easily identifiable as shown in Figures 3.1 and 3.2. Active channel widths were defined by where distinct changes from vegetation (red/green) and water were apparent. Where channel patterns became braided in alluvial regions, both active channel and channel belt measurements were taken (Figure 3.3). Densely vegetated bars (shown in strong red) that were obviously uncovered by even high flow (except perhaps in exceptional events) were not included in active channel width measurements. At points where braided channels were separated by large vegetated bars, active width measurements were taken using the largest or most dominant looking channel. The active channel was defined as the channel that appeared widest and deepest, which was identifiable from the shade of blue that the channel was represented by on the LISS-3 image. As noted by Ashmore *et al*. (2011), there is some difficulty in identifying active channels where rivers become heavily braided, as bed load movement may only be intermittent or wetted channels may not be physically transporting bed material at all. As it was sometimes difficult to determine which was the active channel when there were multiple large channels, the channel belt width (as shown in Figure 3.3) was also measured for comparison.

Using ArcGIS a point shape file was created and a marker was placed every 500 m on the LISS imagery along each reach. At each point, active channel width (herein referred to as 'channel width' unless stated otherwise) was measured using the ArcMap ruler tool. This information was then plotted as a function of down-reach distance. Again, due to the spatial resolution of

these data sets (23.5 m) the accuracy of channel width measurements may be limited. This was notable when trying to identify an abrupt transition between vegetation and water as the image often appeared blurred.

3.2 Channel geometry

3.2.1 Channel geometry in the field

In order to test the relationships derived by Finnegan *et al*. (2005) in equation [6] a number of variables require quantifying. Whilst channel slope, width and discharge data are possible to acquire remotely, field verification is required in regions of particular interest, such as at known fault positions and lithological boundaries, where morphological adjustments may be anticipated. Other variables such as width-depth ratios also require measuring in the field as cannot be done remotely.

Channel Width: Active channel belt/ active channel width was measured at a small number of sites using a hand held laser distance meter. Therefore, sites which could be used relied on there being exposed bedrock on each bank and the visibility of the high water mark as an estimate of high water width. This high water width is likely to represent the active channel belt width (Figure 3.3) attained during annual peak monsoon flows, as below this height there was little vegetation evident. In the instance of the narrower bedrock channels measured, the active channel belt width is also equal to the active channel width due to a lack of permanent in-channel deposits. The range of the laser is also restricted to ~150 m depending on surface reflectance. The laser works best off flat and reflective (white) surfaces such as exposed bedrock, so can only be used in limited parts of the study reaches. Active channel width measurements were taken from the elevation of high water mark so should be directly comparable to those extracted from the LISS-3 dataset. This will also help to get an understanding of the error margins on remotely sensed values.

Width-Depth Ratios: Using a hand-held sonar at regular intervals across a transect perpendicular to the direction of flow; one channel depth profile was constructed across the Gandak River near Devghat in the bedrock region of the channel upstream of the Chitwan Dun. A limited number of depth measurements were also taken just upstream of the HFT. Ideally, more cross-sections would have been completed but there were restrictions due to boat access and the strength of the river flow, which made it difficult to keep the boat still relative to the flow whilst reading the sonar. By reflecting the laser scanner off the high water mark of the bank on each side of the river, the position of each depth reading taken across the cross section was recorded. GPS readings made using a Garmin GPSMAP 60CSx were also taken at the start and finish of the cross-section allowing the transect to be plotted spatially and to provide another reading of total

channel width. To complete the cross section, a meter rule and tape measure were used to measure the height and distance between the water level and high flow mark.

However, as only one detailed cross-section was completed it is not possible to test width-depth ratios within bedrock channel width scaling laws (equation [6]) as there are no downstream depth comparatives to calculate additional width-depth ratios.

3.2.2 Longitudinal Profiles

Using the DEMs produced by ASTER GDEM and SRTM datasets, it was possible to carry out hydrological modelling in ArcMap to ascertain the thalweg of each river. By using the 'fill' command to remove small imperfections in the surface raster and using the flow accumulation tool, a line of concentrated flow approximating the river (thalweg) was constructed. Based on the Root Mean Squared (RMS) error of each dataset (approximately 10 m), a contour interval of 10m was drawn onto the DEMs, as below this level the vertical error of the DEM is too high to be used to a comfortable degree of certainty. As discussed by Wobus *et al*. (2006b) it would be expected for tectonic signals in such a seismically active region to manifest within the landscape at a scale greater than a 10 m contour interval. It is therefore accepted that only minor signals, which may result from the smoothing of DEM data anyway, will be hidden between the 10m contour intervals applied. Jacobsen and Passini (2010) evaluated the height models of both ASTER GDEM and SRTM and found that the height models of SRTM are still marginally more accurate than that of the newer generation of data in ASTER GDEM.

Topographic maps were used in conjunction with SRTM data when extracting longitudinal profiles. After georeferencing maps covering the regions 72A, 63M and 72N it was possible to compare digitised contours with those on the map. However, the scales of many of these maps were large so contours were only represented at large intervals, in some cases only every 500 ft, so could only be used in combination with the DEM derived contour patterns. ASTER GDEM data produced a blocky longitudinal profile with some irregular features, which did not appear to match topography identified on the topographic maps. The same profile was extracted from the SRTM data set, which was then used as appeared more representative.

3.2.3 Channel Slope

Wobus *et al*. (2006b) considered the problems associated with calculating channel slope from the application of moving windows over the surface of the DEM to produce raw pixel-to-pixel slopes, and concluded that elevation data is best resampled at equal vertical intervals, such as at 10m contour intervals. Following this assessment of errors, local channel slope has been derived using the distance between 10m contour crossings and applying the formula:

$$\Delta \, \text{Height} \, / \, \Delta \, \text{Distance} \, = \text{Slope}$$

This information was then plotted as a function of downstream distance. Again, issues arise due to lack of spatial data. In cases where distances between contours are extensive, the channel slope for that section is 'averaged out'. For example, the majority of the 10 m elevation change may be focused in the first kilometre but will be averaged out over the full length. The distance between points is again measured by the ArcMap ruler tool so is subject to human error which is accentuated over longer distances.
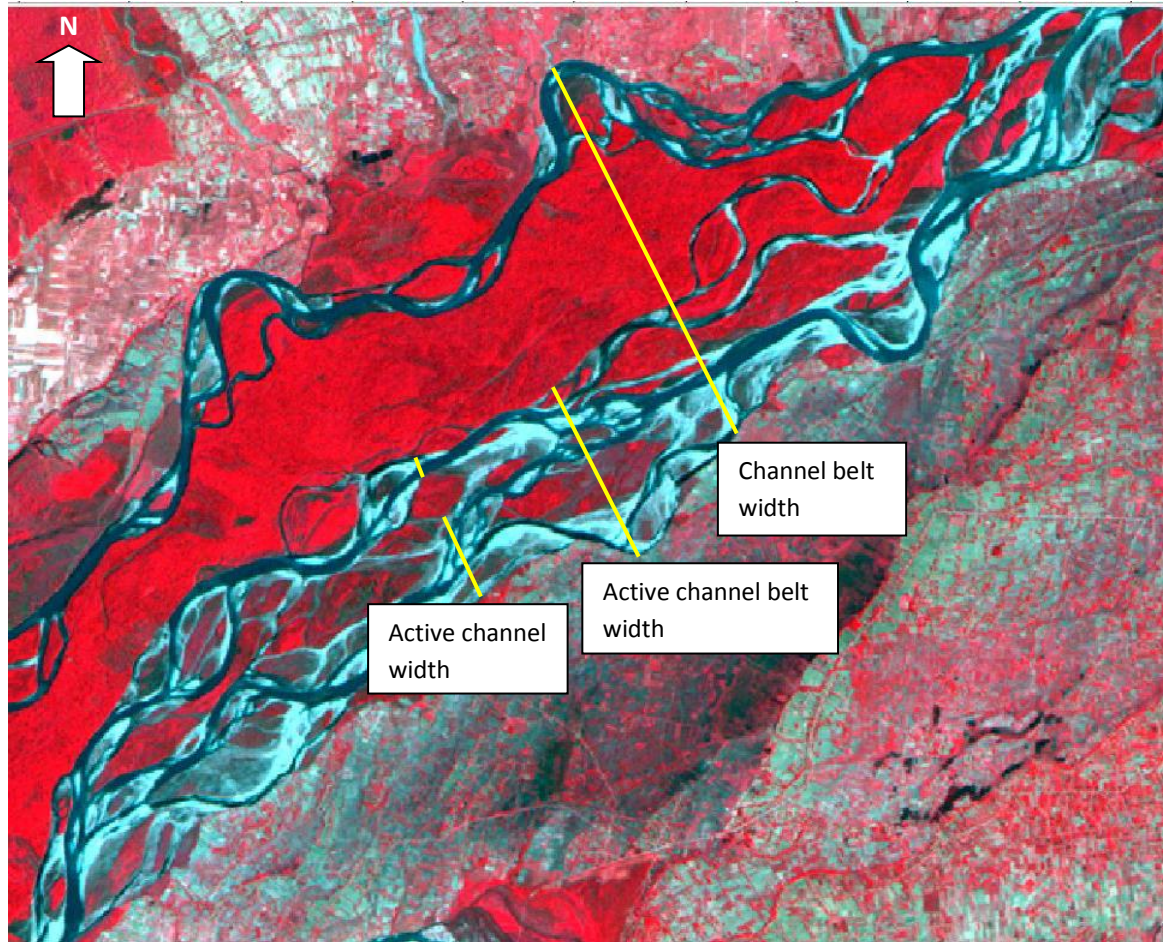
Figure 3.3 *Example of how channel width was measured using LISS-3 imagery on the Gandak River. Where the channel braids are separated by densely vegetated bars (shown in red), which rarely become submerged, the larger more dominant braid to the south of the bar has been measured. Smaller bars which are continuously densely vegetated have been excluded from active channel width measurements, as shown by breaks in the yellow width measurement lines, as are unlikely to become submerged on a regular basis.*

3.2.4 Grain size: field measurements

To establish whether any connections exist between the grain size distribution, sediment inputs and tectonic activity, a series of measurements were taken down each reach in pre-identified locations where such changes may be expected to occur. Using Google Earth to provide the

most contemporary and highest resolution images, transects sites down each river were chosen based on a compromise between access and points where morphological change may be expected to occur. Locations sampled included bars immediately upstream and downstream of fault locations, within 500 m upstream and downstream of major confluences, and 0.5-1 km upstream of major tributaries from their confluence with the main river.

Figure 3.4. *Typical transect path as indicated by the dashed line. The first photo as indicated by the arrow would contain both the GPS and 150 mm scale as shown in the top left corner. Depending on the size of the bar and quality of the exposure, samples may contain up to 100 photos each taken a few steps apart. For reference, this image is facing downstream.*

Photoseiving is an effective method to estimate grain size in exposed areas of gravel bed rivers (Ibbeken and Schleyers, 1986; Sime and Ferguson, 2003; Carbonneau *et al*., 2004; Carbonneau *et al*., 2005) which allows a greater area to be covered in a significantly shorter time period than traditional methods. Dugdale *et al*. (2010) highlighted a significant agreement between photoseiving and Wolman type counting techniques, with coefficients of determination (r^2) falling between 0.88-0.99 (Ibbeken and Schleyer, 1986; Rice and Church, 1996; Rubin, 2004; Buscombe and Masselink, 2009). When identifying suitable bars to sample, care was taken to ensure that the bar was not located on a meander or immediately downstream of any minor tributaries or gravel mining activity. The first image at each sample site was taken with a 150

mm scale and GPS within frame (Figure 3.4 and 3.6), and the height of the monopod remained fixed for images taken at the site to maintain a constant scale. The location of the first image of each sample suite was also recorded using the GPS and a track (active log) produced. Each active log was set up to record GPS points at the lowest interval possible. Then, using a monopod and Kodak C875 Zoom 8MP digital camera, photos of the dry riverbed were taken every few steps along a roughly linear path on the upstream end of the exposed bar as this is where it would be expected for the river to deposit the bulk of its coarse load (Figure 3.4). In cases where the height of the monopod had to be altered, the subsequent photo was taken with the scale in the frame again. Situations where the height of the monopod needed to be altered were when bed material was exceptionally coarse so the height of the camera needed to be increased to capture a significant number of clasts within the shot. A minimum of 50 and maximum of 100 photos were taken in each sample suite.

27 sites were chosen along the study reach of the Gandak River within UTM Zones 44 and 45N. The averaged co-ordinates of each site, calculated as the mean of all points from the active log, are given in Table 3.3.

Table 3.3. Gandak grain size transect locations		
Site Name	**X co-ordinate (UTM)**	**Y co-ordinate (UTM)**
G1	0787412	3038830
G2	0790831	3041472
G3	0791637	3050593
G4	0205246	3051378
G5A	0212934	3051385
G5B	0215490	3051421
G6	0229382	3063123
G7	0239247	3067105
G8A	0245033	3066413
G8B	0246568	3067963
G9	0246814	3067924
G10A	0246247	3071294
G10B	0245886	3071507

G10C	0247127	3071317
G10D	0247130	3071304
G11A	0250206	3074098
G11B	0250466	3073611
G12	0247174	3075932
G13	0247902	3079730
Arung Khola	0792769	3052722
Kiran Khola	0214251	3051498
Girwari Khola	0795757	3052421
Rapti	0234755	3050353
Jharahi Khola	0229562	3063485

Similarly for the Kosi, 7 sites were chosen within UTM Zone 45N and the mean averaged co-ordinates are listed in Table 3.4.

Table 3.4. Kosi grain size transect locations		
Site Name	**X co-ordinate (UTM)**	**Y co-ordinate (UTM)**
K1	0514577	2964624
K2A	0515265	2965655
K2B	0515296	2965581
K3	0514865	2969239
K4	0515663	2976769
K5	0515733	2976737
Tamur (K6)	0517465	2977487

3.3 Grain size: analysis
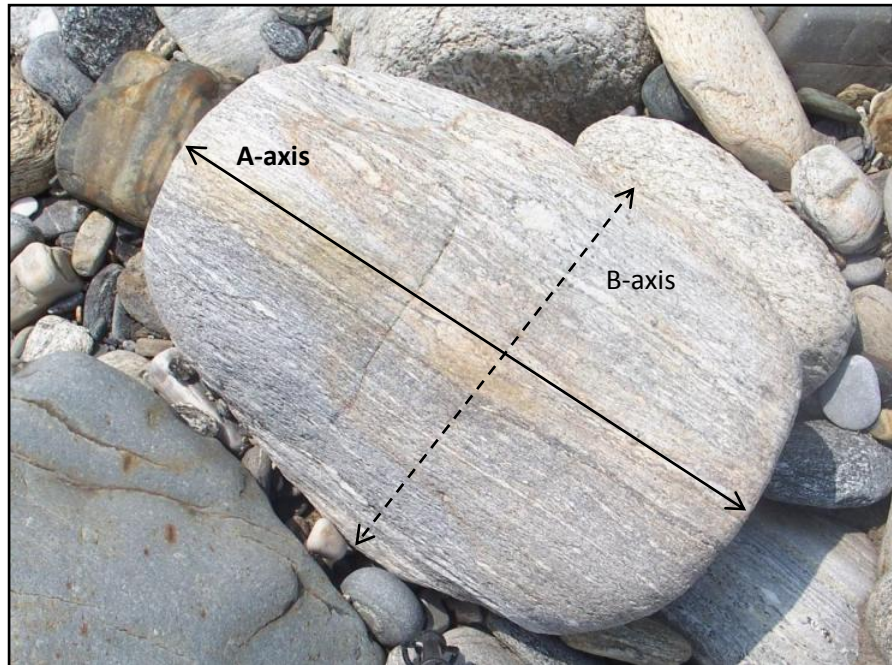
Figure 3.5. *For each clast under a grid intersection, the b-axis as indicated was measured. The b-axis is taken as the largest axis perpendicular to the long axis (a-axis).*

Using a Matlab code and accompanying Graphic User Interface (GUI) similar to that used by Dugdale *et al*. (2010), the b-axis of photographed clasts were measured to produce D_{16}, D_{50}, D_{84} and D_{95} values for each image (Figures 3.5 and 3.6). It was assumed that the a-axis and b-axis of clasts were orientated on a sub-horizontal plane, and that the c-axis was near vertical which appeared consistent with the majority of bars sampled. Each image (approximately 2 MB in size) was imported into the GUI in Matlab R2010a and an 8 x 7 grid was laid over each image (Figure 3.6). The b-axis of the grain under each of the 56 grid intersections was then manually measured to produce a grain-size distribution for the 56 grains sampled in each photo (Figure 3.5 and 3.6). For the majority of the transects, a minimum of 50 photos were analysed. In some instances photos were rejected as were dominated by individual clasts where the b-axis was obscured or incomplete. Instances where large quantities of sand or water were in the image also meant an accurate representation of the grain size distribution could not be taken, so again the photo was rejected.

Lithological variations

A simple assessment of lithological variation was also undertaken to provide a basic indication of how the source of bar material varies downstream. Using techniques similar to photoseiving, lithologies of clasts lying beneath the cross hairs of the Matlab GUI have been categorised as Siwalik, Lower Himalayan or Higher Himalayan in source. Ten photos from each grain size transect were used to calculate proportions of the relevant lithological source groups at each

transect, a total of 56 clasts for each photo. However, due to the large potential errors associated with this technique through misidentification of rarer lithologies and smaller clasts, results should be viewed with caution and treating as a representation of how proportions of different source lithologies vary relative to each other.
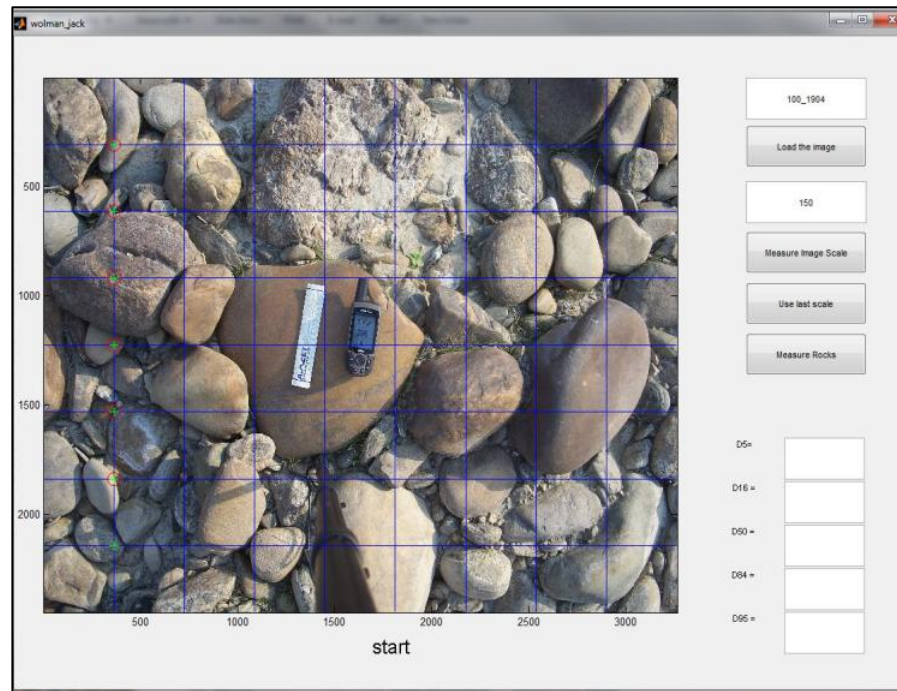
Figure 3.6. *Matlab GUI as used for carrying out photoseiving. For the first photo of each sample, a 150mm scale and GPS were also captured in the image. Under each intersection of the blue grid, the b-axis of the underlying grain was measured.*

3.4 Limitations

Satellite data resolution: The Gandak study area is covered solely by SRTM data with 90 m resolution, whilst the Kosi also has coverage by 30 m resolution ASTER GDEM data. LISS-3 data are also restricted to a spatial resolution of 23.5 m across both areas and the ages of these data sets are summarised in Table 3.1. The LISS-3 data in particular are outdated, as the channel positions are likely to have migrated significantly since the images were captured. When comparing field locations recorded by GPS with the LISS-3 imagery, it was evident that the channel pattern had altered as some exposed bar GPS locations were submerged on the LISS-3 image. When using such data to perform detailed analysis of features such as channel width, the measurements taken will have a degree of error attached based on the resolution and age of the image. Channel width measurements were also made using the laser distance meter in the field to compare with measurements derived from the LISS-3 data, and the difference between readings from the different methods was found to be negligible at only ~1 % (see Appendix). In the case of the DEM, ~10 m of error is also applicable to the vertical axis. The RMS error associated with the ASTER GDEM and SRTM datasets questions how accurate a method this is

for extracting longitudinal profiles in this region. The flow accumulation tool works on the basis of the quantity of accumulated flow in each cell, and in the case of SRTM data each cell covers a 90 m x 90 m horizontal grid size, spanning 1° in latitude and longitude (Hancock *et al.*, 2006). How flow is directed and accumulates in each cell is related to channel slope. In the instance of the Gandak study reach, the overall slope is generally low on the order of < 200 m over a 100 km length. Vertical errors in the region of 10-15 m (based on the RMS error) may therefore alter the direction of flow within an individual cell. With the large cell sizes of these datasets, this may significantly alter the flow accumulation raster. Hancock *et al.* (2006) evaluated SRTM DEMs against high-resolution datasets (10 m) and their use in catchment geomorphology and hydrology, concluding that whilst hypsometric properties are well represented by the SRTM datasets, other properties such as catchment area and relief are poorly captured. Vertical and horizontal accuracies are given as ±16 m and ±20 m respectively further suggesting that hydrological data derived from SRTM data should be treated with caution. In order to improve the accuracy of measurements taken from satellite-derived data, higher resolution images would be needed (e.g. ASTER GDEM of both rivers, and LISS-4 at 5.8 m resolution).

Topographic maps: Topographic maps were used in conjunction with SRTM and ASTER GDEM data to derive longitudinal profiles and channel slope measurements. The majority of these topographic maps were produced 20-30 years ago meaning the thalweg identified in the DEM data was not always consistent with that on the topographic maps. The contour numbering of these topographic maps was often hard to read. As a result, the topographic maps could only be used together with other data. More detailed and accurate profiles could have been constructed with more contemporary maps of a higher resolution (either complete coverage of 1:50,000 or 1:25,000) which were unavailable or inaccessible during the period of this study.

Grain size analysis in Matlab: As raised by Graham *et al.* (2005) and Carbonneau *et al.* (2004) a number of errors existed whilst conducting grain size analysis using photoseiving. Firstly, errors exist due to spatial distortion created by projecting a 3D surface onto a 2D plane, which introduces systematic underestimation of clast dimensions (Carbonneau *et al.*, 2004). Fabric errors associated with grain inclination relative to the plane of the image are also likely to produce significant error, but this was not a significant problem in this study as the a-axis and b-axis of most bars sampled were aligned to a sub-horizontal plane. Some clasts were found to be overlapping, or not completely contained in the photo, and as found by Sime and Ferguson (2003), clasts were also partially buried by fine grained material. Early work by Ibbeken and Schleyers (1986) attributed the biggest difference in grain size distributions between photo-sieving and machine-sieving to the hiding of clasts behind each other (imbrication). Error associated with manual measurement of the b-axis should also be considered as this will be limited by the resolution of the image on the computer screen. The smallest possible grain size which is measurable will also be affected by the resolution of the screen and photo. However,

the number of grains measured using this method (~98,000) far outweighs the number that could have been measured by hand in the field. Through the sheer number of samples taken, it is assumed that sampling and fabric errors will be averaged out.

An additional factor which may introduce significant bias is the over-representation of large clasts within each photo. As the GUI relies on 56-grain measurements per photo to be made, where clasts were large enough to fall under multiple grid intersections, repeated measurements of the same b-axis were taken as the code does not allow samples to be skipped. For instances where clasts were covered by 3 or more grid intersections, the first few measurements were taken of the clast lying beneath the intersection and the remaining taken randomly on surrounding clasts which would otherwise not be sampled. By limiting the number of repeated b-axis measurements to two or three times, it is anticipated that minimal bias will be introduced to the data.

Channel geometry measurements: The accuracy of channel geometry measurements taken in the field was influenced strongly by both the equipment used and external factors. Ideally, more channel cross-sections would have been completed but due to a lack of boat availability, only one detailed profile was completed. One obvious factor introducing error into this profile stems from the strength of the river flow. In the regions of strongest flow, it proved difficult to keep the boat stationary relative to the river bed so rather than the cross-section being conducted in a straight line perpendicular to the direction of flow, the cross-section ended up in a 'U' shape between the two end points on the opposite banks. As the location of each depth reading was taken relative to the bank using the laser scanner, by having a non-linear shaped transect the readings taken will not be perpendicular to flow if taken from the same spot of the bank. This will introduce a horizontal component to the distance measured that would need correcting for. Additionally, if the reading by the scanner was taken perpendicular to flow at all locations, the overall channel width may change at points of the transect. At the point furthest downstream (mid-transect) the relative depth of the channel bank may vary to that of the start and end. The GPS reading taken at either end of the transect also introduces a further element of error as is only accurate to the nearest 4-5 m, which may be a significant influence if used to calculate channel width (~5 % error based on channel widths < 300 m).

Chapter 4: Results

The geomorphological data collected during this study shall now be presented in the following order: longitudinal profiles, channel slope, channel width and grain size. Prior to this, there will be a brief description of field observations concerning lithology and features of interest. The chapter shall conclude with a section concerning calculated Shields stress and critical stream power for points along the study regions.

The locations of the MBT, MDT and HFT faults are as shown in Lave and Avouac (2001) but are not to be taken as exact. Lateral segmentation of the MBT by transverse tectonic features (Kayal, 2001) complicates mapping the MBT as a single linear feature. Instead, the location of the MBT is given over a wider range or 'zone' along the Kosi River, because a single geographical location of the fault trace cannot be defined, referred to as the MBT zone.
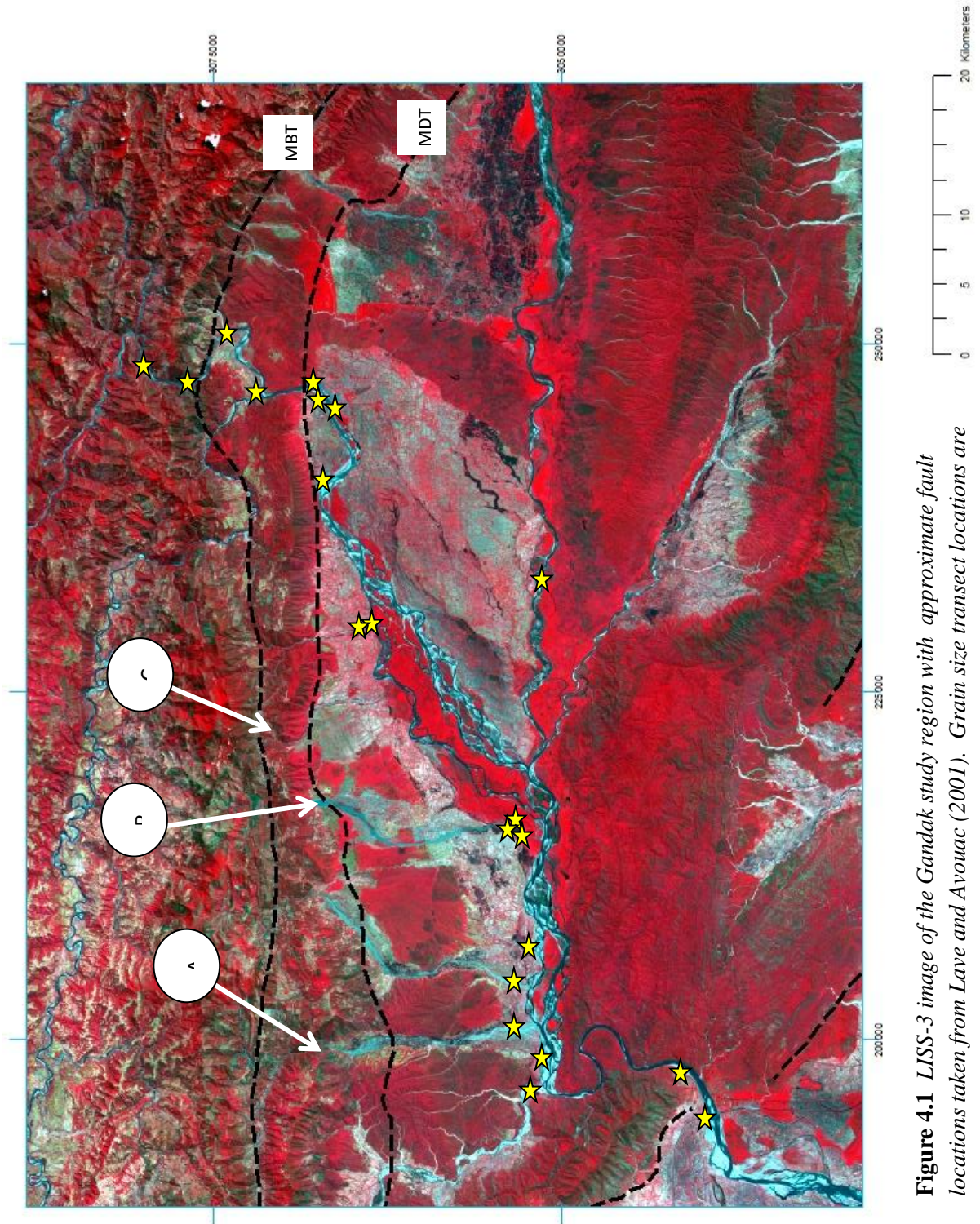
Figure 4.1 *LISS-3 image of the Gandak study region with approximate fault locations taken from Lave and Avouac (2001). Grain size transect locations are also identified by yellow stars*
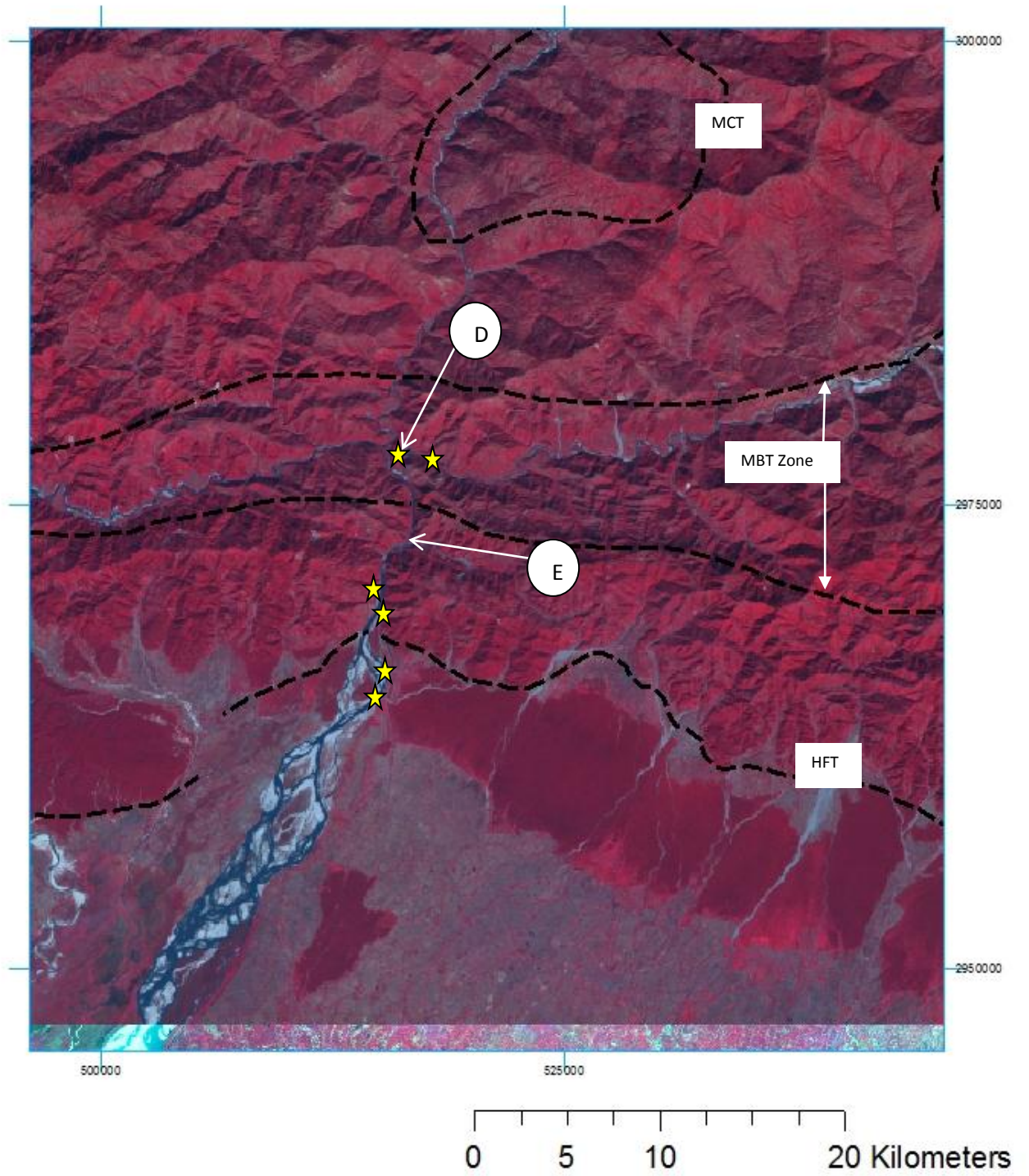
Figure 4.2 *LISS-4 image of the Kosi study reach, fault traces and grain size transects*

4.1 Field observations

Gandak

At locations G10-13 which lie north of the Chitwan Dun and MDT, approximately 30-45 % of the lithology sampled across the grain size transect paths was classified as Greater Himalayan. The majority of this Greater Himalayan proportion was Lesser Himalayan phyllites, quartzites and low grade schists with only a minor contribution (<5 % of overall lithology) from Higher Himalayan crystalline rocks. Within the Dun, this proportion of Greater Himalayan lithologies dropped to < 5 %. There were also frequent exposures of Siwalik bedrock and bedding. In the region of G12, there was a notable difference in landscape with a dramatic increase in hillslope elevations from ~250 m to up to 700 m over a distance of less than 2 km. This is likely to reflect the presence of the MBT. Large conglomerate boulders (more likely a tectonic diamictite) also characterised left bank deposits, which may have originated from intense but localized deformation about the MBT fault plane, further supporting the presence of the MBT. Between sample locations G9 and G10a-d, there was an exposure of coarse-grained conglomerate that was distinct from the lithologies about G10a-d. Dip of the bedding was also significantly reduced from 22° to 7° suggesting that the MDT is likely to be situated close by.

The upper reaches of the Kiran Khola (location B on Figure 4.1) revealed terraces of Siwalik rock (0216801 3066169) above a wide, shallow and heavily sediment choked channel (Figure 4.3). These elevated Siwalik deposits were interpreted as hanging-wall deposits of an unmapped fault, or potentially the MDT. The upper reaches of the Arung Khola (location A on Figure 4.1) also revealed mudstone inter-bedded within sandstone exposures, with evidence of an anticline structure at 0790612 3064868.

The upper reaches of the Deswa Khola (location C on Figure 4.1) were dominated by ancient debris flow deposits, which are currently being slowly reworked by the modern river. The valley was choked by massive unsorted boulders with evidence for faulting at 0221473 3068402. On the upstream side of this exposed section, bedding was dipping strongly north in comparison to the near horizontal bedding planes downstream of the crushed zone. This has been interpreted as either a fault, or the edge of a fault zone.

Figure 4.3 *Dry and* s*ediment choked reach of the Kiran Khola*

Figure 4.4 *Steep bedrock gorge incised by the Tamur River. Remnants of coarse landslide deposits are common at the bases of these unstable hillslopes.*

Within the Dun at points G7, G5b, G3 and G4, gravel lithologies were predominantly Siwalik sandstone with < 5 % Lesser Himalayan lithologies. Within the Kholas entering from the northern margin of the Dun, there was a marginally higher proportion of Lesser Himalayan lithologies (~5 %), yet the coarsest grained material (> 400 mm length in b-axis) remained Siwalik in lithology. There was also a notable increase in maroon coloured sandstone within the Kholas, which may be attributed to an increase in Lesser Siwalik sediment supply (Valdiya, 1998). The reach of the Rapti that was visited contained limited gravel exposures that were not heavily mined or reworked by human activity, yet the lithology of these deposits was > 95 % sandstone. Upstream of the Binai Khola confluence, there were thick (> 3 m in height) sand deposits with intermittent gravel exposures. Near to its confluence with the main Gandak River, there was a bedrock exposure on the right hand bank of the Binai Khola.

Kosi

At the Arun and Tamur confluence bar (K5 and location D on Figure 4.2) there was a mix of well rounded Greater Himalayan low grade metamorphic, and mica schist lithologies in addition to coarser and more angular fragments of Siwalik lithologies. At the Tamur sample (K6), the bar deposit was dominated by angular landslide fragments and massive boulders (> 3 m in diameter) such as those visible in Figure 4.4. The lithology of these deposits was a combination of low grade metamorphic rock such as phyllite and schist, and Siwalik sandstone. At K4, coarser Siwalik gravels dominated the side of the bar closest to the river. Further towards the bank there were fine grained Greater Himalayan lithologies mixed within coarser Siwalik clasts. This was the downstream limit of Greater Himalayan lithologies noted along the Kosi within this study. Further downstream at K2a and K2b, these limited gravel bar deposits were exclusively Siwalik lithologies.

At the village of Barakshetra (0516540 2972815), observations were made of the landslide/stream deposit entering into the left hand bank of the Kosi (location E on Figure 4.2). Large (some > 1 m in diameter) angular to sub-angular boulders and clasts characterised this feature, which has also been heavily reworked by both human activity and the small stream that flows down the deposit. Further downstream between this location and K4, there were multiple pathways noted that hill slope material may enter the Kosi via, such as from landslide deposits and small sediment laden mountain streams.

4.2 Longitudinal river profiles

The Gandak River shows an overall decrease in elevation of 150 m across the 120 km length of the study reach (Figure 4.5). The rate of elevation decrease is greatest just upstream of the Chitwan Dun. There are two significant breaks in slope with drops in elevation of 10 m within this section, the starts of which coincide with the positions of the MBT and MDT as given by Lave and Avouac (2001). These steep sections only persist for 1-2 km along profile however. On entering the Dun, the elevation continues to decrease at a lower and more consistent rate with an overall loss of 70 m in height, over more than 60 km in distance. Upstream of the HFT, the profile flattens out for just under 10 km, before another more abrupt 10 m drop in elevation ~12 km downstream of the HFT. Due to the distance between this break in slope and the HFT, it can be assumed that this is an independent event which is more likely to represent a hole in the DEM which was not 'filled' properly. The RMS error associated with the SRTM data (~10 m) also makes it likely that drops in elevation are insignificant where they are only of 10 m as this lies within the vertical error boundaries of this dataset. The decrease in slope upstream of the HFT is likely to be a reflection of movement along the tectonic boundary. Overall, changes in elevation across the Gandak longitudinal profile, as shown in Figure 4.1 are relatively subtle but the two significant breaks in slope about the MBT and MDT, and the flattening of the profile upstream of the HFT would suggest that a geomorphic response to differential uplift is present.

The Kosi River longitudinal profile (Figure 4.6) displays a more stepped shape than that of the Gandak. Overall, there is a decrease of 110 m in elevation over a distance of ~40 km which is significantly steeper than the Gandak River over a similar tectonic reach. There is one significant break in slope within the MBT zone (at ~19 km down the reach), where elevation drops 20 m over a 100 m distance. Despite the break in slope being an amount greater than the RMS error of the SRTM data set, it is still likely that it may represent a hole in the DEM (Figure 5.4). There are two other regions of slightly increased gradients, the first just downstream of the MCT and the second ~4 km upstream of the HFT. The latter change in gradient may reflect a migrated knick-point associated with earlier surface rupture of the HFT, or a hole in the DEM which was not correctly filled. There is also a subtle shallowing of the profile prior to the MBT break of slope.

The main points of interest which have been raised from the longitudinal profiles of both rivers are that the Kosi study reach is steeper overall and that tectonic structures have influenced channel bed slope on both examples to some degree. As the overall gradients of the profile are still relatively low, it is probable that some of the features have been accentuated or are direct results of imperfections on the vertical axis of SRTM datasets and should be treated with caution.

Figure 4.5. *Longitudinal profile of the Gandak River as extracted from SRTM data using Arc GIS v.9.3. Highlighted are the position of the MBT, MDT and HFT faults (red dashed lines) and the region which flows through the Chitwan Dun (indicated by the green box on the x-axis scale). The direction of thrusting as indicated in the bottom left hand corner is applicable to all faults in this study.*
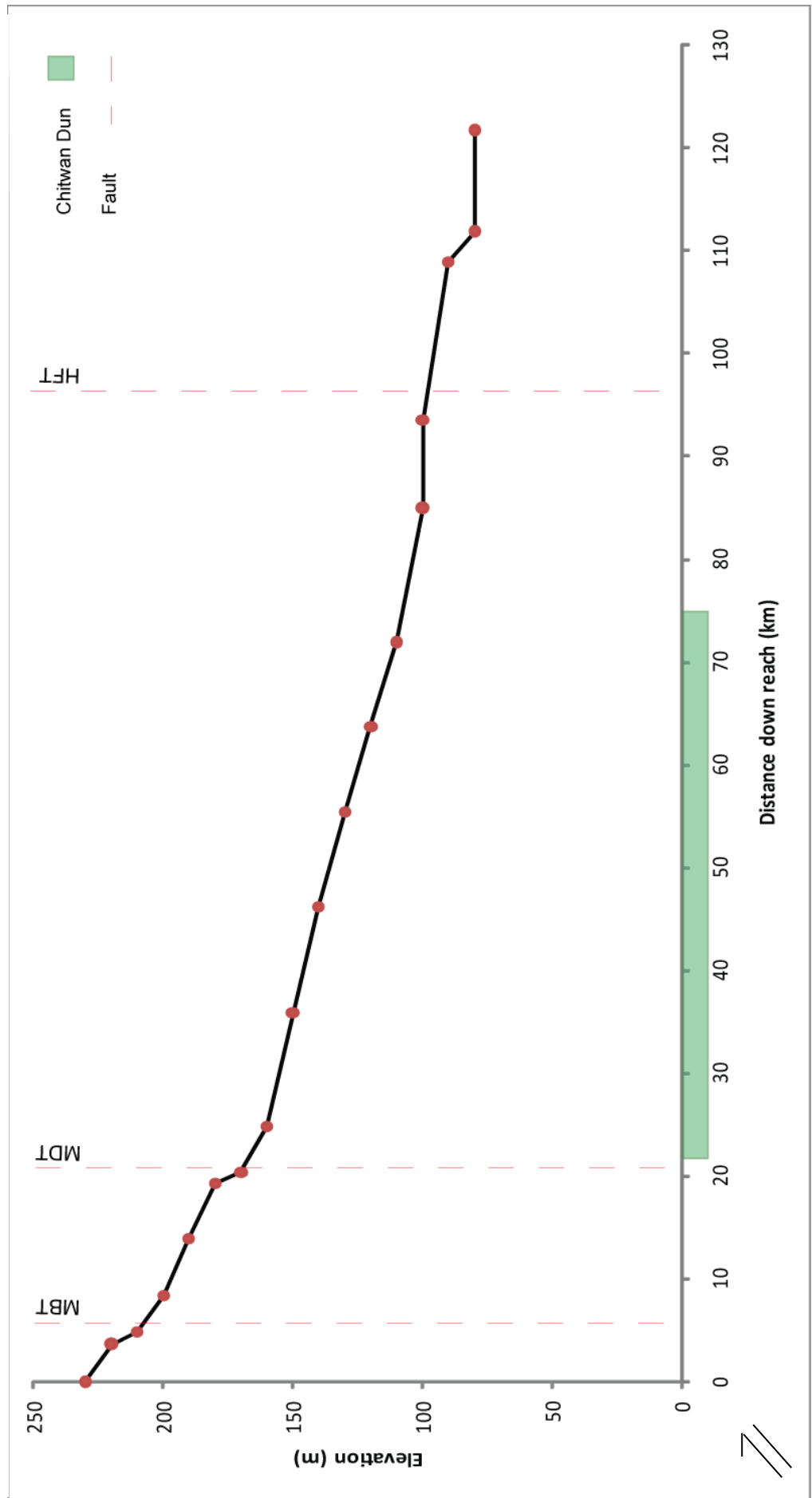
Figure 4.6. *Longitudinal profile of the Kosi River as extracted from SRTM data. Indicated are the positions of the MCT and HFT faults and also the MBT 'zone' but the pink box.*
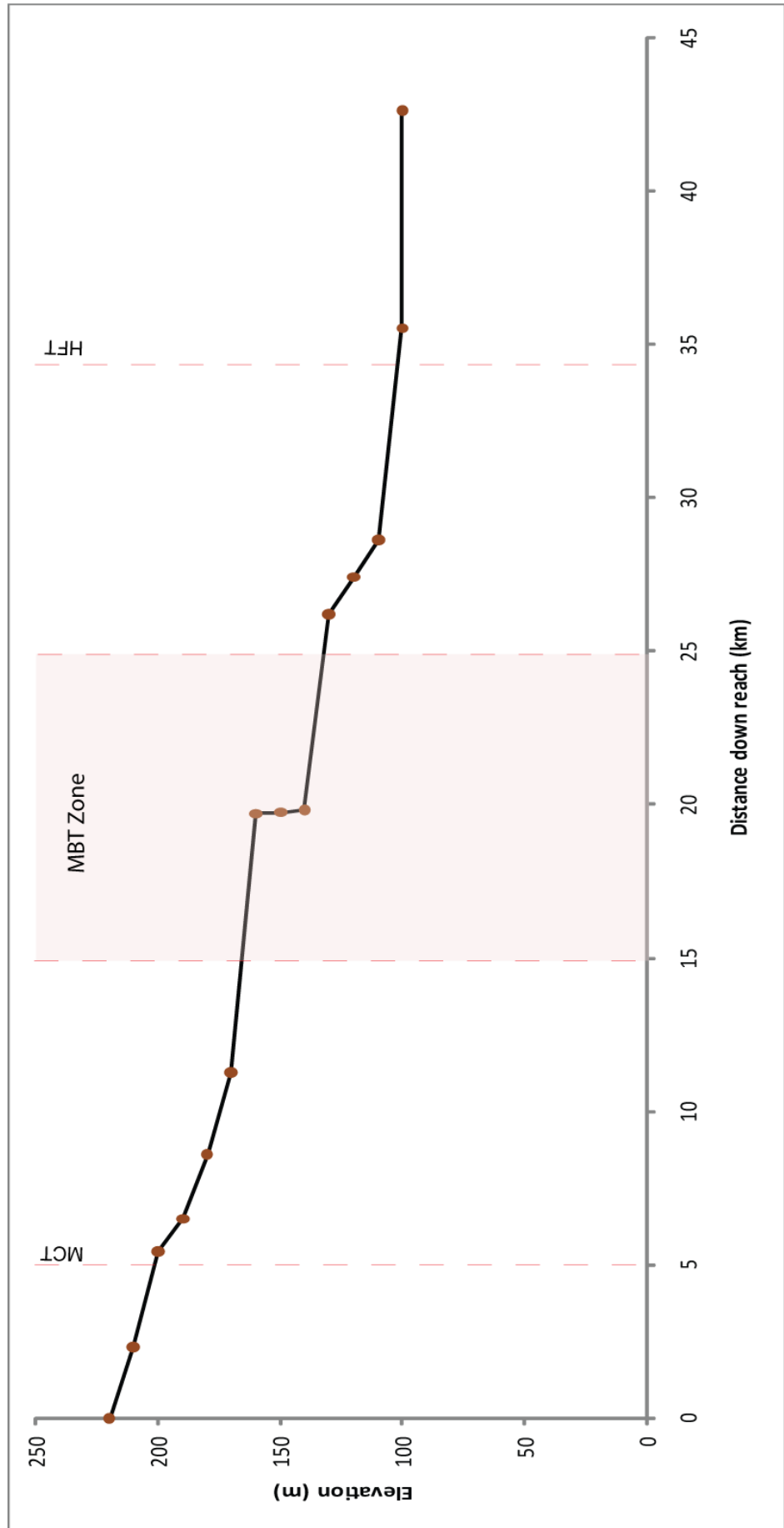
4.3 Channel slope

Using successive points on the longitudinal profiles, channel slope has also been calculated for each river using the methods as described in Chapter 3.

The Gandak channel slope as represented in Figure 4.7 shows to peak values of 0.0089 m/m and 0.0098 m/m for points coinciding with the MBT and MDT respectively (4.8 and 20.3 km downstream). Between these points, channel slope is reduced to ~0.002 m/m. On entering the Chitwan Dun, channel slope drops to ~0.0009 m/m and increases very gradually to ~0.0012 m/m. On exiting the Dun, channel slope drops again to a minimum of 0.00046 m/m approximately 300 m upstream of the HFT. On crossing the HFT, slope increases marginally to ~0.0007 m/m. Overall, there is a gradual reduction in slope on passing through the Gandak study reach. The two main points of interest are focused around the MBT and MDT boundaries.

Channel slope for the Kosi River (Figure 4.8) is dominated by a large peak in slope values, occurring within the MBT zone at ~20 km downstream. At this point, slope values rise from 0.0012 m/m to 0.28 m/m, before dropping off rapidly to 0.14 m/m and 0.0016 m/m by 26 km downstream. There are two other minor rises in channel slope, the first located at 6.5km downstream with slope rising briefly to 0.0093 m/m for ~2 km and the second at 27-28 km downstream where slope values briefly rise by the order of 0.0065 m/m. The first of these minor slope rises occurs ~2 km downstream of the MCT and the second is ~3 km upstream of the HFT. As the rise in slope is only minor, it is possible that they relate to holes in the DEM, or may be ancient fault scarps that have migrated upstream from the HFT and MBT. To determine if these rises in slope are related to tectonic uplift, a comparison to other morphological variables such as channel width and grain size will be required to see if similar changes are noted at these points in the study region.

The number of slope values that could be obtained from the longitudinal profiles is low leading to questions of the reliability for both sets of slope data. This is a direct result of the overall low gradient of both study regions that restricted how many contour-thalweg intersection points could be used, as contours could not be constructed at intervals less than 10 m due to the RMS error of both data sets.

Figure 4.7. *Gandak channel slope variations as calculated from the longitudinal profile extracted from SRTM data in Figure 4.1.*
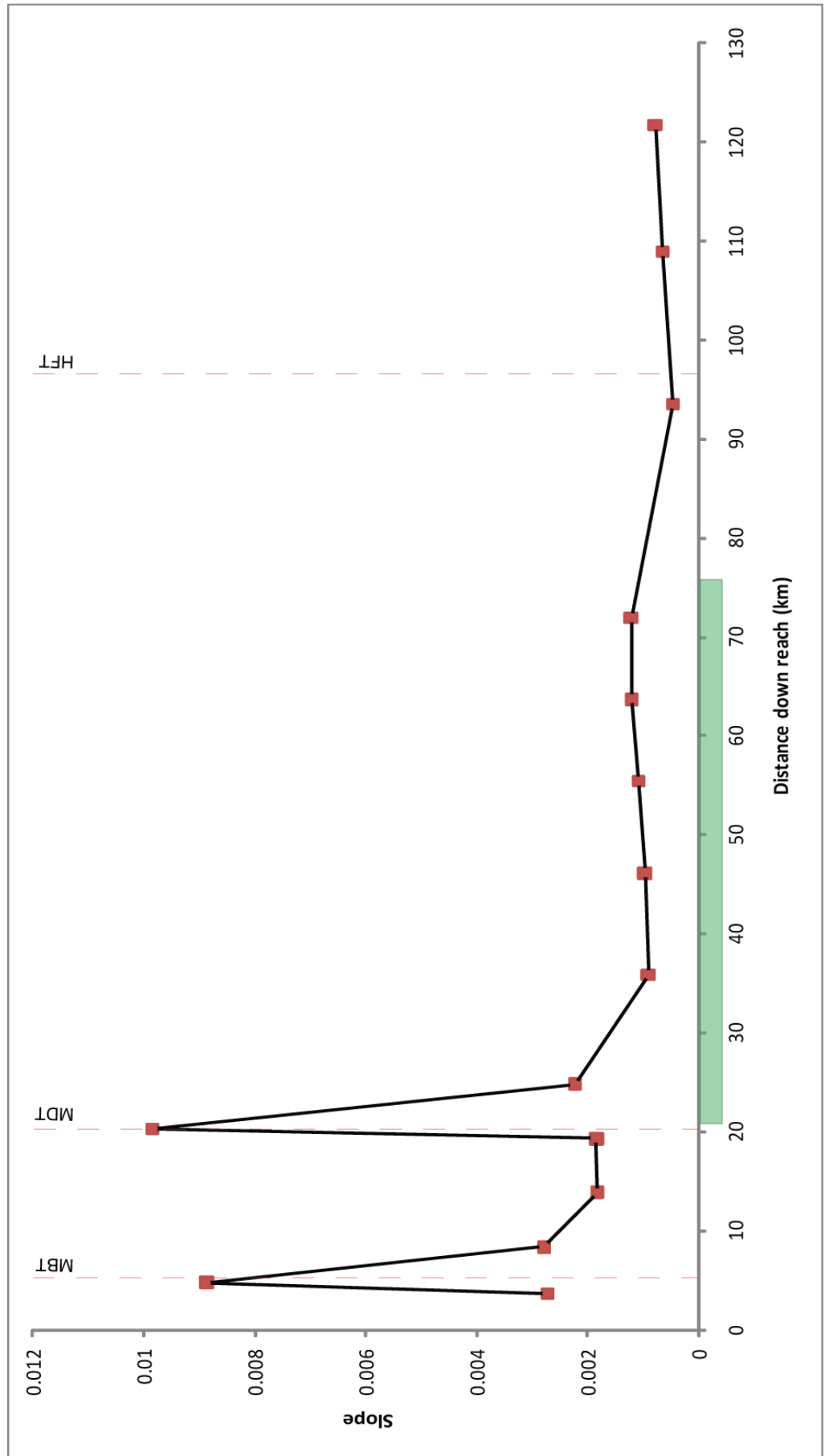
Figure 4.8. *Kosi channel slope variations as calculated from the longitudinal profile extracted from SRTM data in Figure 4.2.*
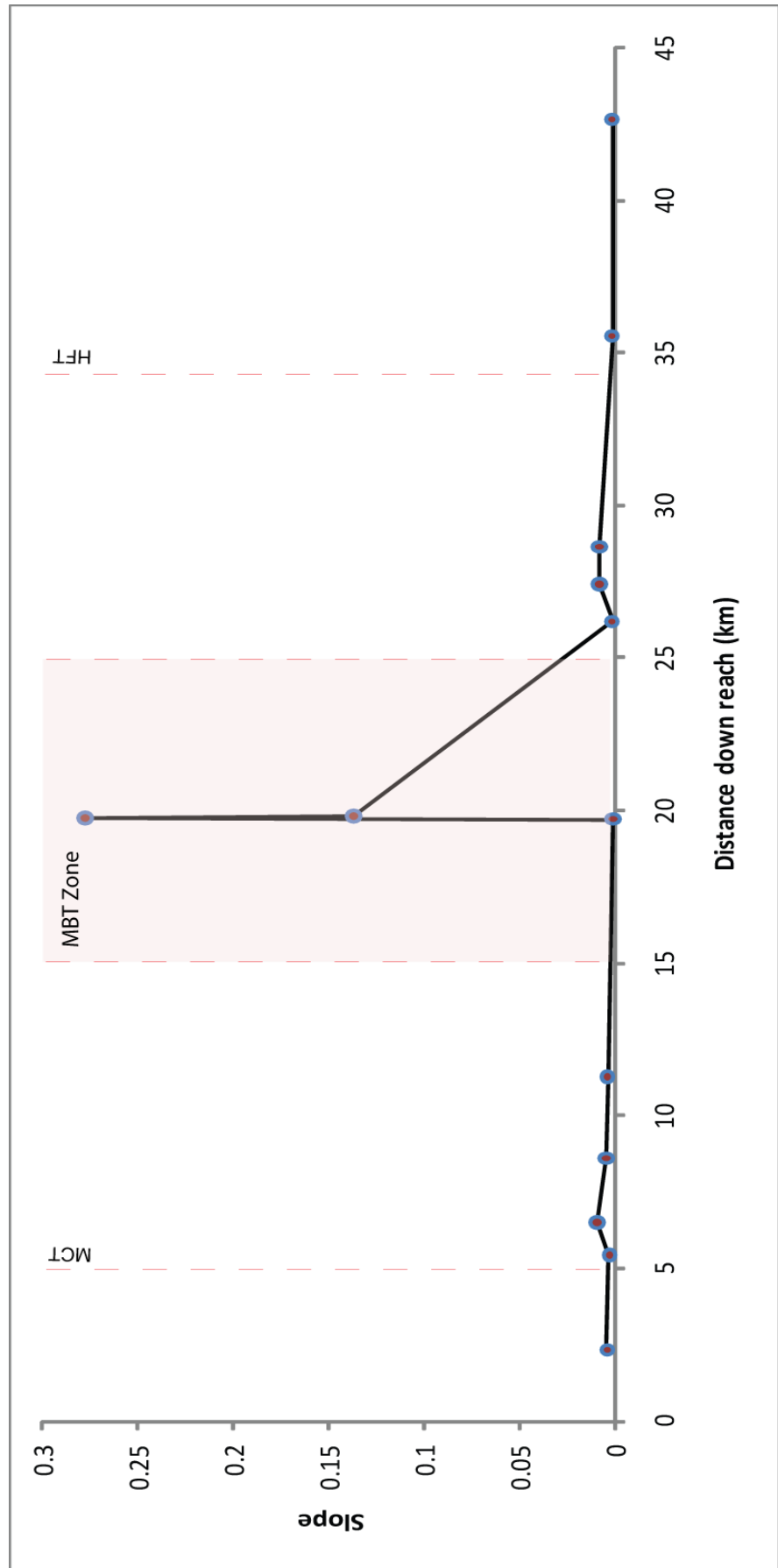
4.3 Channel width

Both active channel and channel belt measurements as defined in Chapter 3 were extracted from LISS-3 datasets on the Gandak and Kosi Rivers. Active channel widths for the Gandak increase downstream within the study reach as shown in Figure 4.9. The most notable feature where channel width is drastically different is as the river flows through the Chitwan Dun. Prior to entering the Dun, channel width does not exceed 430 m as it passes through the Siwalik Hills. Similarly, between the exit of the Chitwan Dun and the frontal fold at the HFT, channel width remains below ~400 m. On entering the Dun, active channel width both increases and fluctuates quite dramatically until reaching a maximum width of >1600 m at 46.5 km. Channel width continues to fluctuate between ~600 m to ~1100 m until the river exits the Dun and enters the restricted bedrock channel of the final topographic barrier (Siwalik Hills) of the Himalayan mountain front. Within a distance of 1 km (77-78 km), channel width drops from 1010 m to 390 m. On approaching the HFT, there is also a significant increase (~500 m) in channel width starting approximately 5 km before the position of the fault as given by Lave and Avouac (2001). However, the Gandak Dam is situated 1 km downstream of the HFT and affects the measured channel widths in this region. Therefore, it is exceptionally difficult to distinguish whether the dam or the fault controls the observed change in channel width without data collected prior to the dam construction. Upstream of both the MBT and MDT there are minor increases in channel width (~50 m and ~250 m respectively), followed by equally small reductions downstream of each fault.

A similar pattern is also noticeable with Gandak channel belt width variations (Figure 4.10), in that belt width is drastically elevated within the Chitwan Dun reaching a maximum value of ~5100 m at 47.5 km. Interestingly, there is a significant but short reduction in channel belt width within the Dun at ~60 km where the channel width is restricted to 596 m. Unlike active channel widths, channel belt measurements within the Dun also increase much more smoothly from ~32 km to the maximum width at 47.5 km. After passing through the Chitwan Dun and frontal fold, channel belt width increases to ~2400 m from ~800 m (in the space of <10 km) downstream of the Gandak Dam. Again, there is only a minor change in channel belt width on approaching the MBT and MDT. On both datasets however, between 11-14 km, width measurements are briefly elevated yet remain <500 m. There appears to be no significant relationship between channel width and the position of tributary confluences either.

As can be seen in Figure 4.11, the active channel widths of the Kosi River are significantly smaller than the Gandak active channel widths in Figure 4.9. For the first 20 km of the study reach, there is no clear increase in channel width. Prior to crossing the MCT there are two 'spikes' representing elevated channel widths before quickly narrowing on the downstream side

of the fault. Active channel width then fluctuates about 100 m until 22.5 km where width starts to increase to ~360 m just upstream of the HFT. On crossing the HFT, active channel width decreases again to ~150 m before rising rapidly to ~650 m at 40 km. By this point, the Kosi has exited the mountain front and is passing over its alluvial mega fan surface. Two areas of interest can be inferred from Figure 4.11, both relating to regions of elevated active channel width. The first is upstream of the MCT where channel width is briefly elevated (the widest part in the first 30 km) before reducing to pre-MCT widths. The second region is prior to the HFT where again, channel width is briefly elevated for a couple of kilometres prior to the thrust fault. Interestingly, there is no major increase as the Kosi flows through the MBT zone, except at perhaps 23 km where active channel width increases to 216 m. This figure is only 50 m higher than any other width within the MBT zone however, so should be treated with caution.

Kosi channel belt widths as displayed in Figure 4.12 display similar trends to those described in Figure 4.11. There is no significant change in channel width until ~30 km after which point channel belt width increases steadily for 5 km to ~2000 m before crossing the HFT. A minor increase in belt width is evident upstream of the MCT (~200 m) and there is no obvious change on crossing the MBT 'zone'. The most significant finding from channel belt measurements is the dramatic increase in width prior to the HFT.

Figure 4.9. *Active channel width variations as taken every 500m on LISS-3 imagery down the length of the Gandak study reach. Also shown are the positions of the confluences of the major tributaries.*
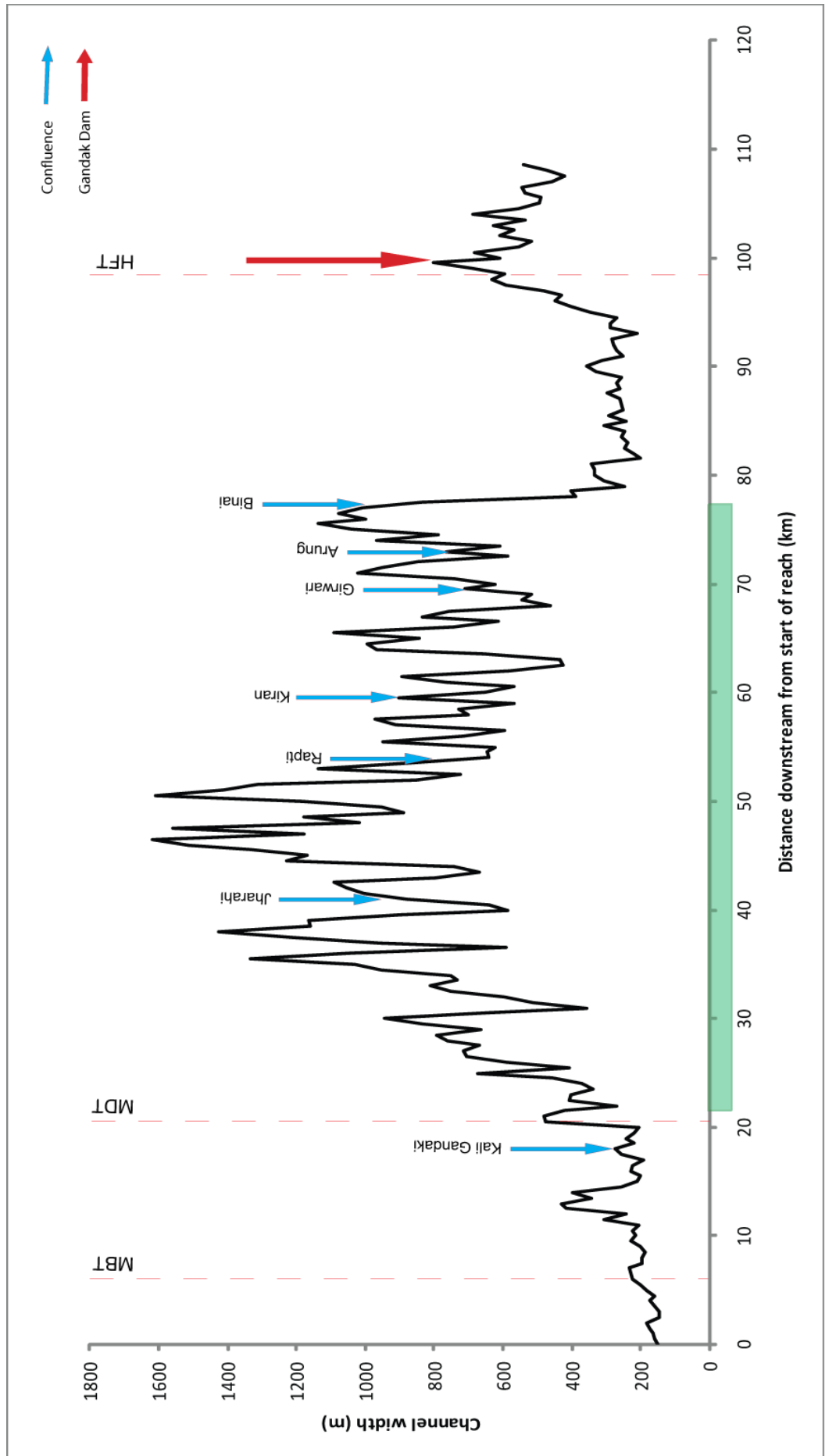
Figure 4.10. *Channel belt width measurements as taken every 500m on LISS-3 imagery down the length of the Gandak study reach.*
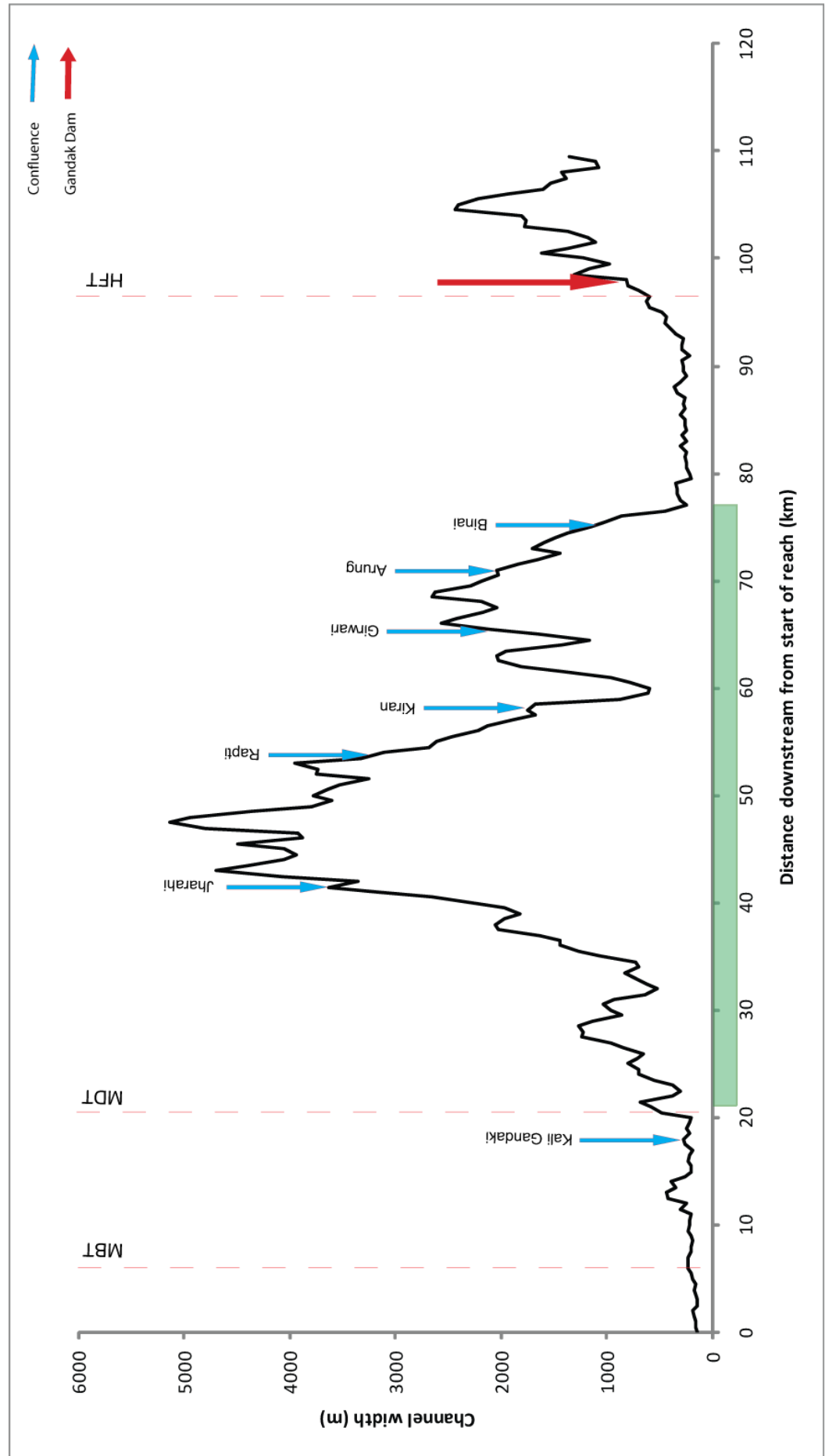
Figure 4.11. *Active channel width measurements as taken every 500m downstream of the Kosi River study reach on LISS-3 and LISS-4 imagery.*
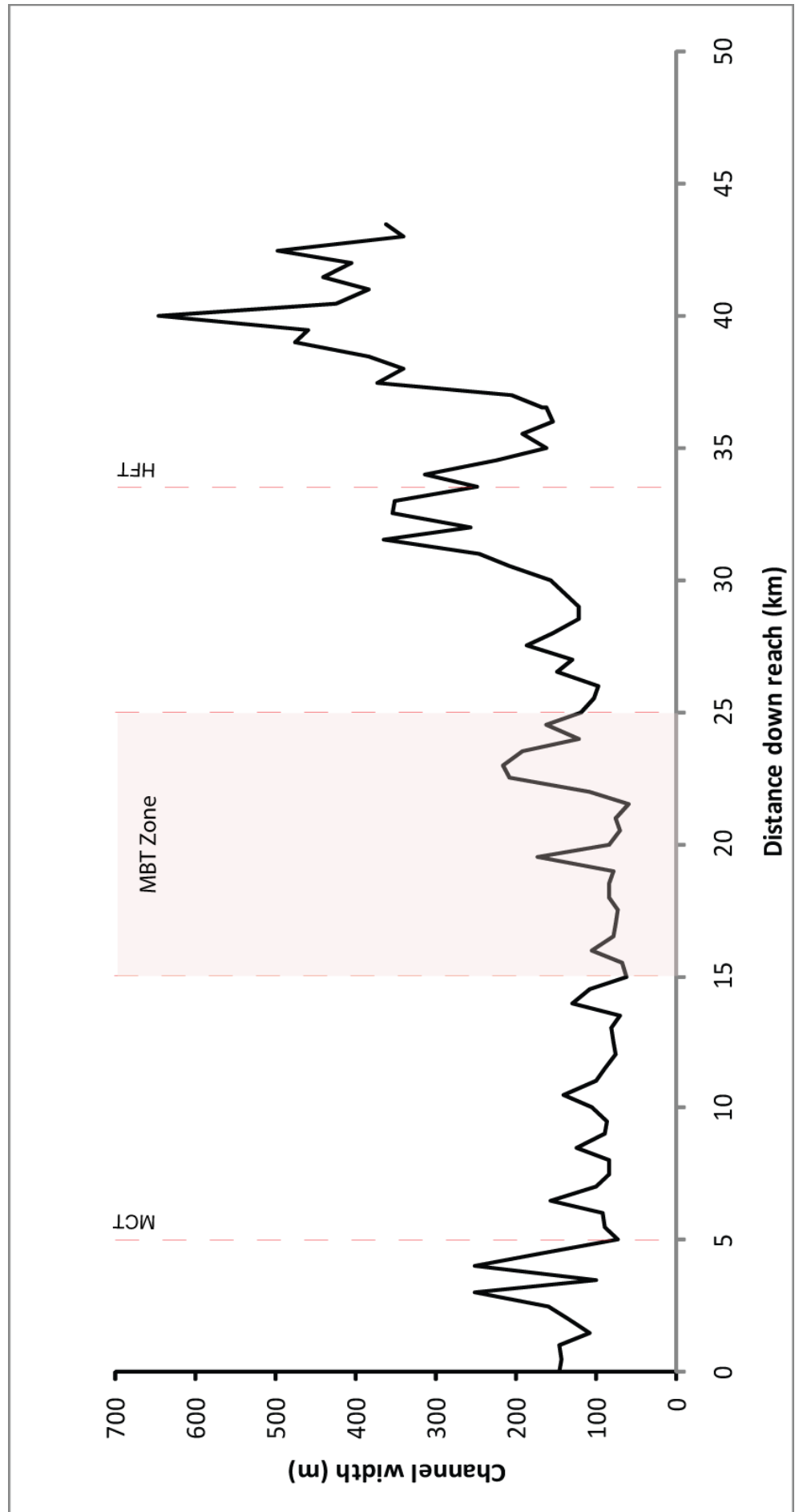
Figure 4.12. *Channel belt width measurements as taken every 500m downstream of the Kosi study reach using LISS-3 and LISS-4 imagery.*
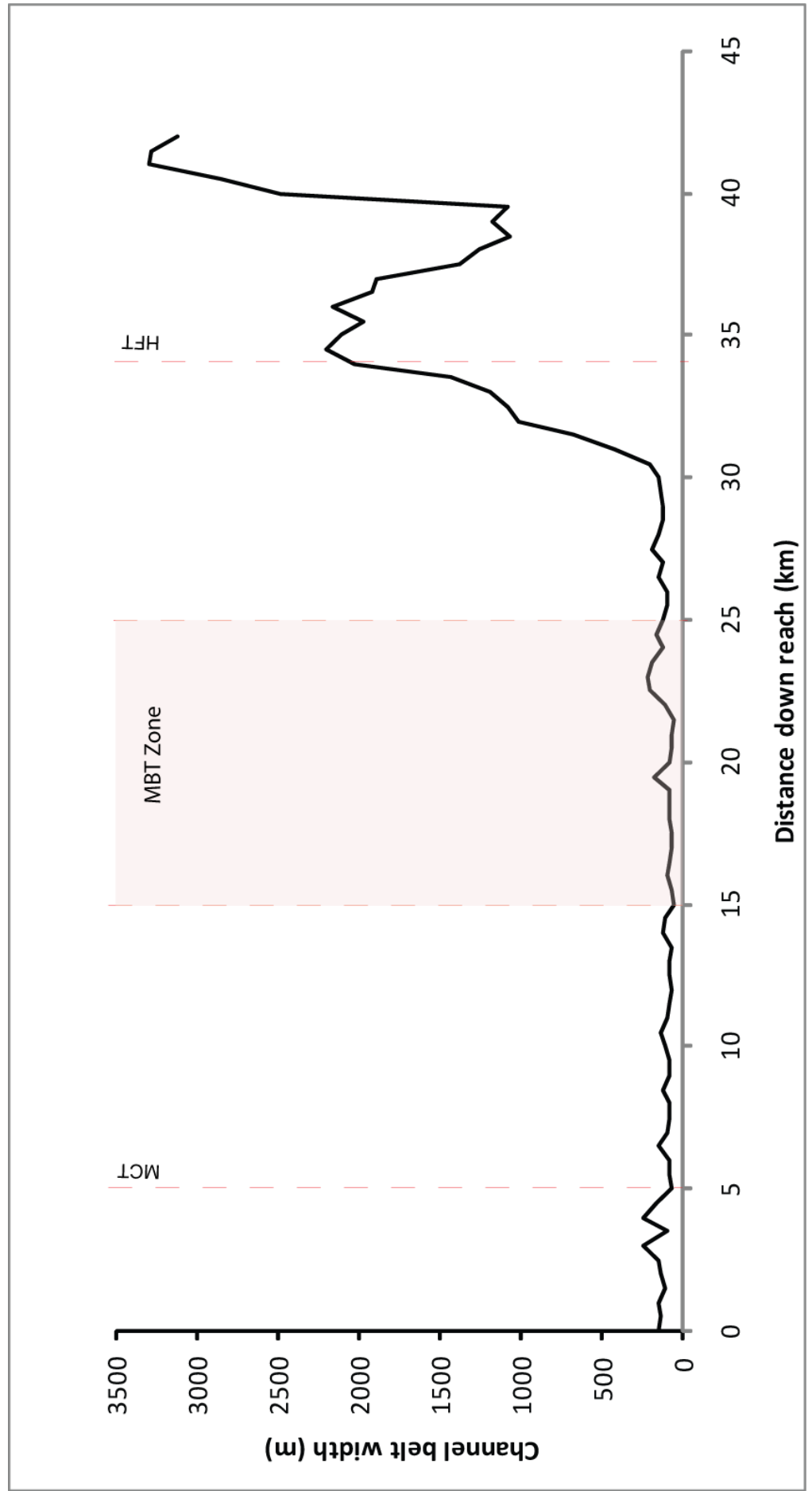
4.5 Grain size and grain size distribution

As is apparent in Figure 4.13, there is an overall reduction in D_{84} along the Gandak River through the study reach. In the first 20 km of the study reach, D_{84} shows its most significant reduction in size from ~190 mm to ~145 mm a couple of kilometres upstream of the MDT. Within the Chitwan Dun, D_{84} grain size for samples from both the Gandak River and its tributaries lie between 70 mm-160 mm. A gradual coarsening of D_{84} on passing through the Chitwan Dun is also apparent in main stem river samples. Interestingly, tributary samples display a smaller D_{84} value than main stem samples, which questions what is the source of coarse sediment that produces an increase in D_{84} within the main river as it passes through the Dun. The two samples taken before the HFT (G1 and G2) are quite small in comparison to the upstream non-Dun samples (G13-G9), but there is a step up in D_{84} size on approaching and passing the HFT. A similar increase in D_{84} is also visible upstream of the MDT.

To reflect the spread of D_{84} values taken from each sample location, the values from each photo have been plotted in Figure 4.14 with Box and Whisker plots in Figure 4.15 to demonstrate the Q1, Q3, median, maximum and minimum values for the D_{84} data . Interestingly the samples with the largest spread of data, and therefore standard deviation, occur within the first 20 km, which also corresponds to the samples with the highest average D_{84} as shown in Figure 4.8. On entering the Dun, the spread of D_{84} within each sample is generally much smaller (excluding G7 at 30.5 km, which has one outlier that is nearly 100 mm greater than the rest of the values). Again, this raises an excellent point for discussion in Chapter 5. Similar trends in grain size distribution inside and outside of the Dun are noticeable in D_{50} and D_{16} Box and Whisker plots (Figure 4.16 and 4.17) but with a smaller contrast between differences in these two settings, and in general the spread of D_{16} and D_{50} sizes is more restricted. The median values for D_{50} and D_{16} Box and Whisker plots lie within ~150 mm and less than 50 mm of each other respectively, and median values of the D_{84} plots lie in the excess of 300 mm of each other which is a significant difference.

D_{84} variations along the Kosi are represented across a much smaller number of sites (Figure 4.18). Overall, there is a decrease in D_{84} over the study reach. There is also a significant coarse input from the Tamur tributary (K6) as the Kosi passes through the MBT 'zone' at 23.5 km. By the next sample at 31.5km (K4) this coarse signal is no longer evident. Based on a small number of samples, there is an increase in D_{84} upstream of the HFT followed by an abrupt decrease downstream of the structure, but there are insufficient sample sites to draw firm conclusions.

Figure 4.13. *Averaged D_{84} values for each grain-size transect site along the Gandak River. The average D_{84} for each tributary transect is shown in red.*
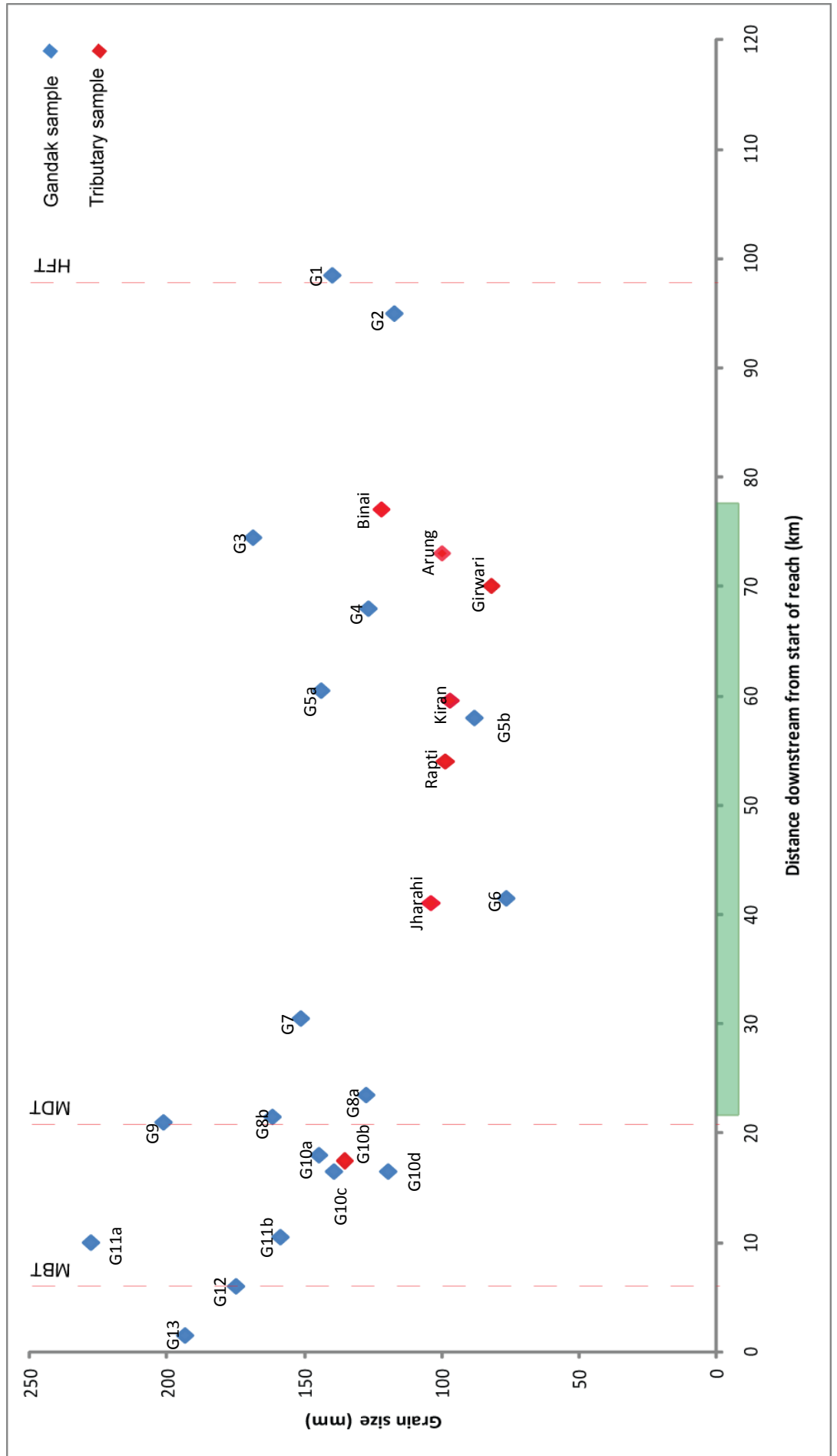
Figure 4.14. *The D_{84} value for each individual photo at each Gandak transect site is plotted to demonstrate the spread of D_{84} values at a single location. The average D_{84} is also plotted.*
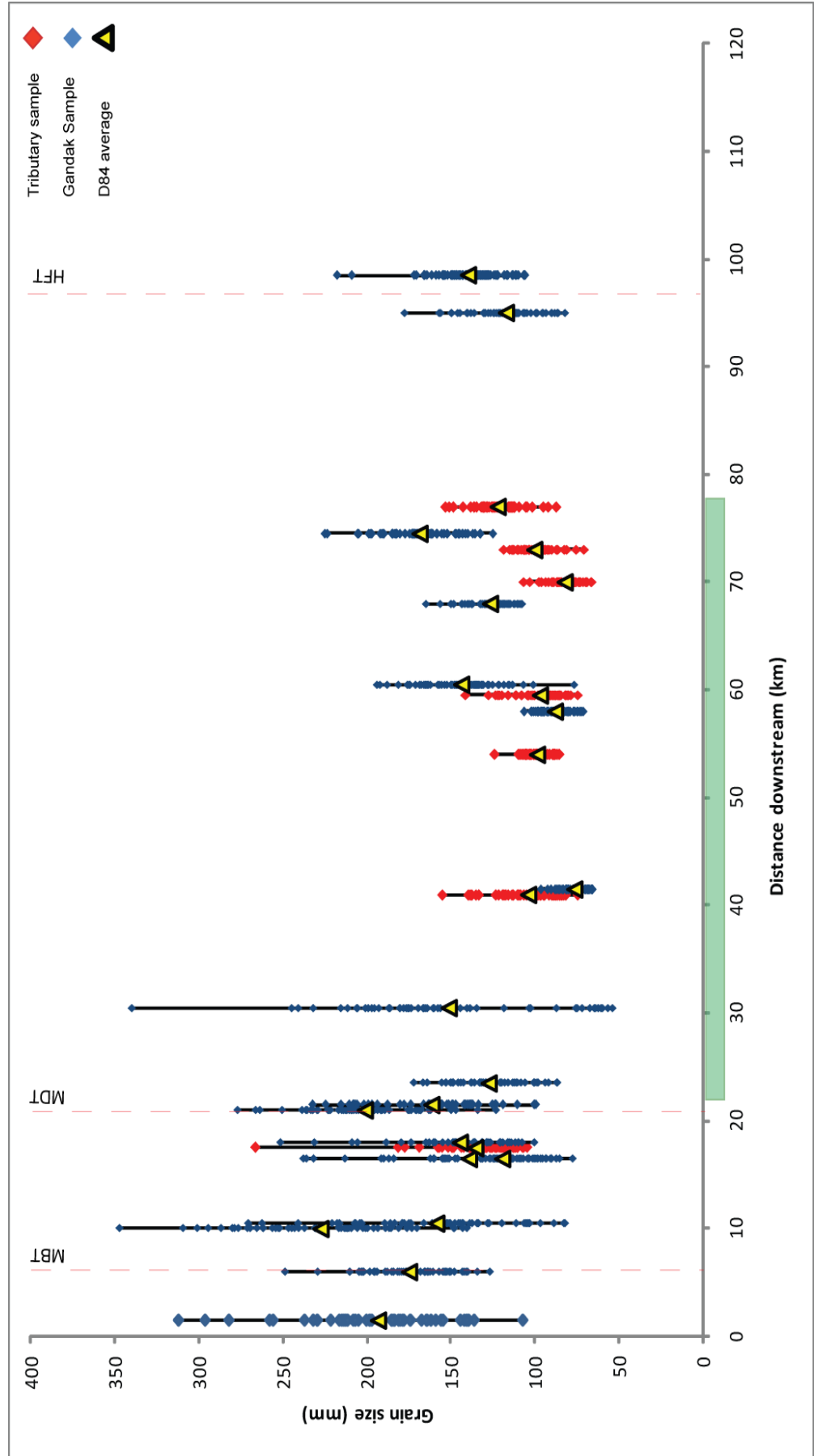
Figure 4.15. *Box and Whisker plots for the D_{84} values taken within the Gandak study reach*
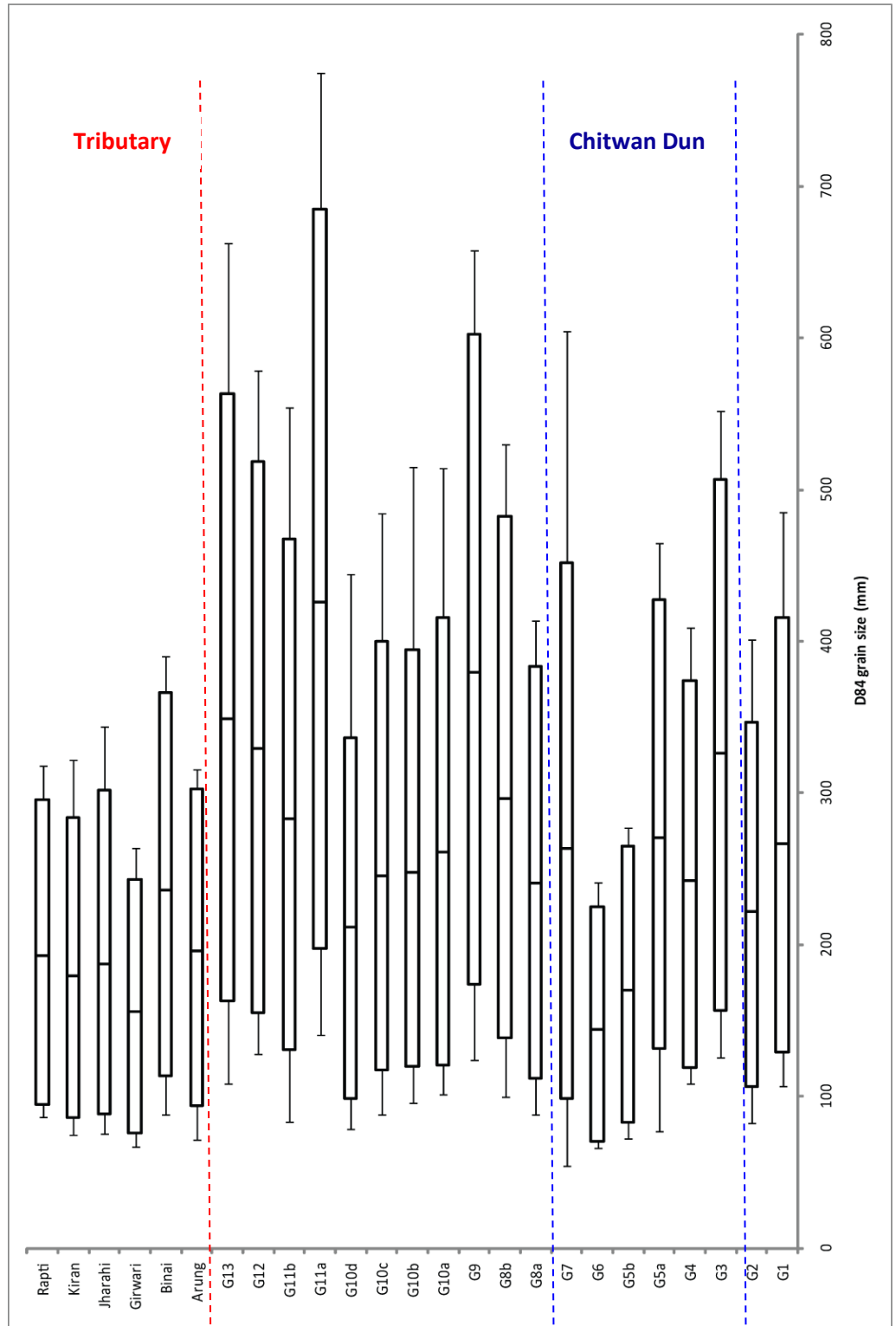
Figure 4.16. *Box and Whisker plots for the D_{50} values taken within the Gandak study reach*
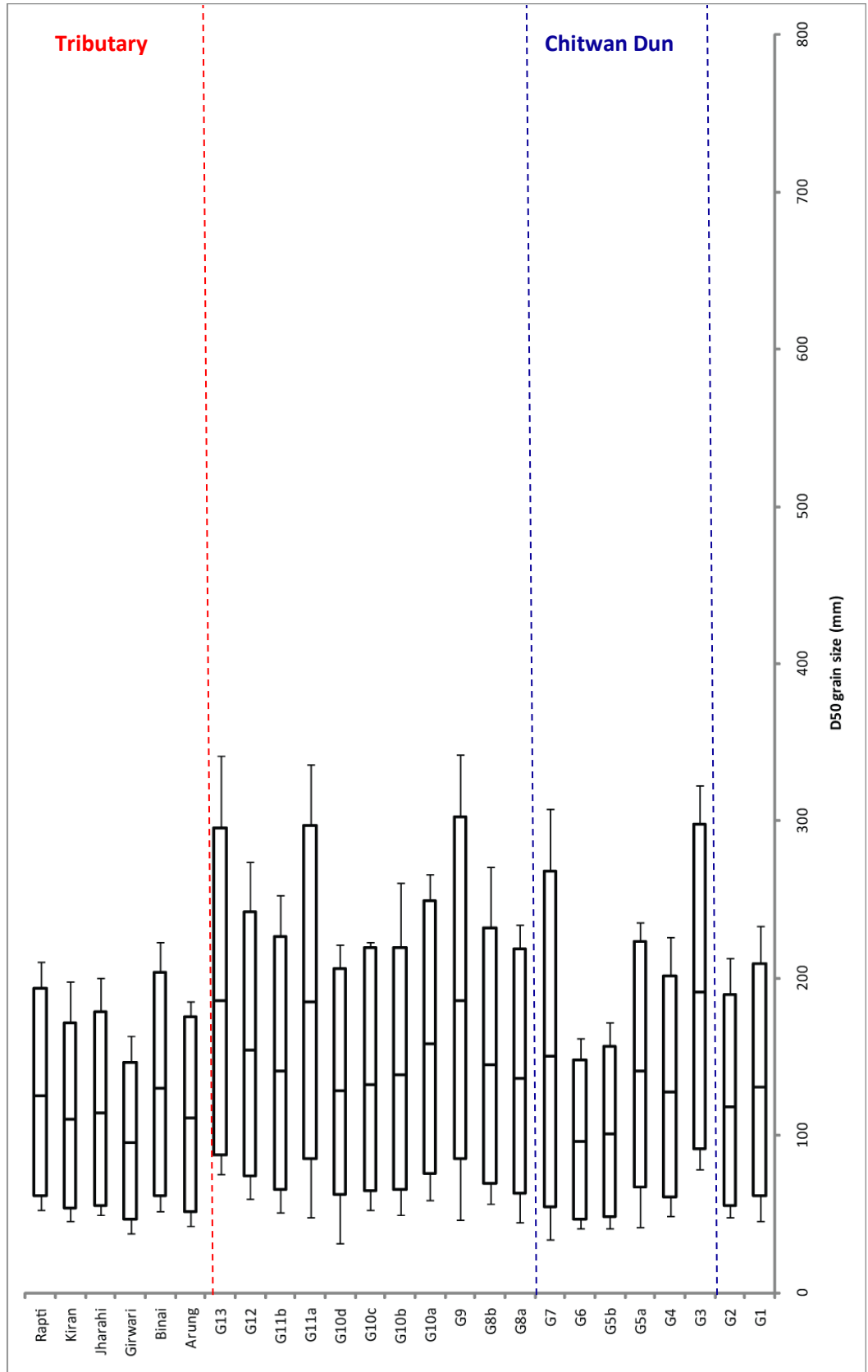
Figure 4.17. *Box and Whisker plots for the D_{16} values taken within the Gandak study reach*
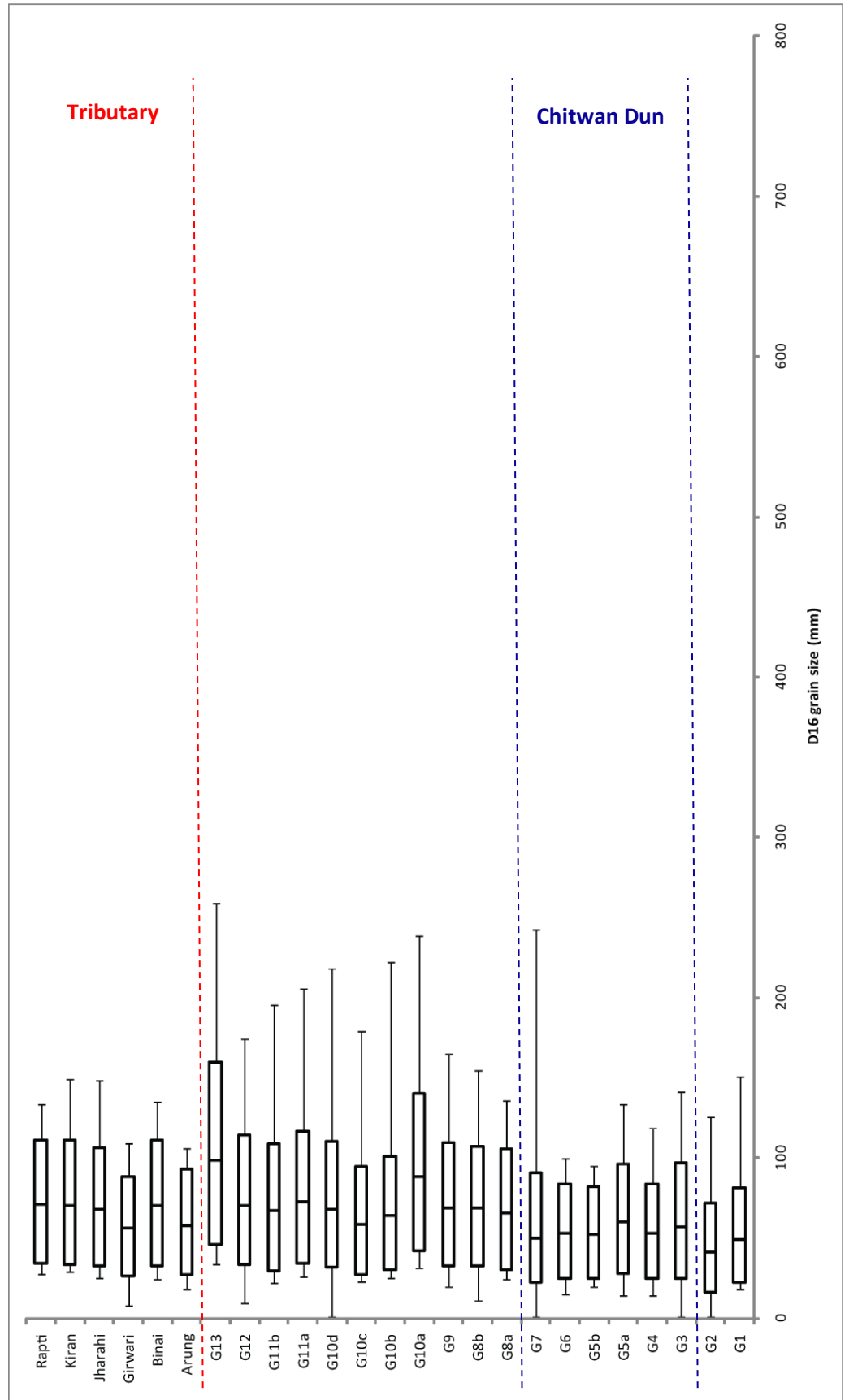
Figure 4.18 *Both the individual and averaged D₈₄ values of photo-sieving images from each transect along the Kosi River.*
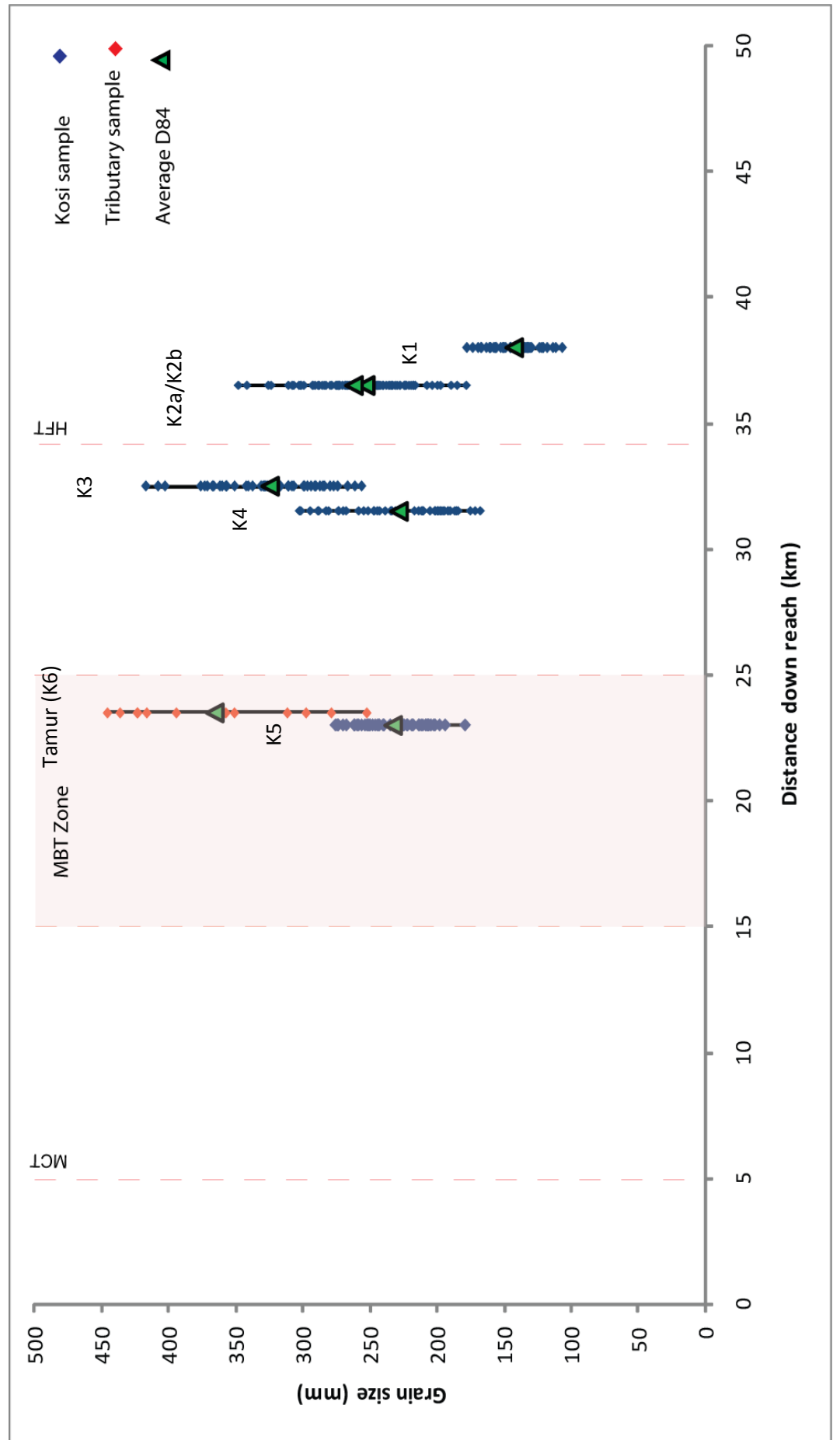
4.6 Shields stress and critical stream power

The Shields stress or Shields number of a flow is a dimensionless measure of shear stress exerted by flow on a bed that enables us to quantify the ability of a flow to mobilise sediment of a particular size (Church, 2006):

$$\tau^* = \frac{\rho g S d}{g(\rho_s - \rho)D} \qquad [7]$$

Where ρ_s and ρ are the sediment and fluid densities (kg/m^3), g is the acceleration due to gravity (9.81 m/s), S is channel slope, d is flow depth (m) and D is the grain size to be moved (m). A critical Shields stress for entrainment (τ^c) is estimated at ~0.045 when D is equal to D_{50}. Where grains are imbricated, larger grains will shelter smaller ones. When these larger grains are entrained at the critical value for entrainment (τ^c), smaller grains will quickly follow suit (Church, 2006). Applying this formula to grain size data collected in the field, DEM derived slope value and flow depth measurements taken in the field or estimations from observations, it is possible to see how the Shields number varies downstream. By rearranging the formula, the D_{50} value that the flow should be capable of entraining, at the critical Shields value, may also be calculated. By comparing this value of D_{50} with the observed values in the field, it should be possible to determine whether the sediment deposits are transport or supply limited. If the field value of D_{50} is significantly higher than that estimated from equation [7], it would suggest that the system is transport limited. Alternatively, if the calculated value of D_{50} exceeds the field value, it would be expected for the system to be supply limited as the flow is capable of carrying much larger grain sizes. The Shields stress which is formulated in equation [7] also allows for the classification of river channels into broadly defined categories including jammed ($\tau^* =$ 0.04+), threshold ($\tau^* =$ 0.04-0.15), transitional ($\tau^* =$ 0.15-1.0) and labile channels ($\tau^* > 1.0$) (Church, 2006). Each category has characteristic features based around sediment type, sediment transport regime, channel morphology and channel stability.

Above a critical level of stream power, bed load transport dramatically increases. Building on Bagnold's original equation for critical stream power, Ferguson (2005) presents a new definition which allows for the partitioning of grain size between what the flow is capable of transporting, and the grain size that acts as a representative size for the bed surface. Furthermore, it does not rely on flow depth but rather channel slope as shown:

$$\omega_{ci} = 0.104 \frac{D_b^{1.5}}{S^{0.17}} \left(\frac{D_i}{D_b}\right)^{0.67} \qquad [8]$$

Where the median grain size of the bed is denoted as D_b (mm), and the grain size capable of being entrained (as calculated using the critical value of entrainment in equation [7]) as D_i (mm). Critical stream power (ω_{ci}) is given units of Wm^{-2}.

Applying equations [7] and [8] to a number of locations down the Gandak and Kosi study reaches, the results in Table 4.1 are produced. Slope values have been taken directly from 10 m contour values of the DEM in methods described in Chapter 3, and depth values from a combination of averaging readings made during a channel cross-section construction at Devghat, one estimate made from isolated depth readings whilst crossing the Gandak at G2, and estimates based on field observations. The density of sediment has been taken as 2500 kg/m^3 as is a combination of Siwalik sandstone and Lesser Himalayan pyllite/quartzite lithologies.

Table 4.1. *Results obtained from Shields number and critical stream power calculations*

Location	Shields Number	Observed D_{50} (mm)	D_{50} (mm) calculated from critical value of entrainment	Critical Stream Power (Wm^{-2})
G12	0.584	81	1052	943
Devghat (G10d)	0.116	67	174	315
G3	0.0325	100	72	261
G2	0.0287	65	41	147
K5	0.0702	134	209	651
K4	0.0620	109	150	445

At G12, the D_{50} value calculated at critical Shields stress is over ten times the size of the observed D_{50}. At G10d, the magnitude in difference is reduced so that the calculate value is less than three times the size of the observed D_{50}. Within the Dun, the observed D_{50} is larger than the calculated by a margin of <40 % of the observed value. At the two sites considered along the Kosi, the calculated D_{50} is larger than the observed D_{50} but lies within a margin of ~50 % of the observed D_{50} value.

Critical stream power reduces downstream in both instances. The samples G2 and K4 are both just upstream of HFT yet K4 displays a significantly higher critical stream power value, which is over three times the value of G2.

4.7 Chapter summary

The key findings which may be taken from these results are:

1. Upstream of the HFT, the Gandak longitudinal profile flattens out and slope is reduced. On crossing the MBT and MDT there is a sudden 10m drop in elevation of the Gandak, which is also reflected by peak slope values (Figures 4.5 and 4.7).

2. The Kosi displays one major and two minor breaks in slope (of 10-20 m change in elevation). The first minor and the major drops in elevation coincide with the MCT and the MBT respectively. For the other minor change, it is possible that it represents a migrated knick-point from an ancient surface rupture about the HFT. There is no evident change in slope or elevation about the modern HFT (Figures 4.6 and 4.8).

3. There are no significant changes in channel width about the MBT or MDT on the Gandak River. There is significant widening of the channel on approaching the HFT however, but it is likely that there is an influence from the Gandak Dam which will disguise any geomorphological response from the Gandak to the HFT.

4. Upstream of both the MCT and HFT on the Kosi River there is a notable increase in channel width. No such trend is apparent about the region of the MBT.

5. There is a subtle increase in D_{84} on approaching the MDT along the Gandak River. A subtle increase is also evident on approaching and passing the HFT. Whilst in the Chitwan Dun, grain-size values for D_{84}, D_{50} and D_{16} are more homogenous with less spread in the data than samples north and south of the Dun, indicating a greater level of sorting. There is also an increase in D_{84} within the Dun before exiting the Siwalik Hills, despite the small grain sizes displayed in the major tributaries (Figures 4.13, 4.14, 4.15, 4.16 and 4.17).

6. There are too few grain size samples from the Kosi to draw firm conclusions but there appears to be an increase in D_{84} prior to the HFT (Figure 4.18).

7. Within the Gandak River, tributaries contain a greater proportion of Greater Himalayan lithologies than deposits within the Dun, but the coarsest grains remain Siwalik in lithology.

8. There is adequate connectivity between hill slopes and rivers for substantial quantities of Siwalik sediment to enter the non-Dun regions of the Gandak and Kosi River systems.

9. There is an overall decrease in Shields stress and critical stream power values downstream in the Kosi and Gandak study reaches. At the mountain front, the Kosi River displays a higher critical stream power than the Gandak (Table 4.1).

Chapter 5: Discussion

Both the Gandak and Kosi Rivers display morphological adjustments on exiting the Himalayan mountain front. Along both rivers there are distinct changes in channel width, slope, elevation, grain size and grain size distribution which are broadly found to correlate with tectonic boundaries and inputs of hillslope or tributary sediments. The following chapter will consider and differences between morphological responses on the Kosi and Gandak Rivers, and to use evidence from this research to challenge or satisfy the original hypothesis as stated in Chapter 1.

5.1 Morphological adjustments to tectonic features at the Himalayan mountain front

There is significant evidence to suggest that channel morphology is at least partially controlled by the positioning of major tectonic structures across the Himalayan foreland. The key morphological responses displayed by both the Kosi and Gandak Rivers to the HFT are a reduction in channel slope and an increase in channel width initiating within 10 km upstream of the fault, as might be expected on the uplifted (relative) hanging wall of an active thrust fault (Figure 5.1). The impact of the Gandak Dam on channel morphology is likely to enhance any increase in channel width associated with the HFT, however.

Further upstream, there are notable changes in slope evident about the MBT (or MBT zone on the Kosi), MDT and the MCT as highlighted on Figure 5.1. At both the Kosi and Gandak MBT and Gandak MDT, there is an increase in slope in the region of the respective faults. This change in slope or drop in elevation is less pronounced downstream of the MCT on the Kosi. Above the MCT on the Kosi, there is also a short reach of ~ 3 km of increased channel width, which narrows again downstream of the fault. Trends in channel width about the MBT on the Kosi are not as pronounced, with only a minor increase in channel width upstream of the fault followed by a narrowing of a similar magnitude on crossing it. There appears to be minimal change in channel width about the MBT on the Gandak. In the case of the MDT however, there is a more prominent increase in channel width for 1-2 km on the hanging wall. This is followed by a sharp, but short-lived (over ~1 km distance), narrowing of the channel that corresponds with an increase in channel slope as the Gandak passes onto the footwall. The Kosi MCT and Gandak MDT display typical responses to tectonic uplift whereby on the uplifted hanging wall, channel width is forced to widen immediately upstream of the thrust fault. In such instances, a decrease in slope has reduced the stream power and transport capacity of the flow, resulting in deposition of its load and reduction in flow depth on approaching the fault boundary (Holbrook and Schumm, 1999). Where bedrock channels then cross tectonic boundaries, the channel should increase in slope and decrease in width (Finnegan *et al.*, 2005) immediately after crossing the fault, before returning to a state similar to that upstream of the hanging wall block. Based on the findings of this research, it would be expected for the river to return to the state it was upstream of the fault within 2-3 km downstream of the structure.
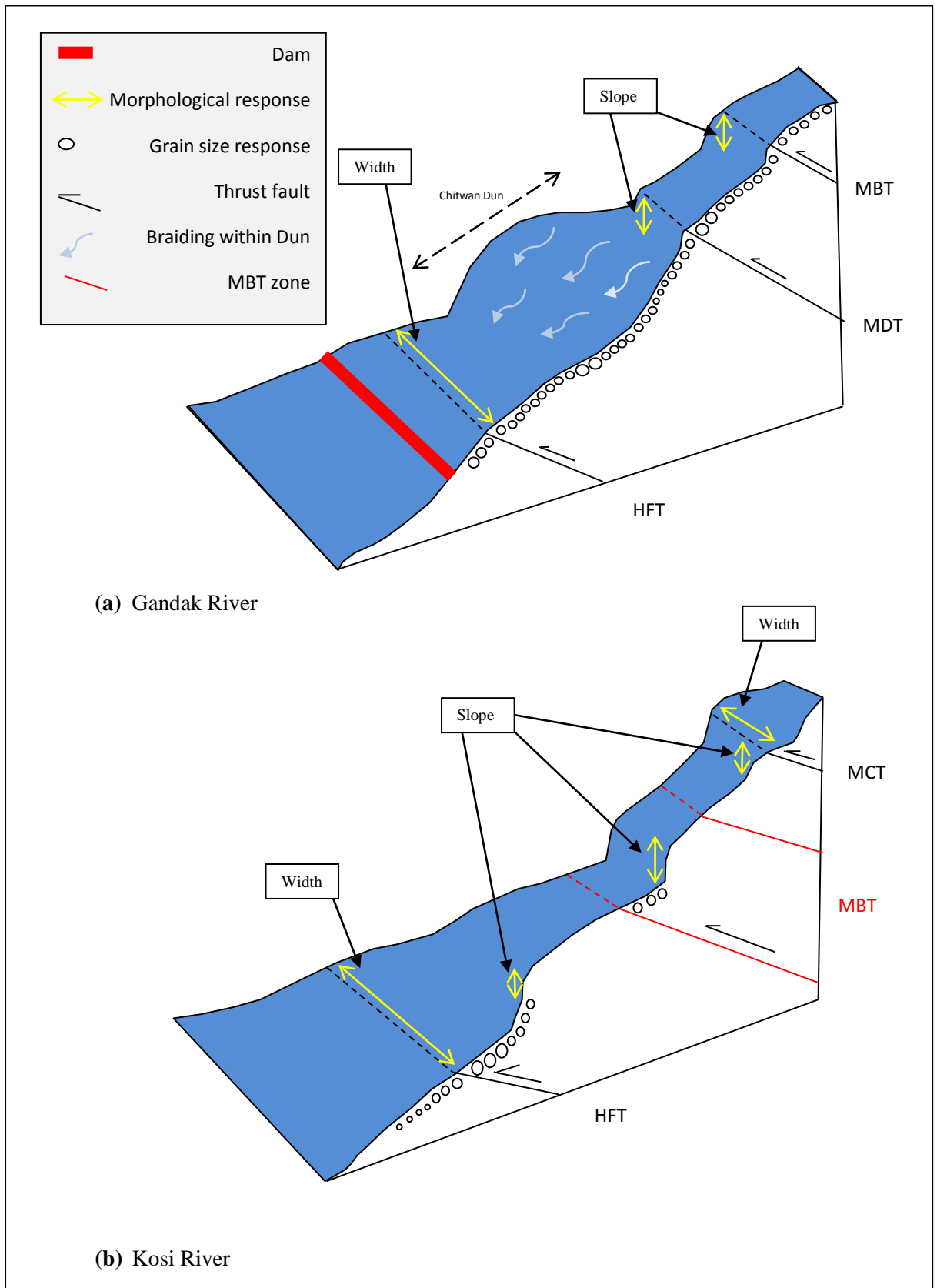
Figure 5.1 *Summary and graphical simplification of morphological responses to tectonic structures along the Gandak and Kosi Rivers on exiting the mountain front.*

In the case of the Kosi River, a potentially interesting knick point is highlighted in Figure 5.2a whereby a significant increase in channel slope is evident within the MBT zone, yet there is minimal change in channel width. Yanites *et al.* (2010) described similar findings along the Peikang River about the Meiyuan fault. The explanation given for this morphological response was that the channel had already achieved a minimum width, whereby channel walls accounted for too large a proportion of the wetted perimeter. In such instances, there is a large loss of energy and boundary stress via the channel walls and an insufficient amount left for vertical incision to balance the imposed rate of uplift. An increase in slope would be the only way to enhance vertical incision resulting in the creation of knick points along the Peikang River. Channel width about the MBT on the Kosi and Gandak Rivers is generally quite narrow, so the elevated slope values would fit with this hypothesis given by Yanites *et al.,* (2010).

The increase in width displayed by both rivers (Figures 5.1, 5.2a and 5.2b) on crossing the HFT reflects the removal of lateral restrictions imposed by the Siwalik Hills. This is also applicable to the Gandak River on entering the Chitwan Dun. On entering the alluvial stretch of the Chitwan Dun and the Gandak and Kosi mega fans, the critical shear stress for erosion of channel boundaries is significantly lower than that in the bedrock-dominated channels within the Siwalik Hills. This allows for lateral erosion of the channel banks at a significantly faster rate producing much wider and shallower channels. The reduction in slope upstream of the HFT is consistent with an uplifted hanging wall which is being actively incised by the river, but there is no increase in slope immediately downstream of the back-tilted block that might be expected about a fault associated with such high rates of rock uplift. Similarly, Lave and Avouac (2000) noted a near uniform gradient between the MDT and 10 km south of the HFT along the Bagmati River. Here, the uniform gradient surrounding the zone of active uplift was attributed to the large drainage area, and therefore stream power, of the Bagmati River that is able to maintain equilibrium with the high rates of rock uplift at the Himalayan foreland. Alternatively, the absence of channel slope change about active tectonic structures may arise from the channel's ability to accommodate a change in shear stress, which is suffice to balance tectonic uplift, entirely through changes in its width. This change in width would then set stream power at a rate sufficient to balance tectonic uplift with an equally high rate of vertical incision, removing any physical signal relating to a change in base level, such as a knick point. As discussed in Chapter 1, the high sediment loads of the Gandak and Kosi may also steepen the relationship between channel width and slope (Yanites and Tucker, 2010) so a more significant change in channel width rather than slope would be anticipated about the HFT.
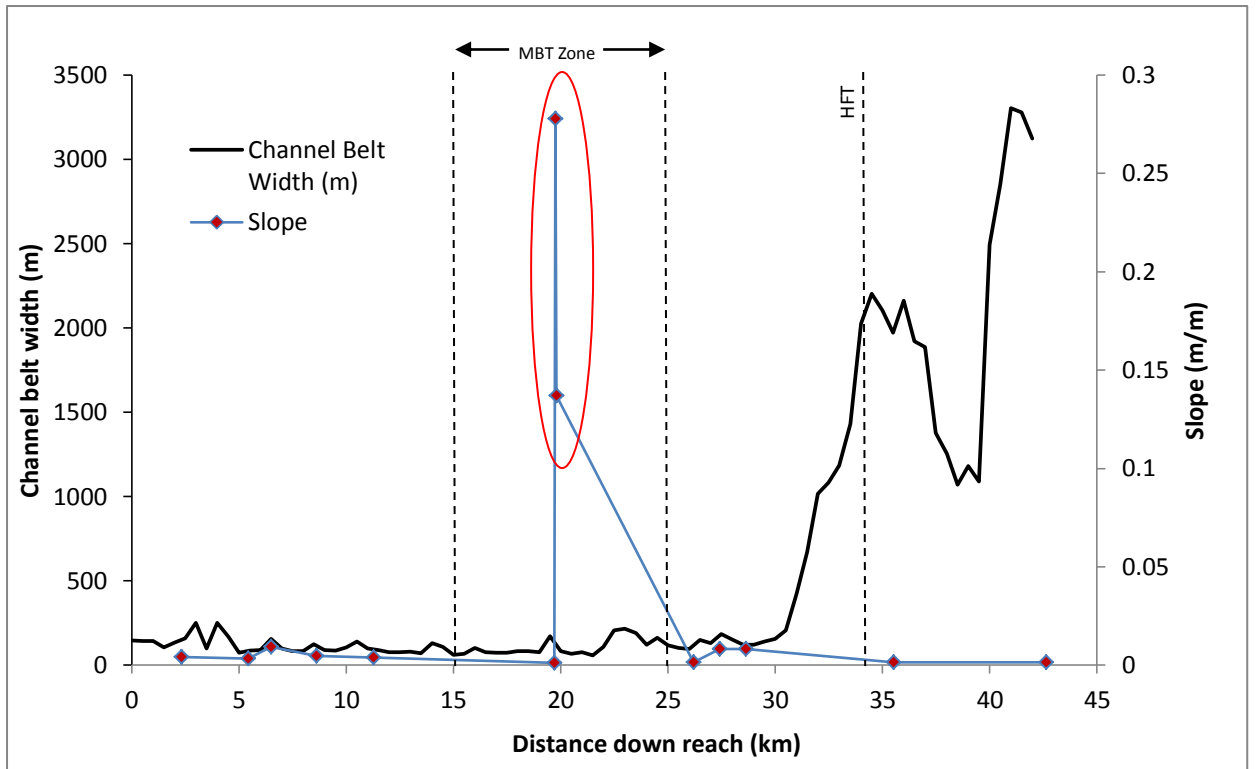
Figure 5.2a *Comparison of channel belt width and channel slope along the Kosi River, highlighted in red is the knick point identified within the MBT zone.*
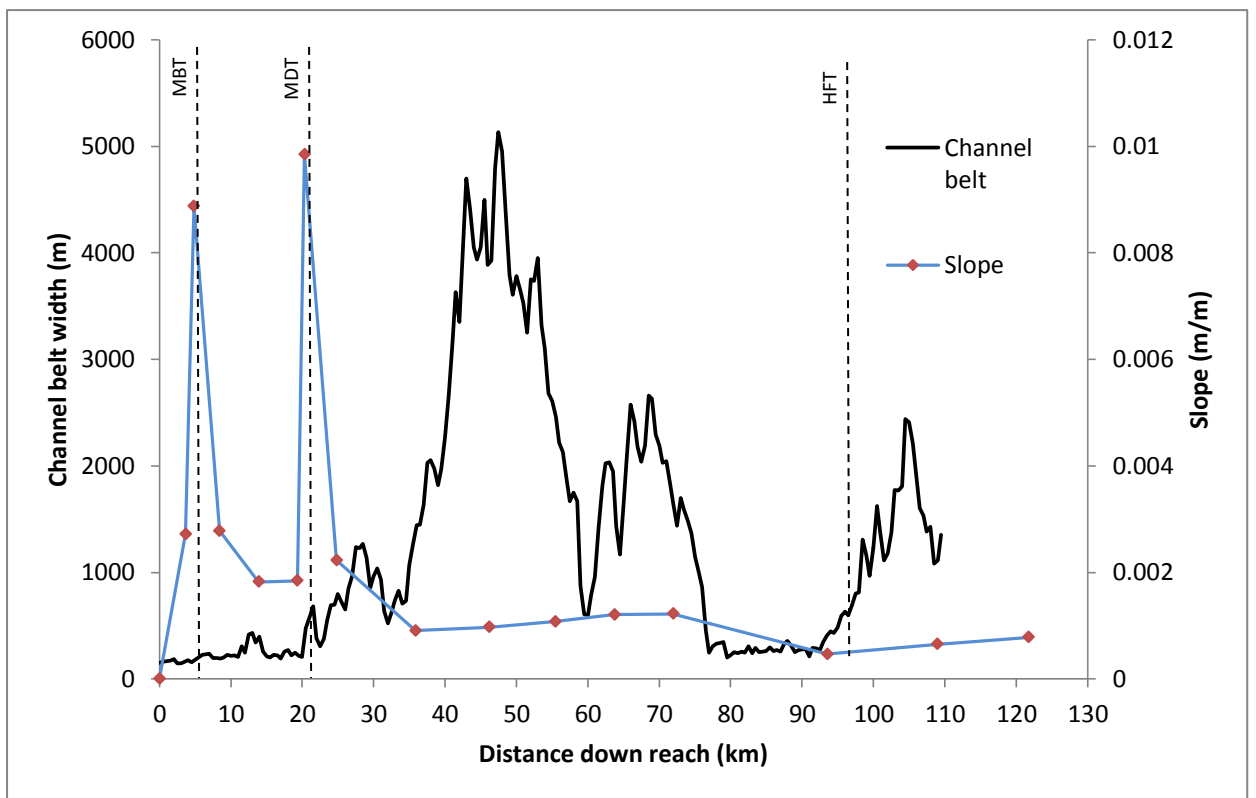
Figure 5.2b *Comparison of channel belt width and channel slope along the Gandak River*

Lithological differences between the bedrock of reaches about the MBT, MDT and HFT may also explain differences between responses. More resistant and higher-grade Lesser Himalayan metamorphic lithologies about the MBT and MDT may result in more obvious knick points about the fault surface ruptures, as the river's ability to incise in response to a change in base-level requires a greater level of stream power. Weaker Siwalik lithologies about the HFT require a much lower stream power to erase changes in base level from the longitudinal profile, so a much faster response and ultimately removal of the knick point, is expected. Upstream of the HFT on the Kosi (~ 7 km), there is a knick point that appears independent from any pre-identified faults. It is likely that this represents an ancient surface rupture of the HFT that has since migrated upstream, but it is also possible that it is a product of, or exaggerated by, vertical error within the SRTM data. Figure 5.4 highlights the effect of vertical error associated with SRTM data, and the influence this has on the contour patterns which have been extracted to ascertain longitudinal profiles and slope values. Highlighted is the MBT knick point on the Kosi River, and the difference in contour patterns between the raw and filled DEMs highlight that knick point features extracted from this data should be treated with caution.

Figures 4.13 and 4.14 display the grain size responses in D_{84} in relation to the MBT, MDT and HFT along the Gandak River. It would be anticipated for an increase in grain size to occur as the river passes over the hanging wall block immediately upstream of the fault as a function of the decreased transport capacity of the flow where channel slope is locally reduced (Holbrook and Schumm, 1999). On the Gandak River, there is an increase in grain size on approaching the MDT, but there are insufficient data to draw conclusions about grain size response upstream of the MBT or downstream of the HFT. There is a gentle increase in gradient throughout the Chitwan Dun (~35-72 km downstream) which may correlate with a slight increase in D_{84} within the Dun (Figure 5.3). This would suggest that the grain size distribution is independent from channel geometry within the Dun, as in areas of increasing slope it would be anticipated that grain size would decrease. The Kosi River lacks sufficient data from which to draw firm conclusions, but an overall decrease in grain size is shown down the study reach. In the case of both rivers, there is a higher level of variation in median D_{84} values in comparison to variation of median values of D_{50} or D_{16} (Figures 4.16 and 4.17). This would imply that the coarse fraction displays the clearest response. The initiator of this response is more difficult to establish, as so far it is shown that there is only a weak correlation between grain size and fault locations.
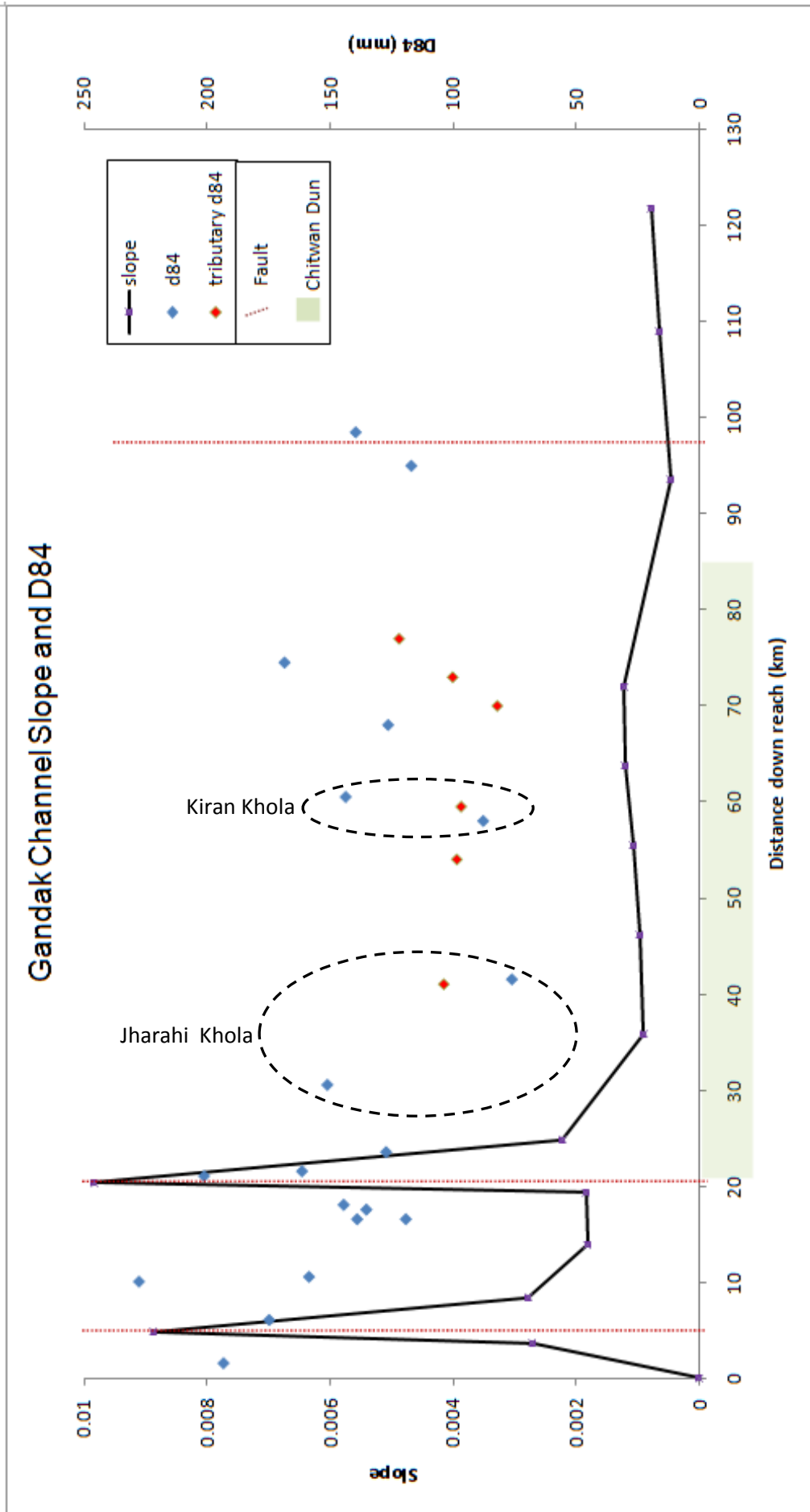
Figure 5.3 *Graph of Gandak channel slope and D_{84} values. This graph reveals a lack a correlation between morphological responses (in slope) to differential uplift and grain size. Highlighted by the black dashed ellipses are the changes in D_{84} associated with the Jharahi and Kiran Kholas.*
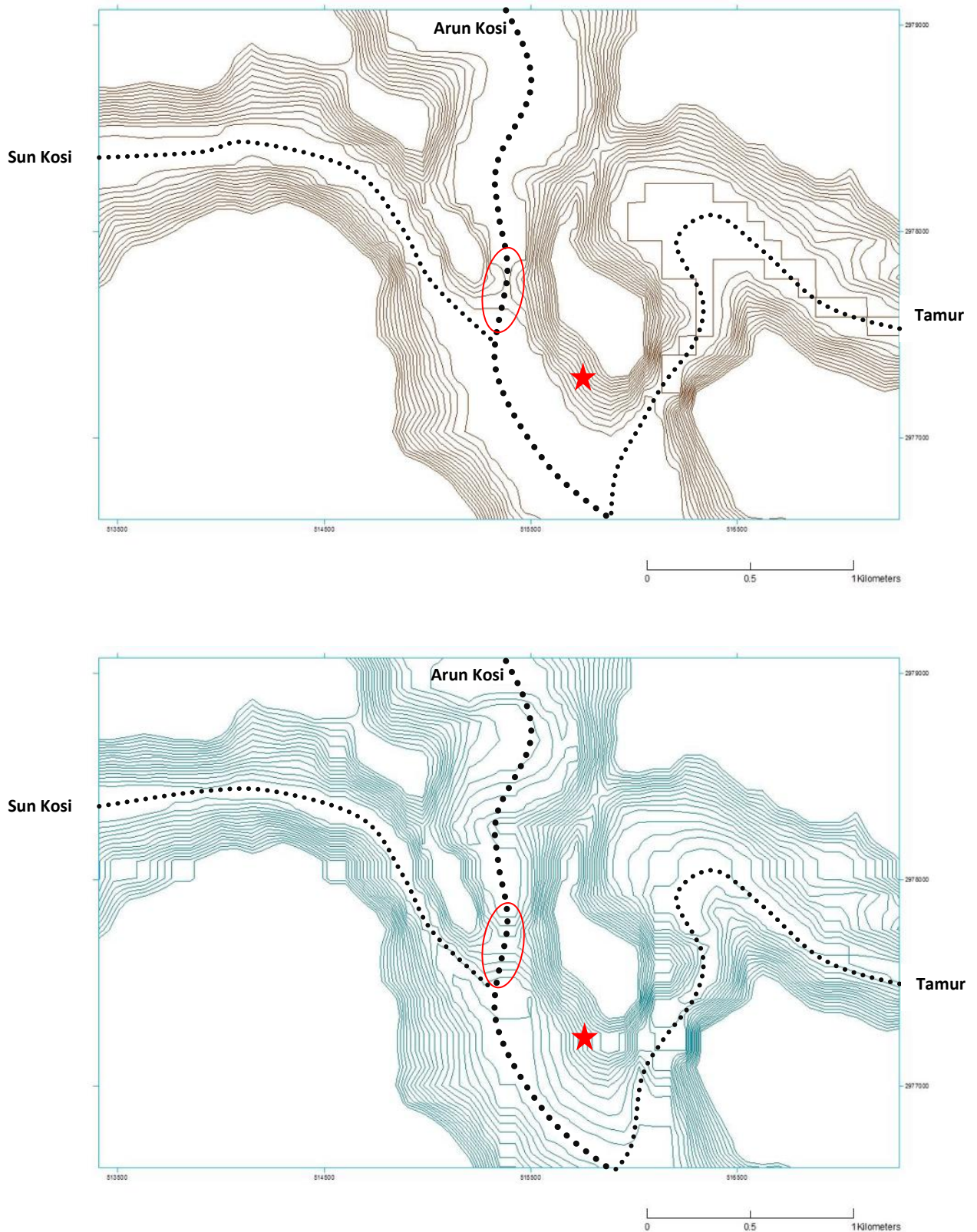
Figure 5.4 *Comparison of 10m contour patterns on filled (upper picture) and raw (lower picture) SRTM derived DEMs. The maximum contour drawn is at 270 m. Grain size transect K8 is represented by the red star, and the black dotted lines represent the channel thalweg as identified by the flow accumulation tool on ArcGIS. The thicker black line along the Arun represents the line that the longitudinal profile was extracted from.*

78

5.2 The effects of sediment input at the Himalayan mountain front

There are clear trends which can be identified in both averaged D_{84} values and grain size distributions, as highlighted in Chapter 4. One of the more striking patterns revealed in Figure 4.14 is the dramatic increase in sorting, or reduction in data spread, of D_{84} values within the Chitwan Dun. The second pattern which is worthy of consideration is the slight increase in average D_{84} values within the Dun. Finally, the difference in grain size between the finer tributary inputs and coarser main river sediments will also be examined.

5.2.1 The Gandak

Grain size distributions

North of the MDT, the range of D_{84} values at each grain size transect is considerably larger than that of transects south of the fault. The reduction in the range of D_{84} values is likely to be a function of both hydraulic and sediment supply processes. In terms of hydraulic processes, selective transport works on the basis that differential transport of clasts occurs as a function of their size (Rice and Church, 1998). It would therefore be expected that smaller and more mobile clasts would be transported further downstream than the coarser fraction of the distribution, resulting in a finer grained and more homogenous grain size distribution beyond the MDT and within the Dun. Differences in sediment supply also exist, where outside of the Chitwan Dun lateral sources of sediment are distinct from those within the Dun. Where steep bedrock channel walls confine the Gandak in the Siwalik Hills, sediment inputs are dominated by directly delivered hillslope deposits derived from vertical incision by the Gandak and consequential steepening and destabilisation of hillslopes. These deposits vary hugely in terms of grain size from fine sands that are immediately washed downstream, to meter-scale boulders that remain on river bars for considerably longer periods of time, and are either immobile or rely on peak monsoonal flows to mobilise them. Landscapes about the MBT are characterised by amphitheatre-shaped landslide scars, steep relief and sparse vegetation (Figure 5.5) that reflects the unstable nature and high frequency of hillslope events which are capable of delivering sediment into the Gandak River. The Chitwan Dun is bound by the Siwalik Hills to the north and south, and lateral inputs into the Gandak within the Dun are predominantly from seasonal tributary sources on the northern (or right hand) bank. These tributary inputs are well-sorted with more homogenous grain size distributions in comparison to direct hillslope deposits, which would explain the narrowing of main stem grain size distributions, as observed within the Chitwan Dun. With a reduction in coarse hillslope inputs, it would be anticipated that selective transport mechanisms would dictate grain size distribution patterns of the main stem within the Dun, producing a finer and more homogenous grain size and grain size distribution.

Figure 5.5 *Photo from transect G12 demonstrating the steep relief, sparse vegetation and amphitheatre-scarred landscape associated with the MBT.*

Lithology

Lithological differences between clasts in non-Dun and Dun reaches of the Gandak River may also influence grain size and its distribution. By considering the lithologies of clasts which are large enough to identify individually (minimum b-axis of ~50 mm), similar techniques to photo sieving have been used whereby the lithologies of clasts underneath grid intersections have been recorded to gauge an estimate of the proportions of major lithologies at each transect. North of the Chitwan Dun and MDT, lithology is more variable with a large fraction (~30 %) of Lesser Himalayan rocks amongst Siwalik sandstones. Within the Dun, lithology is nearly exclusively Siwalik (> 95 %) as represented in Figure 5.6. A significant drop (15 %) in Greater Himalayan lithologies is notable on entering the Dun between transects G10d and G7 (Figure 5.6). As it is unlikely that significant abrasion of these resistant clasts would have occurred over such a short distance (~ 10 km), I infer instead that they have been deposited close to the northern boundary of the Dun. It is possible that such accommodation could be provided in the footwall of the MDT. The more resistant nature of the Lesser Himalayan rock in comparison to the easily erodible Siwalik rock is also likely to have some influence over grain size distribution patterns. Siwalik lithologies should quickly be abraded as they are transported downstream, producing homogenous grain size distributions with relatively small average grain sizes. Where Lesser Himalayan lithologies are also present, there should be a slower downstream fining effect on this rock type as the rock is more resistant to fluvial abrasion. This fraction of the load should remain coarser for further downstream, and in combination with the finer abraded Siwalik sandstone should produce a more varied grain size distribution, and if the relative proportion of the coarse fraction is significant, may also produce a larger average grain size. Within the Dun,

lateral inputs from the Kholas are found to be predominantly Siwalik (> 90 %). Experimental findings by Attal and Lave (2009) reveal that sandstone lithologies have the potential to lose up to 10 % of their mass per kilometre transported in flow. Clasts within the Kholas will have undergone significant abrasion whilst transported for distances of > 15 km in the months where flow was sufficient to transport them, so it would be expected for significant abrasion of the sandstone lithologies to have occurred. This is likely to produce narrow grain size distributions, as is found to be the case of the Kholas sampled.
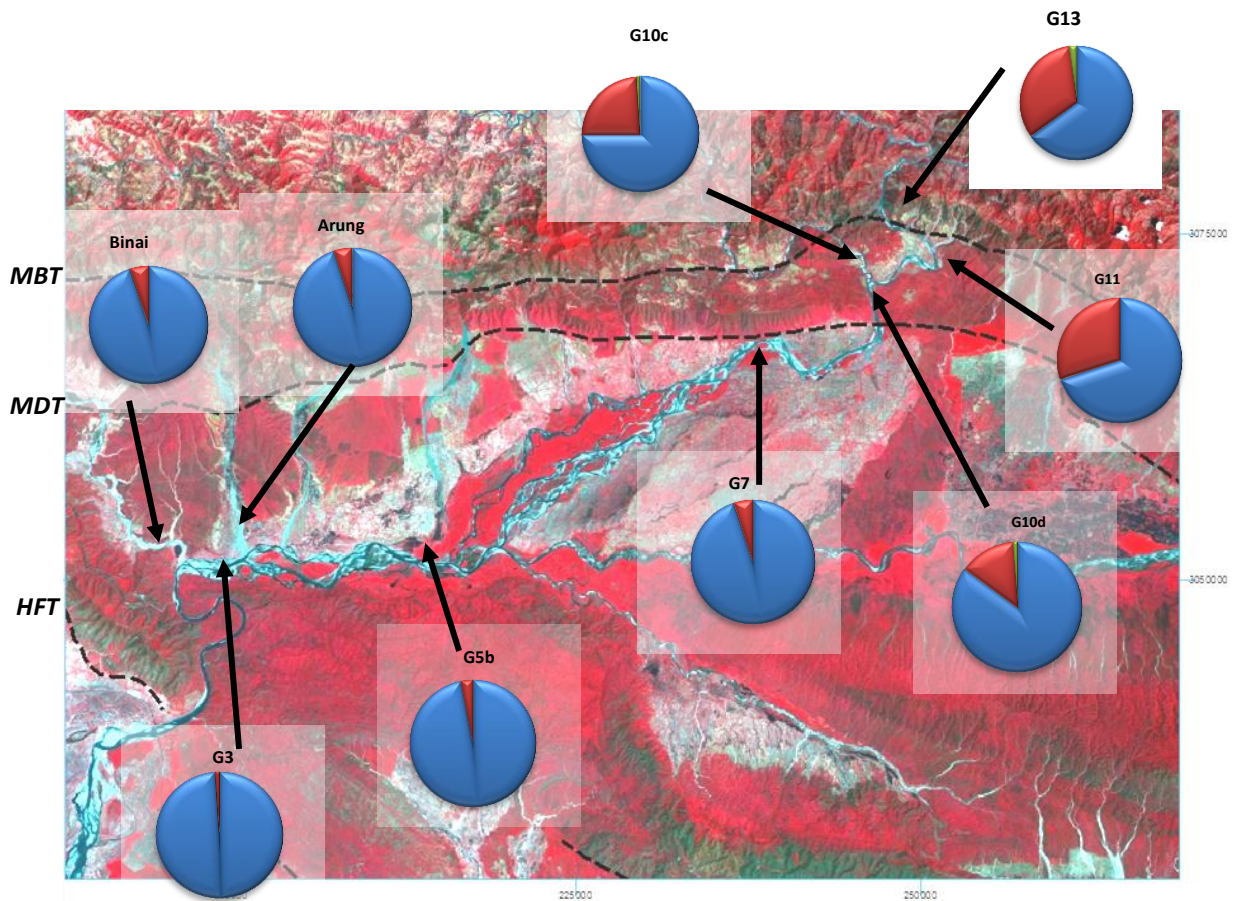
Figure 5.6 *Changes in contributions of Siwalik, Lesser and Higher Himalayan lithologies within the Gandak study reach*
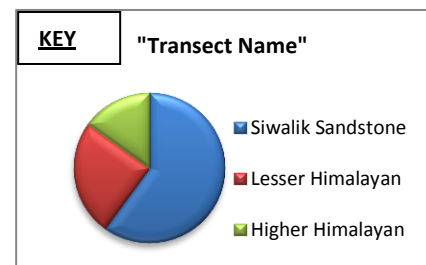
Grain size within the Chitwan Dun

Selective transport cannot account for the slight increase in D_{84} along the Gandak main stem within the Dun. With an increase in slope within the Dun, this grain size pattern is contrary to what is expected in terms of a morphological response as outlined in Chapter 1. Grain size

analysis reveals that samples taken from the Binai, Arung, Girwari, Kiran, Rapti and Jharahi Kholas generally have smaller D_{84} values across a narrower distribution than the main Gandak samples within the Dun (Figure 4.14). However, main stem grain size transects taken directly upstream and downstream of tributary confluences, such as G5a and G5b about the Kiran Khola (highlighted on Figure 5.3), reveal an increase in D_{84} by over 50 mm immediately downstream despite only a marginally larger D_{84} input from the tributary. This pattern is not consistent with other tributary confluences, however. For example, there is a 75 mm decrease in D_{84} between G7 and G6, upstream and downstream of the Jharahi Khola, despite an input from the Jharahi Khola coarser than that at G6 (highlighted in Figure 5.3). It therefore seems unlikely that the slight coarsening within the Dun is related directly to tributary inputs. Another possibility which must be considered is that the coarsening within the Dun is an anomalous result, with grain size transects G3, G4 and G5a not being accurate representations of the true D_{84} of the gravel bars sampled. Whilst every attempt was made to ensure samples were taken on straight reaches away from the influence of back flow and eddy currents, it is still possible that these samples are biased. On selecting transect locations within the Kholas, large areas were surveyed to find the coarsest deposits, so it seems unlikely that these samples under-represent D_{84} values. Alternatively, the main stem grain size transects sampled may not reflect the true maximum D_{84} across the width of the river, as we were unable to access any of the mid-river and left bank deposits which would introduce inherent variability.

Attal and Lave (2006) found similar downstream coarsening trends further north in the Marsyandi River, despite finer-grained tributary and hillslope inputs. The downstream coarsening of this Marsyandi study was attributed to differences in grain size distributions of lateral sediment inputs, which in this instance were predominantly landslide and glacial moraine material. When this hillslope material reached the river, the fine-grained fraction was assumed to have been rapidly washed out as suspended load leaving the remaining coarse fraction of the deposit over-represented on the gravel bar. Attal and Lave (2006) assumed this would increase both the average D_{84} value and weighting of the coarse fraction of the grain size distribution of the bar. With an increase in landslide material supply further downstream, an increase in average grain size would also be expected downstream. Similar patterns concerning finer hillslope inputs were related by the same study to selective transport of smaller pebbles from hillslopes, resulting in a slower transit time and consequential over-representation of coarse material on main river gravel bars during periods of low flow. Other suggestions to explain the downstream coarsening given by Attal and Lave (2006) included abrasion of smaller clasts during fluvial transport, but the study concluded that within active orogens, grain size is most sensitive to the grain size distribution of hillslope sediment supply.

Whilst considering the findings by Attal and Lave (2006) however, the difference in setting between the Chitwan Dun and the Greater Himalayan reaches of the Marsyandi River requires

appreciation. Tributary inputs are distinct from hillslope deposits upstream of the MDT in terms of their regularity of delivery (seasonal) to the Gandak, and the fluvial governing of grain size distribution within the tributary itself. Unlike the hillslope inputs of the Marsyandi River, Gandak tributary inputs have a narrow range of D_{84} grain sizes, all of which are lower than the bulk of D_{84} values of transect site G3. Upstream reaches of the Binai, Arung, Girwari, Kiran, Deswa and Jharahi Kholas were noted in field observations as being heavily choked with sediment, presumed to have been stripped from the surrounding Siwalik Hills. Fieldwork for this research was undertaken in March/April during the period of low flow prior to the monsoon; therefore, the upper reaches of these tributaries were largely dry and hence unconnected to the Gandak. During the monsoon period from late April-September, it would be expected for sediment delivery from the hillslopes and discharge within these tributaries to be dramatically increased. The main points to draw from this are that tributary inputs are likely to be flashy in that they are only seasonal, and deliver sediment of a more uniform grain size distribution than hillslope inputs. Whilst the lithology of these tributaries has a marginally greater proportion of Lesser Himalayan rocks (Figure 5.6) than the main stem, any effect this may have on grain size or lithology in the main stem is diluted. It is therefore unlikely that tributary inputs are a main contributing factor to the increase in D_{84} within the main Gandak River. Table 5.1 shows D_{95} values for transect locations within the Dun, which reveals patterns in all but the coarsest 5 % of the sediment fraction that flow is able to transport. Comparing this with D_{84} data (Figure 5.7) the general trend is similar, with the only exceptions in the upstream end of the Dun where the D_{95} of the Jharahi sample is greater than that of G7 and G6. Therefore, the maximum grain size is also increasing within the Dun.

In light of the evidence presented, only speculations concerning the cause of the increase in D_{84} within the Chitwan Dun may be made. The data obtained during this research have demonstrated that it is unlikely that tributary inputs within the Dun supply the coarse material required to produce such a trend, and that a difference in lithology between tributary and main stem sediment plays no direct role. Therefore, two possible mechanisms could explain the observed trend. Firstly, grain size transects are not representative of the bulk river loads, and coarser deposits must exist slightly upstream in the Kholas, or at either mid-river or left bank main stem locations which were inaccessible during this study. Secondly, assuming that these results are an accurate reflection of bed deposits across the width of the Gandak River, hydraulic processes may act upon the sediment load to eliminate the finer fraction, resulting in a deposit which has an over-represented coarse fraction. One possibility is that smaller clasts are preferentially abraded or split as they are transported downstream. The D_{16} Box and whisker plots in Figure 4.17 show little variation between the median values of G7-G3. There are perhaps some marginally greater D_{16} median values (by 5-10 mm) at the downstream end of the Dun at G5a, G4 and G3 which could suggest that the fine grained fraction of the bar deposit is

increasing in size through the preferential breakdown and removal of fine grained material. This fails to explain the notable increase in D_{95} (Table 5.1) at G3 however, as D_{95} will not be hugely affected by changes concerning the finer-grained end member.

Table 5.1 *D_{95} values for grain size transects within the Chitwan Dun listed in increasing distance downstream.*

Transect Name	*D_{95} (mm)*
G7	**189**
Jharahi Khola	192
G6	**104**
Rapti Khola	124
G5b	**112**
Kiran Khola	130
G5a	**188**
G4	**162**
Girwari Khola	115
Arung Khola	137
G3	**209**
Binai Khola	173
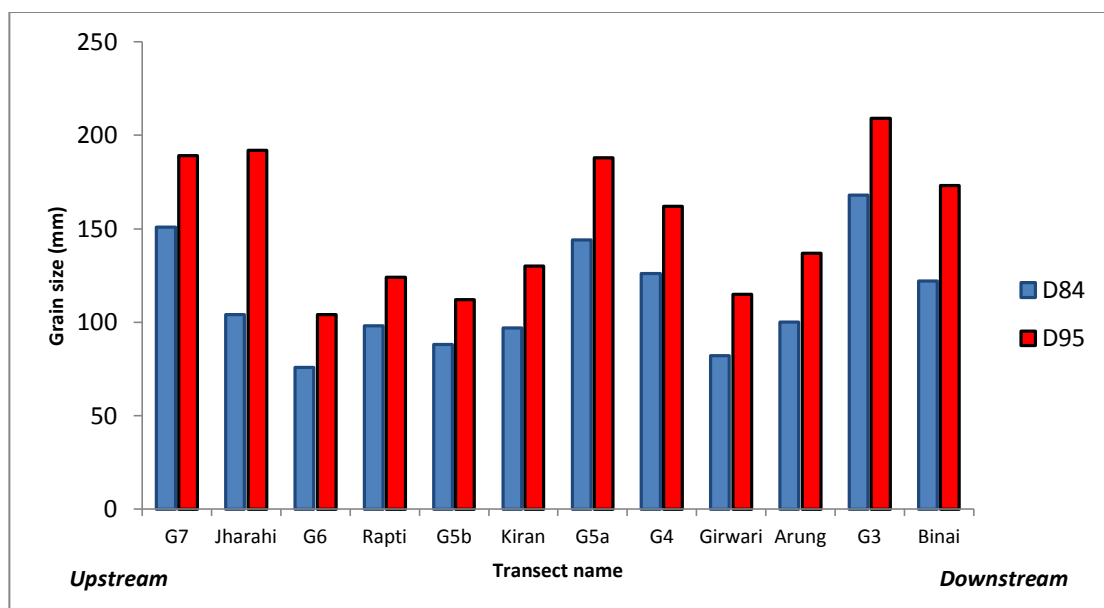
Figure 5.7 *Comparison of D_{95} (red) and D_{84} (blue) of tributary and main stem samples within the Chitwan Dun. The transects are listed in increasing order downstream (left to right).*

5.2.2 The Kosi

With such a limited number of samples from the Kosi River, conclusions drawn from this dataset must be taken lightly. The lack of samples upstream of the Tamur confluence also makes it impossible to discuss how the Kosi responds to either the MCT or MBT 'zone', and whether tributaries other than the Tamur influence grain size further downstream. D_{84} is reasonably consistent between K2, 4 and 5. There is a clear increase in D_{84} at K3, which lies marginally upstream from the HFT so is likely to respond to relative movement of the hanging wall block of the fault, due to a reduction in channel slope. On crossing the HFT, there is a rapid drop in D_{84} between K2 and K1 in response to crossing the gravel-sand transition. Gravel-sand transitions are most common where steep mountain rivers exit a mountain front, and in the case of the Kosi, emerge onto a vast sediment mega fan. This reduction in slope and therefore shear stress, results in a rapid deposition of load and enhancement of size sorting (Ferguson, 2003) due to preferential mobility of smaller grain sizes, producing a much finer bed load. In the case of the Kosi, the gravel-sand transition is abrupt, producing the observed pronounced reduction in D_{84} values.

Unlike the Gandak tributary inputs, transect K6 on the Tamur displays a coarser and wider D_{84} distribution, and the reach over which the transect is located has a higher slope value (Figures 5.8a and 5.8b). Field observation showed that the source of this material at K6 was largely landslide debris covering a range of grain sizes from very fine and freshly eroded rock fragments (tens of mm) to much older and immobile boulders as large as 3 meters in diameter. With only a minor change in D_{84} size and distribution between transect locations K5 and K4, it would be likely that the effects of this input from the Tamur are only short-lived through either dilution of grain size after the Tamur-Kosi confluence, or rapid abrasion during transport.

Girwari Khola

Slope= 0.009 m/m

D_{84}= 82 mm

Arung Khola

Slope= 0.009 m/m

D_{84}= 101 mm

Binai Khola

Slope= 0.007 m/m

D_{84}= 122 mm

G3

Slope= 0.001 m/m

D_{84}= 168 mm

G4

Slope= 0.001 m/m

D_{84}= 126 mm

MBT

MDT

HFT

OUTPUTS (at Ganga confluence)

Q= 49,385 x 10^6 m^3/yr

Q_s = 16,100 t/km^3/yr

[Singh *et al.*, 2008]
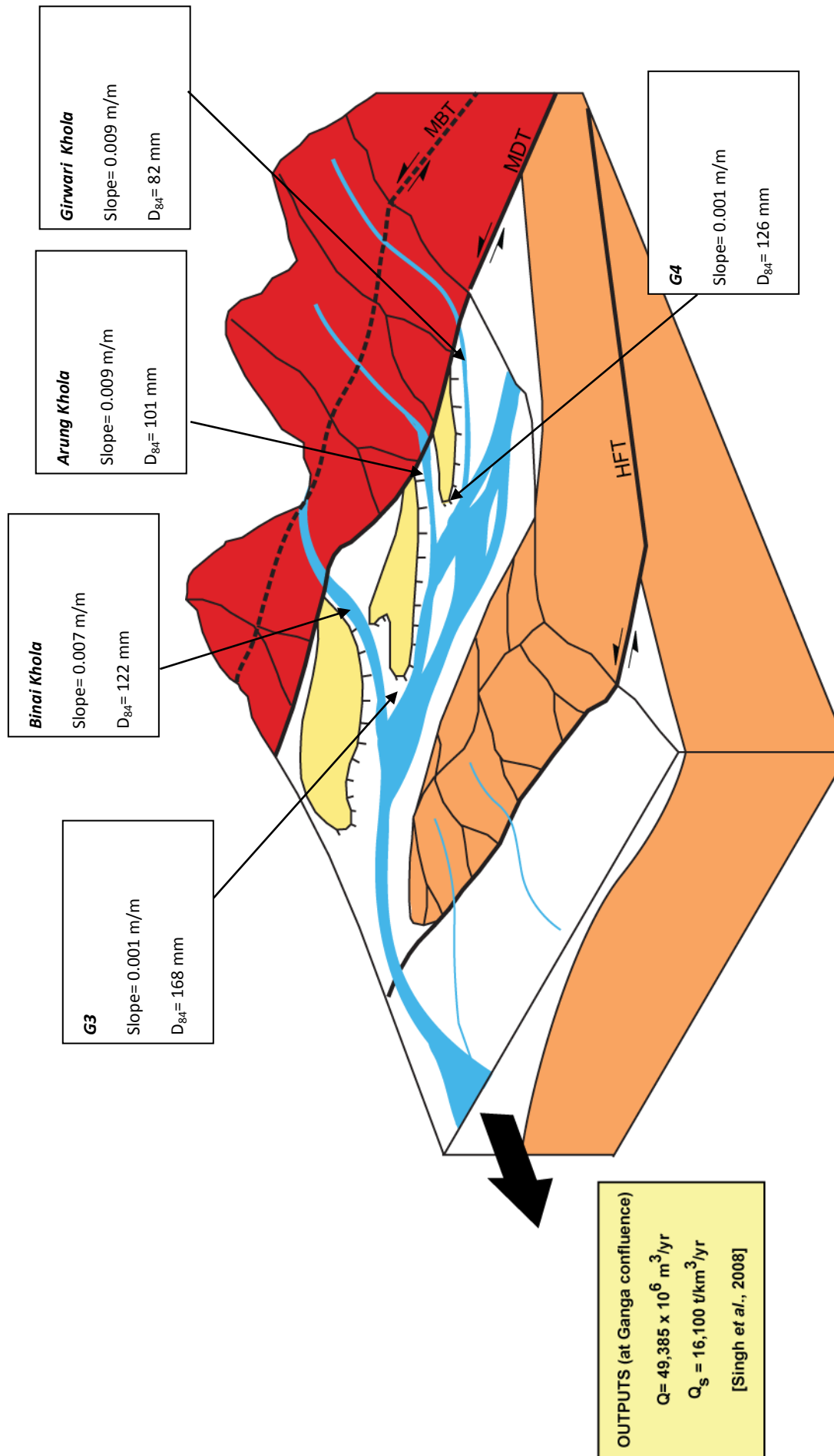
Figure 5.8a *Schematic diagram illustrating relationships between tributary and Gandak River slope and D_{84} values, redrawn after Densmore et al. (2010 EGU poster). Slope values are derived from 10 m contour lines constructed from SRTM datasets and represent the local slope of the transect near the confluence. Annual discharges and sediment yields taken at the Gandak-Ganga confluence by Singh et al. (2008) are also given.*

K5

Slope= 0.002 m/m

D_{84}= 232 mm

MBT

HFT

K6 (Tamur)

Slope= 0.003 m/m

D_{84}= 365 mm

K4

Slope= 0.001 m/m

D_{84}= 228 mm

K1

Slope= 0.001 m/m

D_{84}= 142 mm

OUTPUTS (at Ganga confluence)

Q= 48,155 x 10^6 m^3/yr

Q_s = 1200 t/km^3/yr

[Singh et al., 2008]
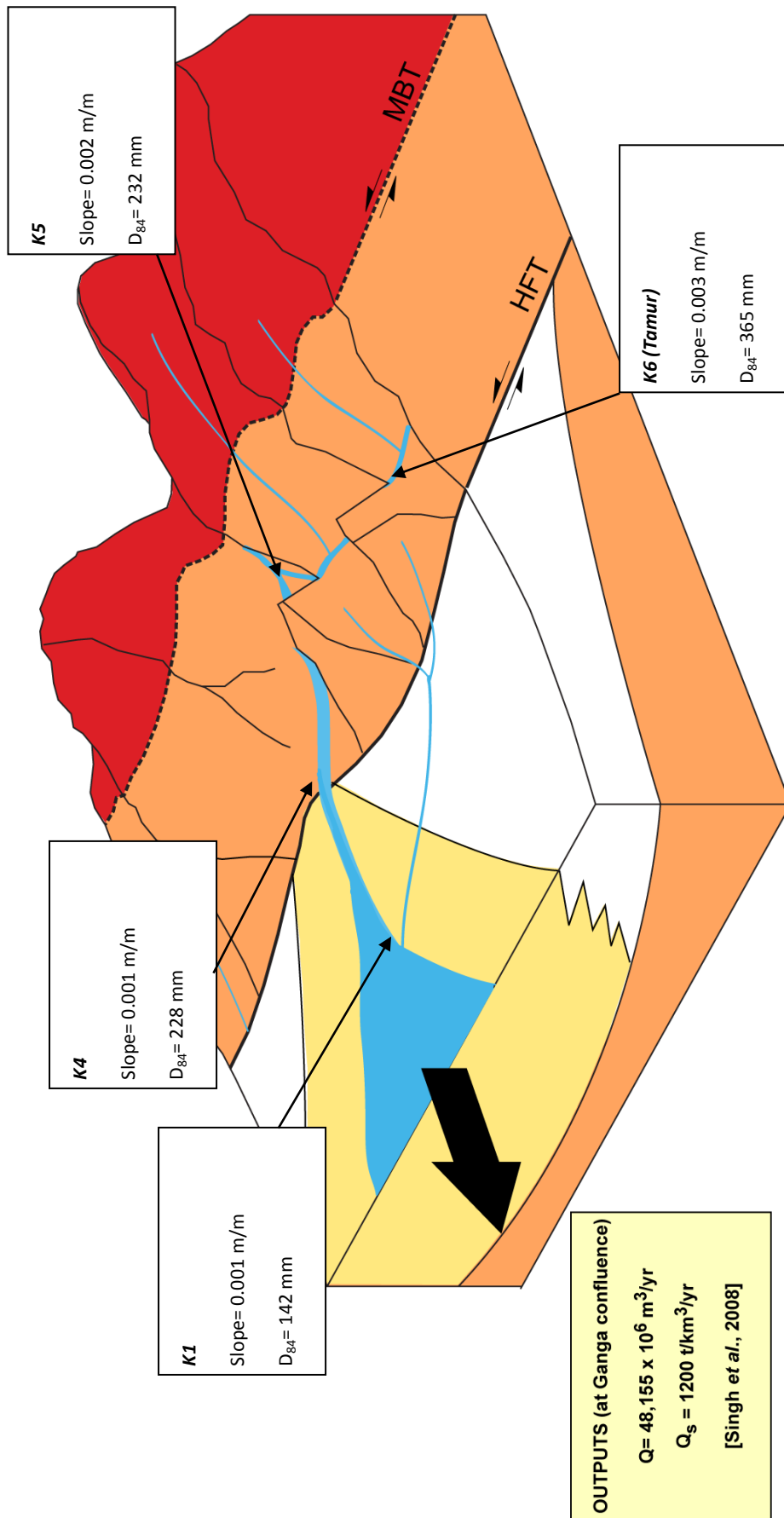
Figure 5.8b *Average D_{84} and local SRTM derived slope values for three sites along the Kosi River (yellow), and one from the Tamur (red), redrawn after Densmore et al. (2010 EGU poster). Annual discharges and sediment yields taken at the Kosi-Ganga confluence by Singh et al. (2008) are also given.*

The narrow D_{84} grain size distribution at K5 is also of interest, as it is situated within a region characterised by steep relief, unstable hill slopes and focused deformation. In such situations, it would be expected for a wider range of D_{84} to occur, such as those noted at transect locations further downstream. K5 is unique from other transect locations on the Kosi as is situated on a mid-river confluence bar between the Tamur and Sun/Arun Kosi Rivers. As a mid-river confluence deposit, the bar is largely submerged during peak monsoon discharge levels resulting in heavy reworking of surface gravels. The high proportion of Greater Himalayan lithologies on the bar reflects a lack of direct local Siwalik hill slope inputs at this location, therefore the grain size distribution of K5 should be a direct reflection of fluvial reworking and selective transport.

5.3 Variations in Shields stress and critical stream power at the mountain front

Flow depth values used in the calculation of Shields stress were crudely derived and likely to have meter scale margins of error attached to them where estimated from field observations. The error associated with DEM derived slope values has been considered in detail in Chapter 3. The large distances (up to 10 km) over which the slope estimates are calculated also means that the values calculated are averaged over the reach, which will ignore any sub-reach scale changes in shear stress. In light of these issues, the values listed in Table 4.1 should only be used as first order estimates. Comparing these values with those from other studies would be unsuitable as the error associated with these absolute values is too large. It would be expected for the results obtained to only be correct to within a minimum of two orders of magnitude. However, to compare values between sites across and along the study reaches is justifiable as a means of direct comparison where values are relative to each other. Values of average shear stress were obtained on the Bagmati and Bakeya Rivers by Lave and Avouac (2001) using slope estimates derived from 1:63,000 maps at 30.5 m contour intervals in combination with GPS/altimeter measurements, channel widths derived from aerial photography/satellite imagery and discharge values. These average shear stress values were then combined with D_{50} values by Lave and Avouac (2001), assumed constant down each reach, to produce a dimensionless Shields stress value. Estimates of Shields stress derived by Lave and Avouac (2001) vary between 0.045-0.085 and 0.065-0.1 between the HFT and 1 km upstream of the HFT, on the Bagmati and Bakeya Rivers respectively. These values are comparable to those estimated about the HFT on the Kosi at site K4 (Table 4.1), but are marginally higher (~ 0.01) than those for the Gandak River in a comparable area relative to the HFT. Additionally, the impact that the Gandak Dam may have on channel morphology, and therefore Shields stress, must be considered when observing changes about the HFT. It may be possible that the dam alters flow depth immediately upstream of itself, which may affect the calculated Shields stress values.

In theory, where observed D_{50} values are considerably smaller than those calculated from the critical value of entrainment, the grain size in the channel should be supply limited. The channel is capable of conveying much larger grain sizes than observed, but with a lack of coarse input, the D_{50} of the representative surface is smaller than what the channel is capable of conveying. Based on the findings in Table 4.1, this relationship between maximum and observed grain size is apparent at G12 and G10d, and to a lesser extent at K4 and G5. In the first two instances, the difference between the observed D_{50} and the value calculated at the critical value of entrainment is by several orders of magnitude. Even with the high error margins associated with these values, it is still likely that these sites are supply limited. Along the Kosi, the difference between observed and theoretical maximum D_{50} values is much smaller. Given the error margins, it is difficult to extract strong conclusions over whether the system is transport/supply limited or somewhere between these two end-members.

Close to the mountain front along the Gandak River at the HFT, the observed D_{50} values are larger than those calculated at channel capacity. In theory, this would imply that the channel is transport or flow limited as based on the criteria used to calculate the maximum grain size the channel is capable of conveying, the river is unable to transport the observed bar material. Similarly to K3 and K4, the difference between the observed and calculated D_{50} values is less than an order of magnitude. Considering the level of error with the absolute values in Table 4.1, patterns identified at these locations must be treated with caution. As a general trend however, it appears that the Gandak River is supply limited north of the Chitwan Dun based on the findings in Table 4.1. Within the Dun, this pattern is less well defined with similar values obtained of observed and calculated D_{50}. This is also the case for the Kosi River. This would suggest that grain size distributions reflect patterns in sediment supply opposed to hydraulic conditions.

Critical stream power reduces downstream. Between G12 and G2 (a distance of ~90 km), the critical stream power reduces to less than a sixth of its original value (943 to 147 W m^{-2}). The reduction from 651 to 445 W m^{-2} between K4 and K3 (over a distance of ~10 km) is also significant. Comparing the critical stream powers closest to the mountain front (G2 and K4) and HFT, also reveals a striking difference between the Kosi and Gandak. Whilst the critical steam power at K4 is close to 450 Wm^{-2}, the critical stream power at G2 only a third of this value at 147 Wm^{-2}. These results show that compared to the Gandak, a greater stream power is required at the Kosi mountain front to mobilize the coarser bed load material found here. This difference in grain size at the mountain front could be attributed to a number of factors. The nature of the sediment input may be an important controlling factor in terms of whether it is directly supplied by the surrounding hill slopes, or whether it has been transported by small tributaries and therefore already undergone significant abrasion and sorting. The grain size distribution on channel bars is also likely to reflect patterns in stream power. Where greater stream power is required to entrain significant proportions of bed material, it might be expected for there to be

an over representation of the coarse fraction on the exposed channel bar as there would have been selective entrainment of the finer material. Expanding on this theme, it should be possible to decipher whether bar deposits are products of the flow that deposited them or whether they are remnants of what is too large to be entrained, based on particular bed form characteristics. The level of organization on exposed bars in terms of imbrication of individual grains, narrow grain size distributions (at select locations) and rare instances of exceptionally large, isolated boulders would suggest that these bar deposits are direct products of flow deposition, as opposed to remnants that are too large for entrainment.
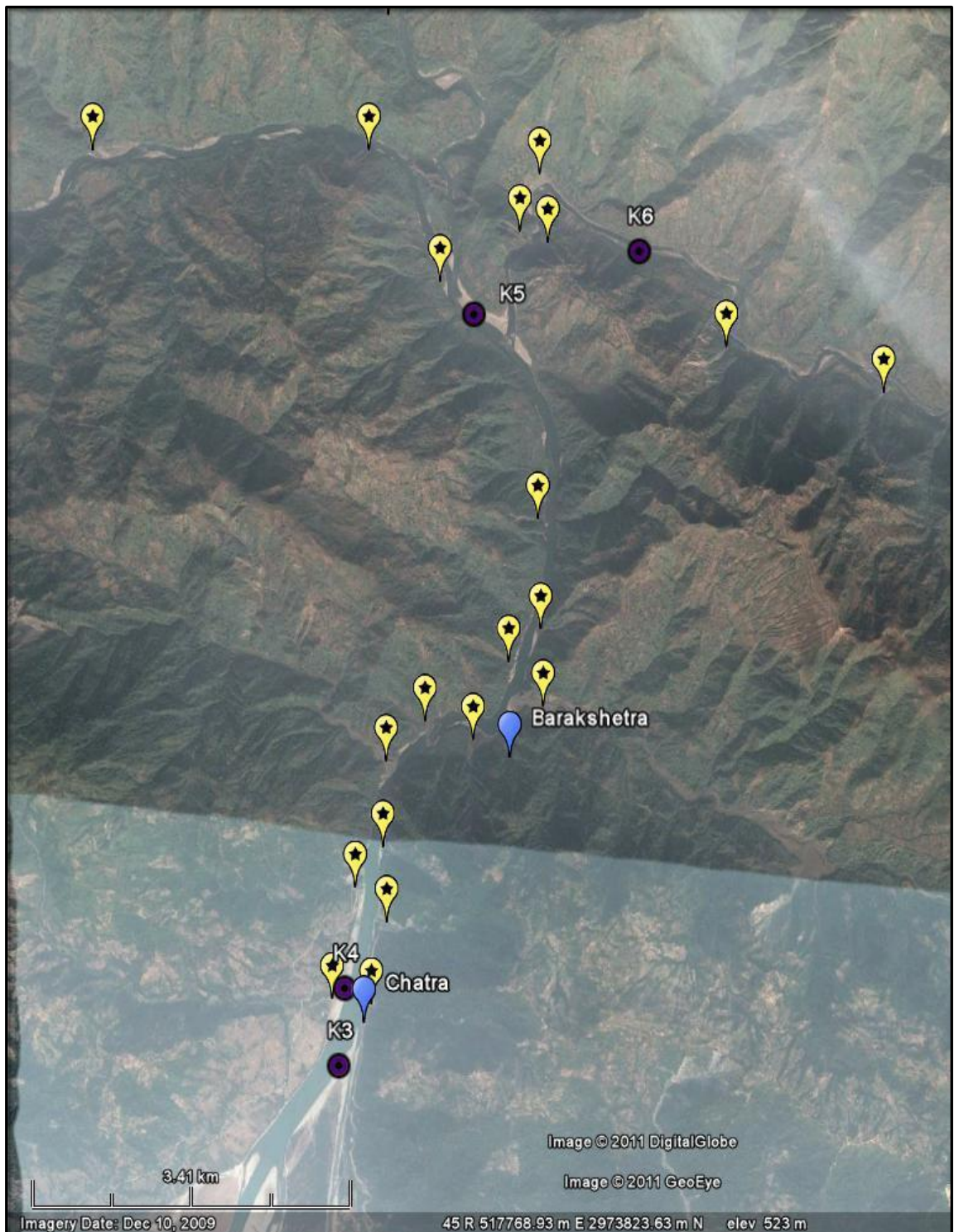
Figure 5.9 *Google Maps image of the Kosi study reach prior to exiting the mountain front. Identified are the grain size transect locations K3-6, the villages of Chatra and Barakshetra, and sites of lateral sediment inputs by the purple circles, and blue and yellow starred markers respectively. These sites have been manually identified from the Google Earth imagery and represent landslide scars and deposits, debris flow tracks or small mountain streams that have at some point been connected to the Kosi River and actively supplied sediment.*

5.4 Hillslope processes and grain size distributions

Colluvial valleys represent 50-70 % of basin relief within the Siwalik Hills (Lague and Davy, 2003) and are therefore likely to influence the long-term dynamics of mountainous drainage basins such as the Kosi and Gandak. Focused deformation at the Himalayan mountain front has produced a dense network of steep and unstable hillslopes along the Kosi River between the MCT and HFT. High rates of vertical incision by the Kosi River initiated in response to relative uplift or back tilting of MBT/HFT hanging wall blocks, enhance the relief of the Siwalik Hills. In agreement with the Indus River and the surrounding hillslopes in the NW Himalaya (Burbank *et al.*, 1996), landsliding allows Siwalik hillslopes to adjust efficiently to the rapid vertical erosion rates imposed by the Kosi River. The threshold for landsliding in such rapidly uplifting regions is a function of the fractured rock strength (Burbank *et al.*, 1996). Considering the weakly consolidated nature of the Siwalik bedrock, the threshold for landsliding in this region should be low which would account for the high frequency distribution of hillslope inputs down the Kosi River study reach (Figure 5.9). This would also concur with findings by Barnes *et al.* (2011) whereby topographic growth in thrust front-foreland settings in the NW Himalaya is limited by fast slip and erosion rates combined with the weak lithology of the uplifted Siwalik rocks. Sediment removal from the Kosi study reach also appears efficient, with the river flowing predominantly over bedrock upstream of the mountain front and considerably fewer exposed bar deposits than the Gandak, suggesting that very little sediment is stored in the channel. This also fits well with Simpson (2010), where it was modelled that foreland basins developed over strong basal decollements produce very little accommodation within such focused regions of deformation.

Whilst the Gandak River receives additional sediment input from numerous lateral sources within the study reach, the nature of these inputs varies from those of the Kosi. Outside of the Chitwan Dun, the majority of sediment inputs are sourced from small mountain streams, and therefore are only connected to the main Gandak River during the monsoon season. By observing patterns of landslide scars and tracks on Google Earth across the Gandak study region (Figure 5.10a and 5.10b), fewer lateral inputs are identified as being directly sourced from hillslope processes or failures, suggesting that Siwalik hillslopes surrounding the Gandak River are more stable. Again, this corresponds well to Simpson (2010) who predicted that foreland basins established over weak basal decollements have distributed deformation fields acting across multiple structures, and over a larger area. This in turn is likely to produce lower relief landscapes than those built over strong basal decollements, and the production of foreland accommodation in piggyback basins (or Duns). The Chitwan Dun would have provided ample accommodation for sediment exported from the rising Greater Himalaya by the Gandak during the early Himalayan orogeny, so unlike the Kosi there is now a vast store of sediment prior to exiting the mountain front. Continual sediment export along the Kosi due to a lack of

accommodation within the foreland also corresponds with expected behaviour from foreland basins developed over strong basal decollements (Simpson, 2010).

With the highly unbalanced modern sediment yields between the Kosi and Gandak (Singh *et al*., 2008), it is anticipated that the Chitwan Dun may be full, and is likely to be in a state where it is no longer capable of storing additional sediment. Should the Dun be full, modern sediment exported from the Greater Himalayas should be directly exported out of the mountain front, which would reflect the high modern sediment yield of the Gandak (Figure 5.8). The sediment yield would also likely be enhanced by Holocene incision of the Dun fill by tributaries across the Dun surface and from the sediment removed from the Siwalik Hills in the north.
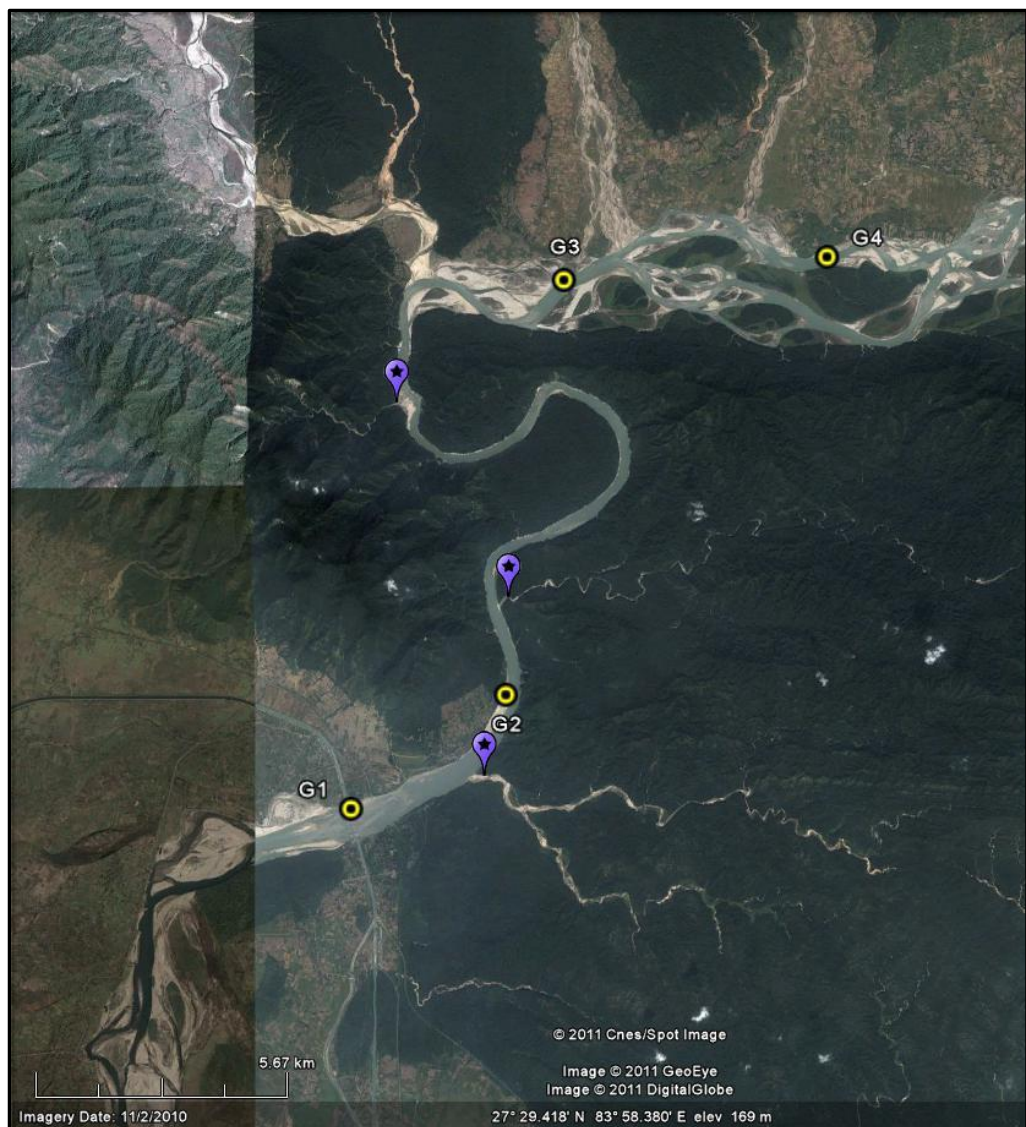
Figure 5.10a *Google Maps image of the downstream region of the Gandak study reach on re-entering the Siwalik Hills. Identified by purple starred markers are manually identified lateral inputs of sediment into the Gandak main stem. These inputs are predominantly small mountain streams.*
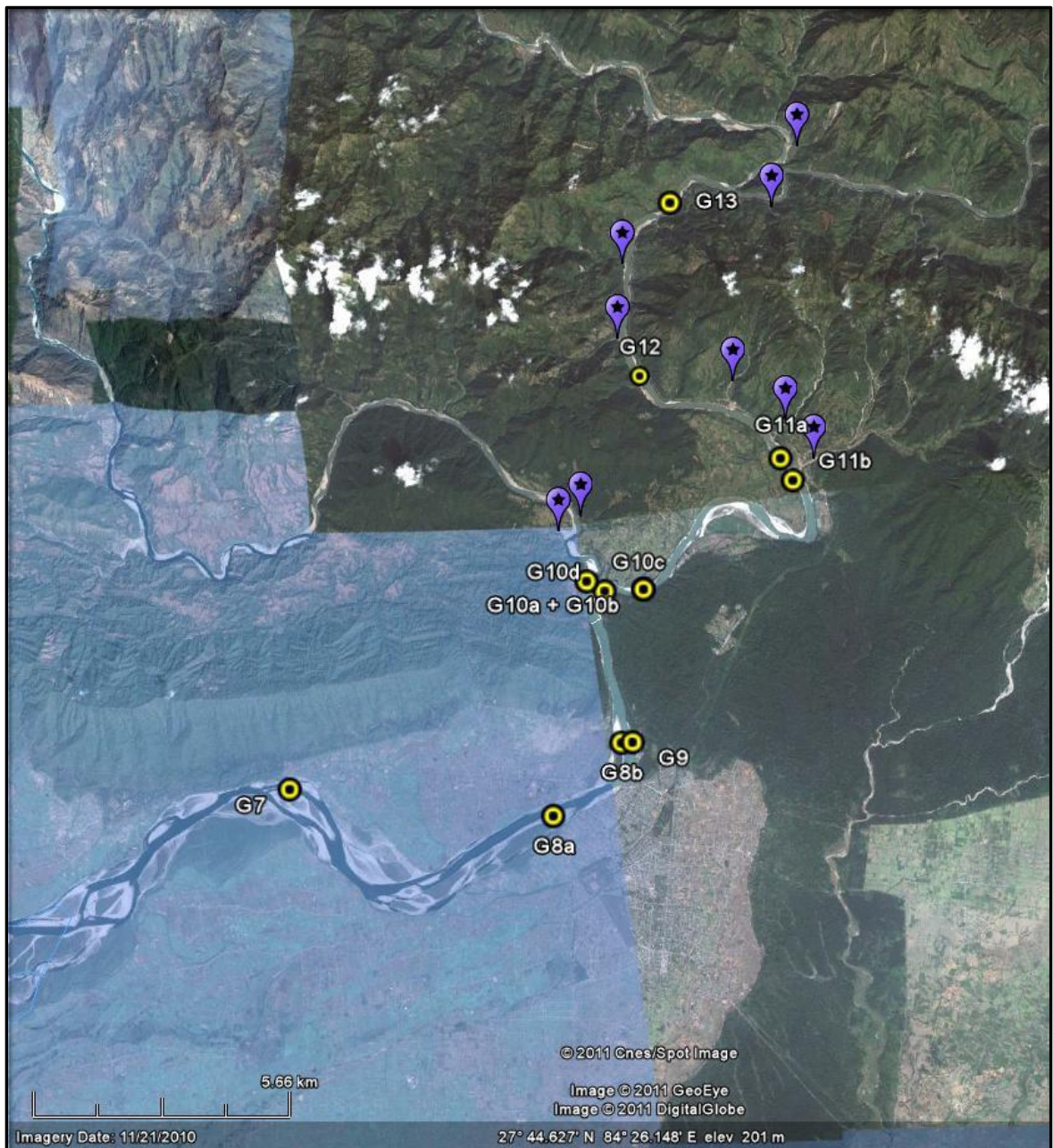
Figure 5.10b *Google Maps image of the region upstream of the Chitwan Dun within the Gandak study reach. Identified by purple starred markers are manually identified lateral inputs of sediment into the Gandak main stem. These inputs are derived from a combination of small mountain streams and landsliding.*

Chapter 6: Conclusions and further research

This study has revealed evidence of morphological response to both tectonic uplift and sediment inputs at the Himalayan mountain front. Changes in channel geometry appear strongly related to the position of tectonic structures, whilst patterns in grain size distribution appear influenced by lateral inputs of sediment. Concerning responses initiated by tectonic uplift, there is discrepancy between the Kosi and Gandak channel geometry, in terms of consistency and magnitude of change around individual faults. For example, an increase in channel width upstream of the HFT is evident on the Gandak but is absent about the MDT and MBT. The Kosi on the other hand, displays a similar increase in channel width upstream of the HFT, but also increases in width upstream of the MCT. The increase in slope about the MBT on the Kosi is also significantly greater than about the MBT on the Gandak, which may reflect a difference in uplift rates along strike of the fault. Many of these interpretations are made from measurements derived from the limits of what can be extracted from the SRTM data. That is to say, the RMS error (~10 m) of SRTM data is likely to influence reach averaged slope values and longitudinal profiles derived from the DEMs. Therefore, changes in channel slope or drops in elevation along the longitudinal profile that relate to the positioning of major tectonic structures may have been influenced by imperfections on the DEMs. Grain size data acquired in the field reveals a more complex pattern, with the most significant change in grain size observed in the coarse fraction of the load (D_{84}). In general, there is a weak correlation between grain size and the positioning of tectonic structures. Sediment inputs however, are likely to play a significant role in the distribution of grain size patterns at the mountain front.

The nature of lateral inputs appears to vary as a function of the style of foreland basin development as modelled by Simpson (2010). Weaker basal detachments produce distributed deformation fields over large areas with sporadic fault activity. This produces less rock uplift above individual faults, and therefore generates lower relief, such as that observed about the Gandak River and Chitwan Dun. As a result, direct hillslope inputs into the Gandak are less common than the Kosi, and within the Chitwan Dun lateral inputs are derived from smaller tributaries that are seasonal in their delivery of sediment to the main Gandak River. The nature of tributary derived sediment differs from hillslope-derived fragments, as has a narrower grain size distribution and is smaller in average median size, indicating that it has undergone significant sorting. This is evident north of the Chitwan Dun, where average D_{84} is notably coarser (119-227 mm) and with a wider range of D_{84} values in comparison to the smaller grained (77-168 mm) and well-sorted deposits within the Chitwan Dun. The Kosi on the other hand, is located over a strong basal detachment, which has produced a focused zone of intense deformation, high relief and rapid uplift above closely spaced individual faults. The Kosi is also characterized by unstable hillslopes that are prone to failure. Along the Kosi, deposits north of the mountain front are characterised by coarse (~ 228- 323 mm) average grain sizes, and wide

D_{84} distributions, with D_{84} values from K6 on the Tamur River tributary representing the coarsest (365 mm) and most widely distributed. This is likely to reflect the dominance of direct Lesser Himalayan and Siwalik hillslope inputs along the study reach. The results of this study reflect a difference in structural development through wider D_{84} distributions and larger D_{84} values at the Kosi mountain front opposed to the Gandak, where a continual supply of hillslope derived material is delivered to and then exported by the Kosi River from the Himalayan mountain front.

Shields stress analysis reveals that north of the Chitwan Dun, the Gandak is likely to be supply limited. The Kosi also reveals similar findings at locations K5 and K4, but to a lesser extent. That is to say that the flow is capable of transporting coarser material, and so grain size distributions reflect patterns in sediment supply as opposed to hydraulic conditions. Therefore, the coarser grain sizes noted along the Kosi reflect the difference in nature of the lateral inputs of sediment within both study reaches, opposed to the competence of the channel flow.

The evolution of the Chitwan Dun has allowed for the temporary storage space of erosional detritus stripped from the rising Himalaya, prior to exiting the mountain front. The Kosi on the other hand, is not capable of storing sediment close to the mountain front as lacks foreland accommodation. The large contrast in sediment yields between the Kosi and Gandak Rivers as documented by Singh *et al*. (2008) is likely to relate to this difference in foreland basin evolutionary styles and production of accommodation at the mountain front. The Chitwan Dun acts as a filter to sediment exported through the Himalayan mountain front. Sediment produced by the rapidly rising Greater Himalaya has been deposited within the Dun, until it has now reached a position where there is no longer any available accommodation, without significant incision of the Dun fill. It is presumed that the Gandak is now directly exporting erosional detritus from the Greater Himalaya onto the Gandak mega fan as is no longer able to temporarily store it within the Dun. Modern erosion of the Dun fill is also likely to enhance the sediment yield. The input of remobilised recycled Dun fill into the Gandak main stem, by Kholas within the Dun, is too small to detect in low flow conditions through grain size analysis or variations in lithology. Whether an input is detectable during high flow conditions would be a worthwhile extension of this research, as flow within the Khola should be great enough to mobilize a more significant quantity of sediment. With a lack of accommodation prior to the mountain front, it is assumed that the Kosi is directly exporting sediment out of the mountain front and therefore the sediment yield is likely to reflect patterns of uplift, climate and erosion within the Greater Himalayas.

Referring back to the initial research hypothesis:

"H1: Channel geometry of trans-Himalayan rivers is a function of active tectonic structures"

There is substantial evidence to suggest that channel geometry (width and slope) adjust about major tectonic structures in the Himalayan foreland, thereby satisfying H1. However, these responses in channel width and slope are not consistent across all of the structures and vary in magnitude. In consideration of the error attached to the SRTM data set as considered in Chapters 3 and 5, patterns in channel width and slope should also be treated with a degree of caution.

"H2: Grain size distributions coarsen as trans-Himalayan rivers exit the Himalayan mountain front as a result of active tectonic structures"

Trends in grain size however, do not consistently display characteristic responses to differential uplift in accordance with patterns outlined in Chapter 1. Whilst appreciating the limited number of grain size transects which could be undertaken on the Kosi River, D_{84} is noted to coarsen upstream of both the MBT and HFT which would suggest that grain size is responding to changes in channel slope related to movement on both structures. Grain size and grain size distribution on the Gandak River appears independent to the relative position of the MBT, MDT and HFT however.

"H3: *Inputs of recycled Siwalik lithologies from local mass-wasting lead to a coarsening of grain size distribution within trans- Himalayan rivers at the mountain front"*

There is also substantial evidence that grain size and grain size distributions are strongly controlled by the nature of sediment inputs. Hillslope and tributary-derived inputs produce distinct patterns in their average D_{84} values and deviation of values within individual bars, with a notable difference also detected between Dun and non-Dun settings.

As a result of differing styles of foreland basin development, the lithology of lateral inputs is also likely to vary between the Gandak and Kosi which is likely to influence grain size patterns. The weakly consolidated Siwalik lithology produces more uniform grain sizes within the Chitwan Dun in comparison to the coarser and wider distributed grain sizes from the more variable Lesser Himalayan lithologies both upstream of the Dun and within the Kosi River. Changes in bedrock lithology as the rivers flow from the Lesser Himalaya onto the Indo-Gangetic Plains are also likely to influence the shape of longitudinal profiles, as a function of the relative hardness of the differing rocks.

"H4: Patterns of sediment storage and release within Dun valleys modulate channel morphology to a greater degree than rock uplift at the Himalayan mountain front"

The contrast in grain size distributions between the Kosi and Gandak Rivers would suggest that the Chitwan Dun, and associated foreland basin development, exerts a strong control on spatial

patterns of grain size (and size distribution) within the Gandak River. Changes in channel geometry however, appear less impacted by the presence of the Dun as changes in channel slope and width appear consistent with morphological responses expected about active tectonic structures.

To summarise, despite the Kosi and Gandak Rivers crossing the same major tectonic boundaries at the Himalayan mountain front there is evidence of subtle morphological inconsistencies, as a result of the style of foreland basin development and resulting form. These inconsistencies are most apparent in grain size and grain size distribution which are modulated by patterns of sediment storage and release from the Chitwan Dun.

<u>Appendix</u>

Quantification of error associated with LISS-3 derived channel widths

To gain an understanding of the error associated with channel width measurements derived from LISS imagery, measurements were taken in the field using a hand held laser distance meter between high water widths on the Kosi River to allow for a direct comparison. Repetitive width measurements were taken at two sites so that an average figure could be produced, as there was some disagreement between repeated measurements, most likely because of the quality of the reflected surface. In spite of this, the inconsistency between readings was within an order of a few meters so was not significant.

Location 1: 0514811 2970257 (UTM zone 45N)

LISS-3 width: 254.85m

Laser width (averaged from two shots): 257.66m

LISS-3 error= 1.09% of laser

Location 2: 0514378 2968889 (UTM zone 45N)

LISS-3 width: 231.51m

Laser width (averaged from four shots): 230.30m

LISS-3 error= 0.52% of laser

Amos, C. B. and D. W. Burbank (2007). Channel width response to differential uplift. *Journal of Geophysical Research-Earth Surface 112(F2).*

Ashmore, P., Bertoldi, W. and Gardner, J.T. (2011). Active width of gravel-bed braided rivers. *Earth Surface Processes and Landforms 36(11): 1510-1521*

Attal, M. and Lave, J. (2009) Pebble abrasion during fluvial transport: Experimental results and implications for the evolution of the sediment load along rivers. *Journal of Geophysical Research* **114**

Attal, M. and J. Lave (2006). Changes of bed load characteristics along the Marsyandi River (central Nepal): Implications for understanding hillslope sediment supply, sediment load evolution along fluvial networks, and denudation in active orogenic belts. *Tectonics, Climate, and Landscape Evolution. S. D. Willett, N. Hovius, M. T. Brandon and D. M. Fisher. 398: 143-171.*

Barnes, J. B., Densmore, A.L., Mukul, M., Sinha, R., Jain, V. and Tandon, S.K. (2011). Interplay between faulting and base level in the development of Himalayan frontal fold topography. *Journal of Geophysical Research-Earth Surface 116.*

Bernet, M., van der Beek, P., Pik, R., Huyghe, P., Mugnier, J. L., Labrin, E. and Szulc, A. (2006). Miocene to Recent exhumation of the central Himalaya determined from combined detrital zircon fission-track and U/Pb analysis of Siwalik sediments, western Nepal. *Basin Research 18(4): 393-412.*

Bilham, R., Larson, K., Freymueller, J., Jouanne, F., LeFort, P., Leturmy, P., Mugnier, J.L., Gamond, J.F., Glot, J.P., Martinod, J., Chaudury, N.L., Chitrakar, G.R., Gautam, U.P., Koirala, B.P., Pandey, M.R., Ranabhat, R., Sapkota, S.N., Shrestha, P.L., Thakuri, D.R., Timilsina, U.R., Tiwari, D.R., Vidal, G., Galy, A. and deVoogd, B.(1997). GPS measurements of present-day convergence across the Nepal Himalaya. *Nature 386(6620): 61-64.*

Burbank, D. W., Leland, J., Fielding, E., Anderson, R.s., Brozovic, N., Reid, M.R. and Duncan, C. (1996). Bedrock incision, rock uplift and threshold hillslopes in the north-western Himalayas. *Nature 379(6565): 505-510.*

Buscombe, D. and G. Masselink (2009). Grain-size information from the statistical properties of digital images of sediment. *Sedimentology 56(2): 421-438.*

Carbonneau, P. E., Bergeron, N. and Lane, S.N. (2005). Automated grain size measurements from airborne remote sensing for long profile measurements of fluvial grain sizes. *Water Resources Research 41(11).*

Carbonneau, P. E., Lane, S.N. and Bergeron, N.E.(2004). Catchment-scale mapping of surface grain size in gravel bed rivers using airborne digital imagery. *Water Resources Research 40(7).*

Chakraborty, T., Kar, R., Ghosh, P. and Basu, S. (2010). Kosi mega fan Historical records, geomorphology and the recent avulsion of the Kosi River. *Quaternary International 227(2): 143-160.*

Church, M. (2006). Bed material transport and the morphology of alluvial river channels. *Annual Review of Earth and Planetary Sciences* **34**: 325-354

DeCelles, P. G., Gehrels, G.E., Quade, J. and Ojha, T.P. (1998). Eocene early Miocene foreland basin development and the history of Himalayan thrusting, western and central Nepal. *Tectonics 17(5): 741-765.*

Desmore, A.L., Sinha, R., Barnes, J., Jain, V. and Tandon, S.K. (2010 EGU poster)

Dugdale, S. J., Carbonneau, P.E. and Campbell, D. (2010). Aerial photosieving of exposed gravel bars for the rapid calibration of airborne grain size maps. *Earth Surface Processes and Landforms 35(6): 627-639.*

Ferguson, R. I. (2003). Emergence of abrupt gravel to sand transitions along rivers through sorting processes. *Geology 31(2): 159-162.*

Finnegan, N. J., Roe, G., Montgomery, D.R. and Hallet, B. (2005). Controls on the channel width of rivers: Implications for modelling fluvial incision of bedrock. *Geology 33(3): 229-232.*

Finnegan, N. J., Sklar, L.S. and Fuller, T.K. (2007). Interplay of sediment supply, river incision, and channel morphology revealed by the transient evolution of an experimental bedrock channel. *Journal of Geophysical Research-Earth Surface 112(F3).*

Frostick, L. E. and S. J. Jones (2002). Impact of periodicity on sediment flux in alluvial systems: grain to basin scale. Sediment Flux to Basins: Causes, Control and Consequences. S. J. Jones and L. E. Frostick. Bath, Geological Soc Publishing House. **191**: 81-95.

Galy, A., France-Lanord, C. and Derry, L.A. (1999). The strontium isotopic budget of Himalayan Rivers in Nepal and Bangladesh. *Geochimica Et Cosmochimica Acta 63(13-14): 1905-1925.*

Graham, D. J., Reid, I. and Rice, S.P. (2005). Automated sizing of coarse-grained sediments: Image-processing procedures. *Mathematical Geology 37(1): 1-28.*

Granet, M., Chabaux, F., Stille, P., Dosseto, A., France-Lanord, C. and Blaes, E. (2010). U-series disequilibria in suspended river sediments and implication for sediment transfer time in alluvial plains: The case of the Himalayan rivers. *Geochimica Et Cosmochimica Acta 74(10): 2851-2865.*

Hancock, G. R., Martinez, C., Evans, K.G. and Moliere, D.R. (2006). A comparison of SRTM and high-resolution digital elevation models and their use in catchment geomorphology and hydrology: Australian examples. *Earth Surface Processes and Landforms 31(11): 1394-1412.*

Hartshorn, K., Hovius, N., Dade, W.B. and Slingerland, R.L. (2002). Climate-driven bedrock incision in an active mountain belt. *Science 297(5589): 2036-2038.*

Hodges, K. V., Wobus, C., Ruhl, K., Schildgen, T. and Whipple, K. (2004). Quaternary deformation, river steepening, and heavy precipitation at the front of the Higher Himalayan ranges. *Earth and Planetary Science Letters 220(3-4): 379-389.*

Holbrook, J. and S. A. Schumm (1999). Geomorphic and sedimentary response of rivers to tectonic deformation: a brief review and critique of a tool for recognizing subtle epeirogenic deformation in modern and ancient settings. *Tectonophysics 305(1-3): 287-306.*

Ibbeken, H. and R. Schleyer (1986). Photo-seiving; a method for grain-size analysis of coarse-grained, unconsolidated bedding surfaces. *Earth Surface Processes and Landforms 11(1): 59-77.*

Jacobsen, K. and R. Passini (2010) Analysis of ASTER GDEM elevation models. *International Society for Photogrammetry and Remote Sensing [online publication: www.isprs.org/proceedings/XXXVIII/part1/09/09_03_Paper_103.pdf]*

Jain, V. and R. Sinha (2003). River systems in the Gangetic plains and their comparison with the Siwaliks: A review. *Current Science 84(8): 1025-1033.*

Jain, V. and R. Sinha (2005). Response of active tectonics on the alluvial Baghmati River, Himalayan foreland basin, eastern India. *Geomorphology 70(3-4): 339-356.*

Johnson, J.P. and K.X. Whipple (2007) Feedbacks between erosion and sediment transport in experimental bedrock channels. *Earth Surface Processes and Landforms 32(7): 1048-1062*

Jouanne, F., Mugnier, J.L., Gamond, J.F., Le Fort, P., Pandey, M.R., Bollinger, L., Flouzat, M. and Avouac, J.P. (2004). Current shortening across the Himalayas of Nepal. *Geophysical Journal International 157(1): 1-14.*

Jouanne, F., Mugnier, J.L., Pandey, M.R., Gamond, J.F., Le Fort, P., Serrurier, L., Vigny, C., Avouac, J.P. and Idylhim Members (1999). Oblique convergence in the Himalayas of western Nepal deduced from preliminary results of GPS measurements. *Geophysical Research Letters 26(13): 1933-1936.*

Kayal, J. R. (2001). Microearthquake activity in some parts of the Himalaya and the tectonic model. *Tectonophysics 339(3-4): 331-351.*

Kimura, K. (1995). Terraced debris and alluvium as indicators of the Quaternary structural development of the north-western Chitwan Dun, central Nepal. *The Science Reports of the Tohoku University, 7th Series (Geography) 45(2): 103-120.*

Kimura, K. (1999). Diachronous evolution of sub-Himalayan piggyback basins, Nepal. *Island Arc 8(1): 99-113.*

Kirby, E. and K. Whipple (2001). Quantifying differential rock-uplift rates via stream profile analysis. *Geology 29(5): 415-418.*

Kirby, E., Johnson, C., Furlong, K. and Heimsath, A. (2007) Transient channel incision along Bolinas Ridge, California: Evidence for differential rock uplift adjacent to the San Andreas fault. *Journal of Geophysical Research- Earth Surface 112(F3)*

Kirby, E., Whipple, K.X., Tang, W.Q. and Chen, Z.L. (2003). Distribution of active rock uplift along the eastern margin of the Tibetan Plateau: Inferences from bedrock channel longitudinal profiles. *Journal of Geophysical Research-Solid Earth 108(B4).*

Knighton, D. (1998) Fluvial forms and processes: a new perspective. *London, Arnold.*

Lague, D. and P. Davy (2003) Constraints on the long-term colluvial erosion law by analyzing slope-area relationships at various tectonic uplift rates in the Siwalik Hills (Nepal). *Journal of Geophysical Research- Solid Earth 108(B2)*

Lave, J. and J. P. Avouac (2000). Active folding of fluvial terraces across the Siwaliks Hills, Himalayas of central Nepal. *Journal of Geophysical Research-Solid Earth 105(B3): 5735-5770.*

Lave, J. and J. P. Avouac (2001). Fluvial incision and tectonic uplift across the Himalayas of central Nepal. *Journal of Geophysical Research-Solid Earth 106(B11): 26561-26591.*

Lave, J., Yule, D., Sapkota, S., Basant, K., Madden, C., Attal, M. and Pandey, R. (2005). Evidence for a great medieval earthquake (approximate to 1100 AD) in the Central Himalayas, Nepal. *Science 307(5713): 1302-1305.*

Leopold, L.B. and T.M. Maddock (1953) The hydraulic geometry of stream channels and some physiographic implications. *Geological Survey Professional Paper 252. United States Government Printing Office, Washington.*

McCaffrey, R. and J. Nabelek (1998). Role of oblique convergence in the active deformation of the Himalayas and southern Tibet plateau. *Geology 26(8): 691-694.*

Meigs, A.J., Burbank, D.W. and Beck., R.A. (1995) Middle-late Miocene (>10 Ma) formation of the Main Boundary thrust in the western Himalaya. *Geology* **23**(5): 423-426

Mohindra, R., Parkash, B. and Prasad, J. (1992). Historical geomorphology and pedology of the Gandak mega fan, Middle Gangetic Plains, India. *Earth Surface Processes and Landforms 17(7): 643-662.*

Montgomery, D. R. and D. B. Stolar (2006). Reconsidering Himalayan river anticlines. *Geomorphology 82(1-2): 4-15.*

Mugnier, J.L., Huyghe, P., Leturmy, P. and Jouanne, F. (2003) Episodicity and rates of thrust sheet motion in Himalaya (Western Nepal). *In: Mc Clay, K.R. (Ed.), 'Thrust Tectonics and Hydrocarbon Systems' AAPG Memoir* **82**: 1-25

Mugnier, J. L., Huyghe, P., Gajurel, A.P. and Becel, D. (2005). Frontal and piggy-back seismic ruptures in the external thrust belt of Western Nepal. *Journal of Asian Earth Sciences 25(5): 707-717.*

Neupane, R. and S. D. Shrestha (2009). Hydrogeologic assessment and groundwater reserve evaluation in northwestern parts of Dun valley aquifers of Chitwan, inner Terai. *Bulletin of the Department of Geology, Tribhuvan University, Kathmandu, Nepal* **12**: 43-54.

Ouchi, S. (1985). Response of alluvial rivers to slow active tectonic movement. *Geological Society of America Bulletin* **96(4): 504-515**.

Pandey, M. R., Tandukar, R.P., Avouac, J.P., Lave, J. and Massot, J.P. (1995). Interseismic strain accumulation on the Himalayan crustal ramp (Nepal). *Geophysical Research Letters* **22(7): 751-754**.

Powell, C. M. A. and P. J. Conaghan (1973). Plate tectonics and Himalayas. *Earth and Planetary Science Letters* **20(1): 1-12**.

Rice, S. and M. Church (1996). Sampling surficial fluvial gravels: The precision of size distribution percentile estimates. *Journal of Sedimentary Research* **66(3): 654-665**.

Rice, S. and M. Church (1998). Grain size along two gravel-bed rivers: Statistical variation, spatial pattern and sedimentary links. *Earth Surface Processes and Landforms* **23(4): 345-363**.

Robl, J., Stuwe, K. and Hergarten, S. (2008). Channel profiles around Himalayan river anticlines: Constraints on their formation from digital elevation model analysis. *Tectonics* **27(3)**.

Rubin, D. M. (2004). A simple autocorrelation algorithm for determining grain size from digital images of sediment. *Journal of Sedimentary Research* **74(1): 160-165**.

Schelling, D. (1992). The tectonostratigraphy and structure of the Eastern Nepal Himalaya. *Tectonics* **11(5): 925-943**.

Schumm, S. A., Dumont, J.F. and Holbrook, J. (2000). Active tectonics and alluvial rivers. *Cambridge, Cambridge University Press*.

Seeber, L. and V. Gornitz (1983). River profiles along the Himalayan arc as indicators of active tectonics. *Tectonophysics* **92(4): 335-367**.

Sime, L. C. and R. I. Ferguson (2003). Information on grain sizes in gravel-bed rivers by automated image analysis. *Journal of Sedimentary Research* **73(4): 630-636**.

Simpson, G. D. H. (2010). Influence of the mechanical behaviour of brittle-ductile fold-thrust belts on the development of foreland basins. *Basin Research 22(2): 139-156.*

Singh, A. K., Parkash, B., Mohindra, R., Thomas, J.V. and Singhvi, A.K. (2001). Quaternary alluvial fan sedimentation in the Dehradun Valley Piggyback Basin, NW Himalaya: Tectonic and palaeoclimatic implications. *Basin Research 13(4): 449-471.*

Singh, H., Parkash, B. and Gohain, K. (1993). Facies analysis of the Kosi mega fan deposits. *Sedimentary Geology 85(1-4): 87-113.*

Singh, S. K., Rai, S.K. and Krishnaswami, S. (2008). Sr and Nd isotopes in river sediments from the Ganga Basin: Sediment provenance and spatial variability in physical erosion. *Journal of Geophysical Research-Earth Surface 113(F3).*

Sinha, R. (2008). Kosi: rising waters, dynamic channels and human disasters. *Economic and Political Weekly: 42-46.*

Sinha, R., Bapalu, G.V., Singh, L.K. and Rath, B. (2008). Flood Risk Analysis in the Kosi River Basin, North Bihar using Multi-Parametric Approach of Analytical Hierarchy Process (AHP). *Photonirvachak-Journal of the Indian Society of Remote Sensing 36(4): 335-349.*

Sinha, R. and P. F. Friend (1994). River systems and their sediment flux, Indo-Gangetic Plains, Northern Bihar, India. *Sedimentology 41(4): 825-845.*

Sinha, R., Jain, V., Babu, G.P. and Ghosh, S. (2005). Geomorphic characterization and diversity of the fluvial systems of the Gangetic Plains. *Geomorphology 70(3-4): 207-225.*

Suresh, N., Bagati, T.N., Thakur, V.C., Kumar, R. and Sangode, S.J. (2002). Optically stimulated luminescence dating of alluvial fan deposits of Pinjaur Dun, NW Sub Himalaya. *Current Science 82(10): 1267-1274.*

Surian, N. and Rinaldi, M. (2003) Morphological response to river engineering and management in alluvial channels in Italy. *Geomorphology 50(4): 307-326.*

Szulc, A. G., Najman, Y., Sinclair, H.D., Pringle, M., Bickle, M., Chapman, H., Garzanti, E., Ando, S., Huyghe, P., Mugnier, J.L., Ojha, T. and DeCelles, P. (2006). Tectonic evolution of

the Himalaya constrained by detrital Ar-40-Ar-39, Sm-Nd and petrographic data from the Siwalik foreland basin succession, SW Nepal. *Basin Research 18(4): 375-391.*

Tamrakar, N. K., Maharjan, S. and Shrestha, M.B. (2008). Petrology of Rapti River sand, Hetauda-Chitwan Dun Basin, Central Nepal; an example of recycled provenance. *Bulletin of the Department of Geology, Tribhuvan University, Kathmandu, Nepal 11: 23-30.*

Tandon, S. K., Gibling, M.R., Sinha, R., Singh, V., Ghazanfari, P., Dasgupta, A., Jain, M. and Jain, V. (2006). Alluvial Valleys of the Ganga Plains, India: Timing and causes of incision. *SEPM (Society for Sedimentary Geology) SEPM Special Publication No.85 (Incised Valleys in Time and Space): 15-35.*

Thakur, V. C. and A. K. Pandey (2004). Late quaternary tectonic evolution of Dun in fault bend/propagated fold system, Garhwal Sub-Himalaya. *Current Science 87(11): 1567-1576.*

Valdiya, K. S. (1998). Dynamic Himalaya. *Hyperabad, India, Universities Press.*

van der Beek, P., Robert, X., Mugnier, J.L., Bernet, M., Huyghe, P. and Labrin, E. (2006). Late Miocene - Recent exhumation of the central Himalaya and recycling in the foreland basin assessed by apatite fission-track thermochronology of Siwalik sediments, Nepal. *Basin Research 18(4): 413-434.*

Wells, N. A. and J. A. Dorr (1987). Shifting of the Kosi River, Northern India. *Geology 15(3): 204-207.*

Wesnousky, S. G., Kumar, S., Mohindra，R. and Thakur, V.C. (1999). Uplift and convergence along the Himalayan frontal thrust of India. *Tectonics 18(6): 967-976.*

Whipple, K.X. and G.E. Tucker (1999) Dynamics of the stream-power river incision model: Implications for the height limits of mountain ranges, landscape response timescales, and research needs. *Journal of Geophysical Research- Solid Earth 104*(B8): 17661-17674

Whittaker, A. C., Attal, M. and Allenn, P.A. (2010). Characterising the origin, nature and fate of sediment exported from catchments perturbed by active tectonics. *Basin Research 22(6): 809-828.*

Whittaker, A. C., Cowie, P.A., Attal, M., Tucker, G.E. and Roberts, G.P. (2007). Bedrock channel adjustment to tectonic forcing: Implications for predicting river incision rates. *Geology 35(2): 103-106.*

Wobus, C., Heimsath, A., Whipple, K. and Hodges, K. (2005). Active out-of-sequence thrust faulting in the central Nepalese Himalaya. *Nature 434(7036): 1008-1011.*

Wobus, C. W., Tucker, G.E. and Anderson, R.S. (2006a). Self-formed bedrock channels. *Geophysical Research Letters 33(18).*

Wobus, C. W., Whipple, K.X., Kirby, E., Snyder, N., Johnson, J., Spyropolou, K., Crosby, B. and Sheehan, D. (2006b). Tectonics from topography: Procedures, promise, and pitfalls. *Tectonics, Climate, and Landscape Evolution. S. D. Willett, N. Hovius, M. T. Brandon and D. M. Fisher. 398: 55-74.*

Yanites, B. J. and G. E. Tucker (2010). Controls and limits on bedrock channel geometry. *Journal of Geophysical Research-Earth Surface 115.*

Yanites, B. J., Tucker, G.E., Mueller, K.J., Chen, Y.G., Wilcox, T., Huang, S.Y. and Shi, K.W. (2010). Incision and channel morphology across active structures along the Peikang River, central Taiwan: Implications for the importance of channel width. *Geological Society of America Bulletin 122(7-8): 1192-1208.*